THE UNIVERSITY *of* EDINBURGH

Application of fire calorimetry to understand factors affecting flammability of cellulosic material: Pine needles, tree leaves and chipboard

Freddy Xavier Jervis Calle

A thesis submitted for the degree of Doctor of Philosophy

The University of Edinburgh

2012

Abstract

Calorimetry, the science of measuring heat from chemical reactions and physical changes, is one to the most valuable tools fire safety engineering have at their disposal. Calorimetric devices such as the cone calorimeter and the fire propagation apparatus (FPA) give us the means to evaluate and understand how different materials burn at a small scale. Due to fire being affected by many different environmental factors, these devices help us to isolate and examine how each factor affects fire as a whole and be able to apply this knowledge to tools that can be used at larger scales.

This thesis reports various pieces of work on different calorimetric studies done on cellulosic material used in today's natural and built environment. All experimental tests herein are done using the FPA, the state of the art calorimeter for fire safety studies. The experimental techniques presented here show how invaluable calorimetry is in giving us key insights on the combustion dynamics of fire related processes.

The thesis is presented in manuscript style. Each chapter is a stand alone research work intended for publication with the exception of the first and last chapter; intended to introduce these and their relevance to the science and the last to summarize on overall findings and recommended improvements.

Chapter 2 presents a study on the burning of live and dead pine needles. Pine forests present a relatively high flammability risk comprised in great part by pine needles. Different moisture content, flow conditions and their interrelationship is studied on the different parameters affecting the combustion processes. Overall, the results show that fire physics and chemistry vary with fuel and flow conditions and that moisture content is not the only difference between live and dead fuels but that the needle bed physiochemical mechanisms matter as well. This is the first time calorimetry data is presented on the burning of live and dead pine needles.

Chapter 3 complements chapter 2 with an added in-depth analysis on the effect of different pine needle species, fuel load and imposed heat insult. Interrelationship between these variables is shown to have a strong effect on the overall combustion process. Fuel load is shown to be an essential condition to know as it gives a direct indication on the intensity of the fire. Flow is shown to have a varied effect depending on the fuel load, it can either aid or be detrimental to the overall combustion process especially relating to ignition times.

Chapter 4 is a study on the effect of leaf morphology to flammability of different natural fuels. This study is a direct extension of the work presented in the paper Belcher et al (2010) in Nature Geoscience. Representative natural fuel samples from the Triassic/Jurassic Boundary, a time period of great importance because it marked a time of major environmental changes, are used to evaluate fire activity as a whole during this time period. The study shows that smaller leaf area and larger surface area to volume ratio show a strong correlation to an increase in flammability of these fuels. The research presents new insight into how leaf morphology can be used as a tool to assess the effect of fire activity around the globe and how closely vegetation is linked to this.

Chapter 5 presents a study on flammability of chipboard. Wood being an inhomogeneous, non isotropic material presents researchers with a complex problem due to its burning behavior. Wood has been a preferred construction material since far back and is widely used in construction today. Different oxygen levels, heat insults, material thicknesses and densities and the interrelationship between these variables are assessed to observe the effect on the flammability of chipboard. Density and thickness is shown to have little effect on the overall burning dynamics with thermally thick samples apart from the increased fuel content. Oxygen levels and imposed heat insults, however, show a wide range of effects and the interrelationship proves to be quite important during the combustion process. The research outlines how char formation is affected by the different variables and how important this process becomes along the overall combustion process.

Calorimetric studies are presented that illustrate the use of these devices to study the effect of varying environmental conditions and the importance of their interrelationships on both natural and built environment fuels. The works highlight the importance of first establishing the dynamics of the combustion process in order to be able to extract combustion parameters that are needed for modeling fires better in both wildland and built environments.

Table of Contents

List of Figures

List of Tables

List of Symbols and Abbreviations

Symbols

A_L	Leaf area (cm^2)
c_p	Specific heat of the combustion product-air mixture (J/kg.K)
$\dot{G}$	Generation rate (g/s)
$\dot{G}^0$	Generation rate at time zero (g/s)
ΔH	Net heat of complete combustion per mass generated (kJ/g)
ΔH_c	Effective heat of combustion (kJ/g)
L_V	Heat required to produce the volatiles (J/g)
$\dot{m}$	Total mass flux of the fire product-air-mixture (g/s)
$\dot{m}''$	Burning rate ($g/s.m^2$)
$\dot{Q}$	Heat release rate (kW)
$\dot{Q}_c$	Convective heat release rate (kW)
$\dot{Q}''_E$	External heat flux applied (kW/m^2)
$\dot{Q}''_F$	Heat flux supplied by the flame (kW/m^2)
$\dot{Q}''_L$	Loss expressed as a heat flux through the fuel surface (kW/m^2)
SA_L	Surface area of a leaf (cm^2)
T	Temperature (K)
τ	Thickness (mm)
V	Volume (m^3)

Subscripts

a	ambient
CO	Of carbon monoxide
CO_2	Of carbon dioxide
d	In the test duct
o	Initial

Abbreviations

ASTM	American Society for Testing and Materials
CDG	Carbon dioxide and carbon monoxide generation
FM	Factory Mutual
FPA	Fire Propagation Apparatus
HRR	Heat release rate
MLR	Mass loss rate

Declaration

This thesis and the work described within has been conducted solely by Freddy Jervis under the supervision of Dr Guillermo Rein and Prof. Jose L. Torero. Where others have contributed or other sources are quoted, references are given in full.

Freddy Jervis

2012

Acknowledgements

First of all, I would like to express my sincere gratitude to my supervisor Dr. Guillermo Rein. His constant encouragements, optimism, support and belief in me has led me this far, Muchas Gracias.

Thanks also to Prof. Jose Torero and Prof Dougal Drysdale for their ample knowledge in the fire safety discipline from which I have learned a lot throughout these years. Thank you for forming such a diverse group here where ideas are constantly exchanged to produce unique research.

This research was funded by BRE Trust, UK. Thank you very much for your financial support these years and my special thanks to Dr. Debbie Smith for her support.

I also wish to thank all my colleagues at the Fire Lab and at John Muir for making all my time in Edinburgh that much more enjoyable. Thanks to Hubert and Paolo for first showing me how things work in the Lab. Thanks to Kate, Wolfram, Rory, Ying, Koo, Ime and Laura for listening to my troubles in the office. Thanks to Nico, Jamie, Rut, Joanne for their continued help. Thanks to Claire for showing me how important it is to look at things outside the box.

For the people in Edinburgh for their invaluable time, thank you. A special thanks to Rory, Ime and Florian for being people who I could always count on. Cecile thanks for telling Guillermo to be patient with me.

Above all, I would like to thank my family, my mom, dad and sister, without your support I would have never been here and to anyone else I owe gratitude Muchas Muchas Gracias.

Preface

This thesis is presented in a manuscript format. Each core chapter is written in the style of a research paper which has been prepared for journal publication. The material is presented in the following order:

- Chapter 2 presents a calorimetric study on the burning of live and dead Pinus halepensis needles using various fuel and environmental conditions.

- Chapter 3 is a manuscript on the effect of different pine needle species, fuel load and imposed heat insult to the burning dynamics of these fuels.

- Chapter 4 is a study on the effect of leaf morphology to flammability of different natural fuels.

- Chapter 5 presents a study on flammability of chipboard with varying densities thickness and under varying oxygen levels and heat insults.

Selected publications

Belcher, C. M., Mander, L., Rein, G., **Jervis, F. X**., Haworth, M., Hesselbo, S. P., Glasspool, I. J. and McElwain, J. C. Increased fire activity at the Triassic/Jurassic boundary in Greenland due to climate-driven floral change. Nature Geoscience, 3(6), doi: 10.1038/NGEO871, (2010).

Jervis, F. X., Rein, G., Simeoni, A., Torero, J. L. Burning Behaviour of Live and Dead Pinus Halepensis Needles using Small Scale Calorimetry Experiments. Proceeding of the Sixth International Seminar on Fire and Explosion Hazards, 973-983, April 2010.

Chapter 1

Introduction

Over the years, the dangers of fires have become more and more apparent. In the United Kingdom alone, direct losses from fire probably exceed £1000 M and over 800 people die each year. [1] The need for understanding fire behavior has become essential to be able to predict and tackle these fires both in the built environment and natural environment. However, fire science as a whole is a relatively young field. Research in this field only started during the middle of the 20th century when knowledge of the basic sciences gave us the background knowledge to start the science itself. Our understanding is still limited and this has forced us to look at ways to bypass our current lack of understanding. [2] In order to do this, fire safety engineers have constantly been developing various tools to allow us to understand various aspects of the fire whether it be fire growth, speed, intensity among others. These have developed from very simple equations describing the burning of a piece of material to complex models involving computational fluid dynamics (CFD) such as the Fire Dynamic Simulator (FDS). [3] Given the many different variables involved in a fire; however, it becomes very complex in nature and very hard to predict; therefore, a strong need for more understanding and good input data for these models has become apparent.

One of the difficulties arises in that we still do not have a full understanding of how different materials burn. Most fires involve combustible solids where a material is subjected to heat and undergoes thermal decomposition or pyrolysis. This allows for flammable volatiles to be released and once it has reached a flammable mixture of air and fuel it can ignite if a pilot source of energy such as a spark. This process is known as piloted ignition. For spontaneous ignition it will slightly differ in that suitable conditions need to be achieved in the absence of a pilot source with a higher heat input overall. Although the process in itself is complex in nature, fire safety engineers have come to rely heavily on small scale tests in order to bypass this complexity. These tests provide

data that can be understood, quantified and be used as inputs to evaluate the fire hazard of a given material. The best examples of these are the cone calorimeter and the fire propagation apparatus (FPA). [4]

Calorimetric devices, such as the cone calorimeter and the FPA, allow us to evaluate how materials burn at a small scale in order to apply this knowledge at a bigger scale. Two main data sets are extracted from these devices: mass loss rate (MLR) and heat release rate (HRR), which has been described as the single most important variable in fire hazard [5]. It essentially tells us about intensity and fire growth; it also basically determines the contribution to compartment fire hazard from materials. [5] There is a large volume of material about these devices and its uses; for more information refer to the Hazards Calculation section in the Society of Fire Protection Engineers handbook. [4]

One of the problems, however, is that much of the research in the literature has been on what we refer to now as "traditional fuels". Fuels such as PMMA and polyurethane have been studied extensively, although we still don't have a full understanding of how these fuels burn. Moreover, in a field where we have to keep up to date with new building materials constantly emerging and models that require good input parameters in order to model this, the understanding of fire dynamics for these new kinds of fuels becomes highly complex.

In an attempt to expand our understanding and knowledge of these new fuels, the studies presented here are done to demonstrate capability of the state of the art in these small scale tests that enable us to gain a better understanding of the combustion dynamics involved during the burning of some these complex fuels. The collection of works herein present calorimetric studies on various cellulose materials in use in today's natural and built environment and how different environmental condition can affect burning of these materials in different ways. Even though natural and built environments differ in many was, the core concepts in material burning are very similar.

Under natural fuels, live and dead pine needles (various species) in chapter 2 and 3 are studied and natural leaves (various species) in chapter 4. Three main concepts have been defined as the group of characteristics defining flammability of vegetation in general: ignitability, combustibility and sustainable of burning. [6] Many factors, however, can have an impact on the way natural fuels burn such as fuel load, composition, configuration, moisture content, porosity among many others and the interrelationship between each other. One of the big problems, however, is how to decide which are the most relevant or influential to the burning of these fuels. It is for this reason that experimental studies become necessary in order to both calibrate and validate the prediction of models. [7] It is the aim of these works to study these relationship and interrelationships of some of these variables affecting the burning of natural fuels at the small scale.

Under fuels used in the built environment, we observe similar concepts in chapter 5. A much wider amount of research is presented in the literature on these fuels, but the fundamental research work still remains limited to mostly "traditional fuels" as highlighted before. Solid burning has been widely studied, one key area, however, in which research is still relatively lacking, has been oxygen concentration studies of the fuel burning process. Oxygen can have very strong effect of the way materials burn mainly due to the effect on the flame itself. Moreover, given that during compartment fires, oxygen concentration can range from ambient (21%) to almost zero [8] and one can reach higher concentrations in industrial sectors where oxygen leaks are a possibility, knowing how this will affect the combustion process has become a key mechanism to understand burning of fuels in this scenario. The work presented in chapter 5 presents burning of chipboard under different levels of oxygen concentration and the interrelationship of this with other parameters important to the combustion process. Chipboard and wood in general is one of the materials most widely used in construction due to its flexibility, availability, among other advantages and have become one of the main materials constituting the fuel load in buildings and homes. [9] Wood, however, has the added complexity of char formation which is still not fully understood today and the effects of oxygen levels and this char formation process are presented herein.

Even though calorimetric devices can be very useful to give us key insight into material flammability and a way of classifying materials accordingly, full scale effects during real fires can sometimes undermine small scale effects. Radiation is a phenomenon that has been observed to not be as important in small scale as it is in large scales. Burning rate will be largely dominated by radiation from the flame if the fuel bed is greater than about 0.3 m in diameter [1] compared to ~0.1m size for calorimetry tests. Markestein also observed that the emissivity of flames above polymethylmethacylate increased approximately three-fold from 0.31 m to 0.73m [10]. In an enclosure, heat dissipated to the environment is not totally lost as the fuel gases are trapped in the ceiling which will be heated. Radiation from the hot gases will then heat the burning fuel and a cycle is created from the fuel generating more hot gases and the gases reradiating heat back to the fuel. [1] Alpert in [11] has also shown the importance of pressure and radiation in large scales which cannot be seen at the small scale. At larger scales, the length scale will be different depending on the scale which will affect the heat and mass transfer like is the case in microgravity [12]. This becomes a problem in wildland fires as well. The flame characteristic and temperature distribution in the fire plume change from the lab to the field due to the different length scales for vegetation and turbulence [13]. Variability and homogeneity is something that is easier to control at the small scale but becomes a real challenge at the large scale.

It is clear we have yet to fully understand how fire works and as Emmons presented in his review of the discipline, we most likely have a long road ahead before we can understand and model fire from first principles. [2] It is for this reason we are still heavily dependent on experimental data such as calorimetric experiments which can give us key insights on the combustion dynamics of these processes.

References

[1] Drysdale, D. An Introduction to Fire Dynamics (Wiley, 1998).

[2] Emmons, H. W., Future History of Fire Science, Combustion Science and Technology, 1984, 40:167-174.

[3] Mcgrattan, K. Fire Dynamics Simulator (Version 5) – Technical Reference Guide. NIST Special Publication 1018-5, 2010.

[4] SFPE Handbook of Fire Protection Engineering, 3rd edition, The National Fire Protection Association Presss, 2002, Section Three Hazard Calculation: pgs 3-38-3-161.

[5] Babrauskas, V. and Peacock, R.D. "Heat Release Rate: The Single Most Important Variable in Fire Hazard," Fire Safety Journal 18, pp 255-272 (1992).

[6] Anderson, H. E., Forest fuel ignitability, *Fire Technology*, 1970, **6**: 312-319.

[7] Mendes-Lopes, J. M. C., Ventura, J. M. P. Flame characteristics in fires propagating in beds of Pinus halepensis needles, in : D. X. Viegas (Ed.), V International Conference on Forest Fire Research, 2006.

[8] Beaulieu, P. A. and Dembsey, N. A. Effect of oxygen on flame heat flux in horizontal and vertical orientation. Fire Safety Journal, 2008, 43: 410-428.

[9] Fire safety in timber buildings - Technical guideline for Europe, SP Technical Research Institute of Sweden, SP Report 2010:19.

[10] Markstein, G. H., "Radiative properties of plastic fires," *Proceeding of the Combustion Institute*, 1979, **17**, 1053-1062.

[11] Alpert, R. L., "Pressure modeling of fires controlled by radiation," *Proceeding of the Combustion Institute*, 1977, **16**, 1489-1500.

[12] Torero, J. L., Simeoni, A., "Heat and mass transfer in fires: scaling laws, ignition of solid fuels and application to forest fires," *The Open Thermodynamics Journal*, 2010, **4**, 145-155.

[13] Santoni, P. A., Simeoni, A., Rossi, J. L., Bosseur, F., Morandini, F., Silvani, X., Balbi, J. H., Cancelleri, D., Rossi, L., " Instrumentation of wildland fire: Characterisation of a fire spreading through a Mediterranean shrub," *Fire Safety Journal*, 2006, **41**, 171-184.

Chapter 2

Ignition and Burning Behavior of Live and Dead Pine Needles

Abstract

Moisture content can be a dominant factor affecting combustion especially in live fuels due to the wide range of moisture content that can be encountered with vegetation. Laboratory experiments are used to study the fire dynamics of Mediterranean Pinus halepensis needles under a range of fuel and flow conditions. A set of 80 experiments with good repeatability were conducted in the Fire Propagation Apparatus (FPA) fire calorimeter. The burning behavior is measured in terms of the evolution of the mass loss rate and the heat release rate from ignition till burn out for different forced flow velocities. Recently collected live and dead needles are compared here for the first time. Additionally, live samples aged for 15 months after collection are presented as an alternative to study changes in live needles. Two different moisture conditions are considered, fresh and oven-dry. The most flammable samples are fresh dead and 15 months aged needles, followed by oven-dry dead, and oven-dry live needles. The least flammable is fresh live needles. Overall, the results show that fire physics and chemistry vary with the fuel and flow conditions, and that moisture content is not the only difference between live and dead fuels, but that the needle bed physicochemical mechanisms matters as well. The loss of volatiles and other changes induced during oven drying is seen to lead to significant differences in the burning behavior.

Keywords: Forest fuel, wildland fires, calorimetry, pine needles

Introduction

The relatively high flammability of a pine forest is due in great part to its pine needles, eg. Mediterranean biome. Needles are fine fuels that spread flames faster than woody fuels [1][2], and also represent an important fraction of the total fuel consumption in pine forest wildfires. Needles are found both in the tree canopies and on the ground. Live pine needles (green needles) are part of the foliage and burn in crown fires. Dead pine needles (brown needles) fall to the ground, accumulating gradually on the litter and humus layers, and burn in surface and ground fires. The presence of live needles on the ground and of dead needles on the foliage is frequent but of less interest since it is short lived and generally occurs in small quantities. A notable exception to this is pine stands attacked by bark beetle that can lead to large amounts of dead needles simultaneously standing on the foliage [3] thus significantly affecting wildfire behavior.

Xanthopoulos et al. [4] lists four aspects of fuel particle factors affecting fire behavior: moisture content, structure (surface-area-to-volume ratio, bulk density and porosity), chemical composition (content in plant tissues of lignin, carbohydrates and ash) and fuel arrangement. Moisture content can be a dominant factor affecting combustion especially in live fuels due to the wide range of moisture content that can be encountered with vegetation. [5] Dead fuel can have fuel moistures that range from 2% to over 40% on a dry weight basis, whereas, in live fuels, the range of fuel moisture varies from 30% to over 300%. [4] Heat of combustion, a direct measure of the fuel content in fuels, is known to be greatly affected by moisture content. The greater the moisture content, the more energy will be required for evaporation and hence affecting the ignition and fire spread in vegetation.

The scientific literature on fire safety of Christmas trees in residential and commercial premises shows that the flammability of trees with fresh live needles compared to dry live needles is very different and most likely due to the different moisture content. [5] Moisture content is also sometimes assumed to be the mechanism governing the burning

behavior of live and dead needles. However, no scientific study can be found in the literature directly comparing live and dead pine needles. [6] Thus, the mechanism still remains unknown.

One of the big assumptions in wildfire behavior has been to categorize live fuel as just very moist dead fuels due to moisture content's strong effect on combustion and neglect any composition difference between live and dead fuels. From *On the need for a theory of fire spread* by Finney et al., [7]: describes how intrinsic fuel characteristics, such as fuel moisture content, is commonly assumed to influence live fuel fire behavior. The assumption was based on early fire spread research in dead fuels that suggested that fuel moisture plays a dominant role in determining the rate of spread and heat release of a fire. Due to the strong apparent dependence of fire behavior on dead fuel moisture, researchers simply assumed that live fuels behave in the same manner. Dead fuels rarely support flaming combustion with moisture contents above 35%; however, fire can spread through exclusively live foliage even though the moisture content is two to three times higher (>100%). Fuel structures and ignition conditions for live fuel fire spread compared to dead fuel beds is suggested to be the cause of this. More importantly, this problem emphasizes our need for more fundamental research in order to have a better grasp of the problem. [7]

This paper aims at filling this gap in knowledge and reports novel laboratory results on the burning of *Pinus halepensis* needles, a common species in the Mediterranean region, using small-scale fire calorimetry experiments of live and dead (both fresh and dried) needles.

Experimental device and protocol

The state of the art scientific methodologies to understand the burning of solid fuels encompass fire calorimetry, solid ignition theory and flame spread models. [8] This scientific knowledge is most frequently used to study fires in the built environment, but

is also applicable to the natural environment. Recently, fire calorimetry is being applied to wildfire research [9]-[12] mostly because the burning conditions can be controlled and varied to provide a fundamental framework of study. As Xanthopoulos et al. [4] has pointed out, flammability studies of this nature represent an improvement in characterizing plant flammability.

We use the Fire Propagation Apparatus (FPA) calorimeter (see Figure 2.1 a) which was initially developed to study the burning behavior of industrial fuels. [13] A sample is introduced inside a chamber 15 cm in diameter. The top surface of the sample is exposed to a uniform radiant heat flux large enough to ignite the fuel and establish a flame. A small pilot source is provided. The mass loss of the sample is measured with a balance. The combustion gases are channeled upwards towards the exhaust exit where the volumetric flow rate is measured by a Pitot tube. The CO and CO2 concentrations are measured using an infra-red system.

The experimental procedures were carried out in accordance to ASTM E2058-03 [14], which outlines the standard operations, but using a specially modified sampler holder. The porous sample holder is a circular basket open at the top and made of stainless steel mesh measuring 13 ± 0.01cm in diameter and 30 ± 0.5mm in depth (Figure 2.1 c). It was developed originally in [11] to account for the important flow conditions inside the fuel bed. The standard sample holder is non-permeable to flow (it is made of solid metallic sheets instead of mesh) and thus leads to uncontrolled flow conditions. The porous holder percentage opening is 63%. The forced flow is 200 $l.min^{-1}$, providing an upstream velocity at the sample centerline of 0.46 ± 0.02 $m.s^{-1}$. The downstream airflow velocity at the sample centerline is between 0.12 ± 0.01 $m.s^{-1}$ for the initial full sample and 0.22 ± 0.02 $m.s^{-1}$ for the empty holder when the sample needles have been consumed.

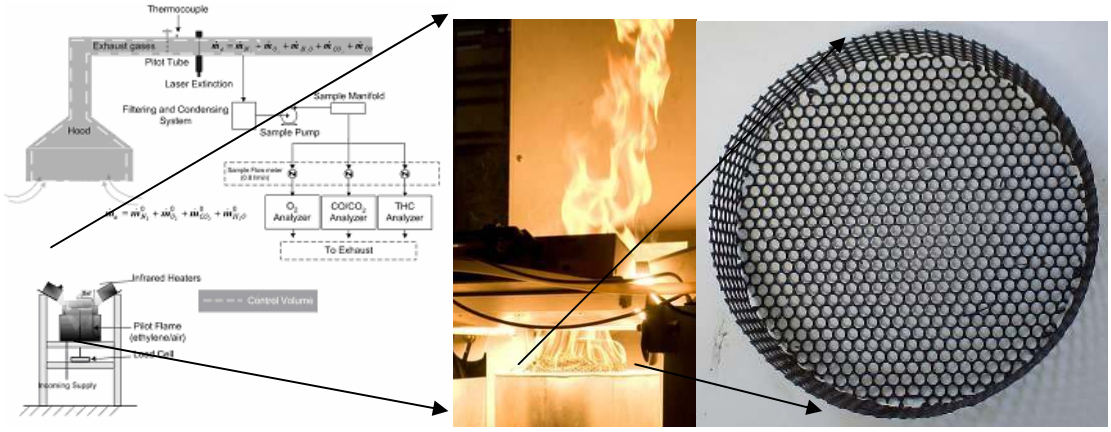

Figure 2.1 ***a) Schematic of the Fire Propagation Apparatus (FPA)***
b) Burning pine needles c) Porous sample holder

We set the infra-red heaters at 50 $kW.m^{-2}$ until burn out of the sample. Experiments are conducted under both natural and forced flow conditions. Each experiment was repeated at least four times and for some conditions up to six times.

Samples of *Pinus halepensis* were prepared with 8 g of needles as seen in Figure 2.2, obtaining an approximate bulk density of 20 $kg.m^{-3}$, similar to that encountered in the litter of some Mediterranean forests. [15] This density is however, much higher than the densities measured in the crowns of pine trees, which has been determined to be around 0.2 $kg.m^{-3}$. [16] The effect of the sample density on the results could be significant but the topic lies outside the scope of this work. The interested reader is referred to chapter 3 of this thesis for more information on the subject.

Figure 2.2 Pinus halepensis needles samples for ***a) Live b) Aged c) Dead d) Ash after burn***

Dead and live samples were studied (see Figure 2.2), each at two different moisture conditions. Live needles of Pinus halepensis were collected from pine stands during spring time in the Mediterranean coast of France. Fresh samples had a wet-base moisture content (MC) of 48 ± 4 % (92% in dry base). These samples were tested rapidly, within one week after collection. Dead needles were collected from the forest litter at the same location and time as the live needles. They were maintained at standard conditions (25°C and 50% air humidity) and tested within five weeks of collection. The measured MC was 7.5 ± 1%. Subsets of the dead and live needles were dried in the oven at 60°C for two days. The measured MC was 2 ± 1% for both. Note that MC for oven-dry samples is not zero because once removed from the oven, the samples quickly reach equilibrium with the atmospheric conditions in the laboratory as previously reported by Marcelli et al. [17] An additional sample series was created to test the effect of aging from a subset of fresh live needles stored at near standard condition (18 ± 5 °C a 40 ± 10% air humidity) during 15 months after collection referred to as “aged needles”. The measured MC was 7.5 ± 1%.

Experimental calculations and parameter estimation

Measurements are obtained following ASTM E 2058 [14], standard practice for using the FPA, combustion test. All other calculations outside this scope are described here. The main sets of data obtained from the FPA are Heat Release Rate (HRR) and Mass

Flux. Chemical HRR is obtained through carbon dioxide and carbon monoxide generation (CDG) calorimetry and convective HRR is obtained using gas temperature rise as described by Tewarson. [18] Mass flux is obtained by deriving mass over time. Due to variability in the load cell, a smoothing algorithm called the supsmooth algorithm is used. [19] Values for energetic constants are obtained from average values described by Tewarson. [18] From these, parameters are obtained and are explained in the figures and equations below:

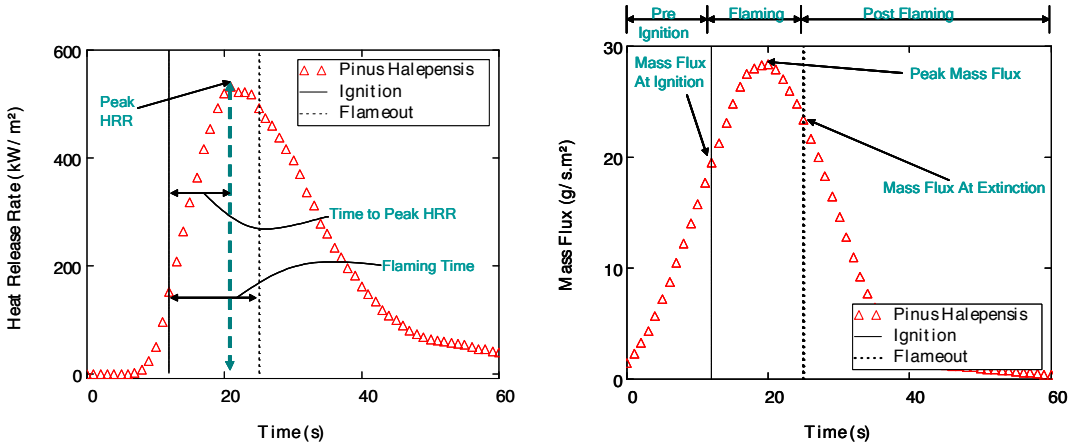

Figure 2.3 ***a) Heat Release Rate b) Mass Flux*** **for fresh dead pinus halepensis needles**

Heat release rate (HRR) is determined using carbon dioxide and carbon monoxide generation to obtain total energy released from the combustion process calculated here as, [18]

$$\dot{Q} = \Delta H_{CO_2}\left(\dot{G}_{CO_2} - \dot{G}^0_{CO_2}\right) + \Delta H_{CO}\left(\dot{G}_{CO} - \dot{G}^0_{CO}\right) \qquad \textbf{Equation 2.1}$$

where $\dot{Q}$ is HRR, ΔH is the net heat of complete combustion per mass generated, $\dot{G}$ is the generation rate, $\dot{G}^0$ is the generation rate at time zero, and CO and CO_2 are carbon monoxide and carbon dioxide respectively. The convective HRR referred to here is calculated using gas temperature measurement difference and pressure difference in the test section duct as,

$$\dot{Q}_c = \dot{m}_d c_p (T_d - T_a)$$ **Equation 2.2**

where $\dot{Q}_c$ is the convective HRR, $\dot{m}_d$ is the total mass flux of the fire product-air-mixture, c_p is the specific heat of the combustion product-air mixture, T_d is the temperature of the combustion product-air mixture in the duct and T_a is the ambient temperature. Effective heat of Combustion (ΔH_c) for these experiments is calculated by integrating the HRR and then dividing by the initial mass, as

$$\Delta H_c = \frac{\int \dot{Q}\, dt}{m_o}$$ **Equation 2.3**

where m_o is the initial mass of the sample.

A series of 80 experiments were conducted. Figure 2.3 a and b are representative of the combustion dynamics for these kinds of experiments. The process can be divided into three main stages: pre ignition, flaming and post flaming stage as can be seen in the mass flux curve. Each stage is important in its own right as they give different indications of what kind of fire can be achieved from the given material and conditions. The start time at zero seconds is the time at which the heat flux is imposed on the material. As can be seen from the mass flux curve, at this time the material starts to degrade and lose mass therein producing pyrolysis gases. Once the concentration of these gases around the pilot flame directly above the sample is sufficient the material will ignite as can be seen identified by the solid vertical line. The sample will then start to rapidly release heat from the flames until it reaches its peak heat release rate as marked on Figure 2.3a. The heat release rate starts to decrease at this point and flameout will occur shortly after. Important parameters are highlighted in Figure 2.3 that are analyzed in detail in the results section such as the mass flux at certain points, different record of time for events in the combustion process such as time to ignition among

others that are important to the combustion dynamics of these fires. A description of parameters of interest to this study is presented in Table 2.1.

Table 2.1 Description of flammability parameters

HRR (kW/m^2)	Heat release rate (HRR) per unit area of sample free surface
Effective Heat of Combustion (kJ/g)	Calculated as the integral of the HRR from ignition to flame out divided by the initial mass (time zero)
Time to Ignition (s)	Time for sample to ignite from when it is first subjected to the heat insult (time zero)
Flaming Time (s)	Duration for which a flame is sustained from ignition to flameout
Time to Peak HRR (s)	Time from ignition to the peak HRR
Mass Flux ($g/s.m^2$)	Mass loss rate per unit area of sample free surface
Normalized Mass Lost (g/g)	Mass lost from the sample normalized against initial sample mass
CO/CO_2 Ratio (g/g)	Ratio of CO production to CO_2 production
Radiative Fraction (kW/kW)	Radiative component of HRR obtained from difference between chemical and convective HRR

Parameters of great importance to wildland fires can be derived from these measurements, such as flame spread rate, depth of the flame front, fire intensity and total heat release. For example, the flame spread rate in real-scale fires is inversely proportional to the time to ignition [8]; so the faster a fuel ignites the faster the flame spread rate. The depth of the fire front is proportional to the flaming time (and the bulk

density); and the fire intensity per unit length of fire front is proportional to the HRR and the depth of the front. Note that we report the effective heat of combustion measured in a fire calorimeter. This is the energy per unit fuel mass that is effectively released in fire conditions. Compare this to the value most reported in the literature, the maximum heat of combustion, which is typically measured in bomb calorimeters and that is only released in ideal combustion conditions (resembling those inside combustion engines) and far from those encountered in real fires.

Results

Transient results

Statistical analysis of the tests was done using the direct and calculated values of various parameters. Discrete and continuous variables are described below. Two different conditions were looked at in this study: natural convection vs forced convection, and moisture comparison (fresh and oven dry needles for live, dead and aged samples). Representative heat release rate and mass loss curves for a given experiment for all these conditions can be seen in the figures below. Statistical results for different parameters are described in the analysis of flammability measurements section.

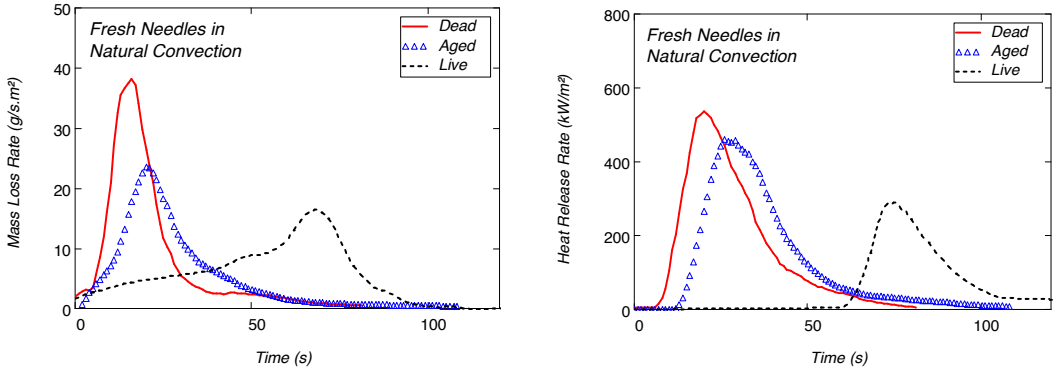

Figure 2.4 ***a) Mass loss b) Heat Release Rate***
for fresh ***Pinus halepensis*** **needles under natural convection**

Figure 2.4 shows the measurements of mass loss and HRR for three needle conditions under natural flow. Test data is fairly repeatable (within 10% variability for most cases and within 20% for all experiments). At the time of ignition (59s average for live, 11s for dead and 13s for aged needles), the HRR sharply increases, reaches a peak value and then decays in two stages. Pre-ignition mass loss is between 45 and 55 % for live needles and between 5 and 10% for the other two needle samples. Considering that fresh live needles MC is 48 % and dead and aged needles MC is 7.5% in wet base, most of the mass loss before ignition would be due to water loss from drying. Flaming combustion lasts between 20 - 40 s so the material is consumed rapidly in this regime. During this time, between 80 and 90 % of the sample mass has burned and what is left is char residues and mineral ash. After flaming, the much slower stage of smouldering combustion takes place burning the char.

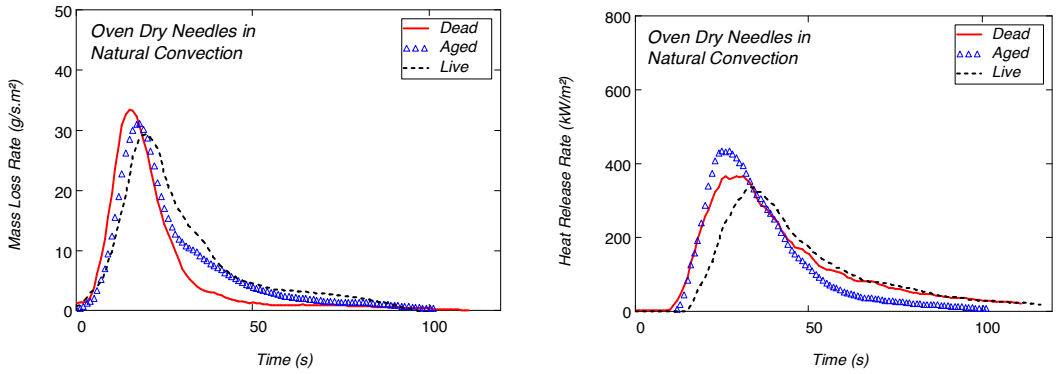

Figure 2.5 ***a) Mass loss b) Heat Release Rate***
for oven-dry ***Pinus halepensis*** **needles under natural convection**

Similarly, Figure 2.5 shows measurement of mass loss and HRR for the three needle conditions in their oven dry state. For live needles, there are large differences between fresh and oven-dry conditions in terms of time to ignition and peak HRR. Fresh live needles ignite later and give off lower HRR. On the other hand, dead and aged needles

have small differences in time to ignition but peak values for dead are smaller compared to aged needles in oven-dry conditions.

Figure 2.6 and Figure 2.7, like the figures before, show measurements of mass loss and HRR but in forced convection. Overall, larger peak values for both mass loss and HRR were observed in forced convection except for fresh live needles, where the differences were small. Times to ignition were greater overall and flaming times lower with again the fresh live needles having negligible differences. Between fresh and oven-dry conditions in forced convection, similar behaviour as seen in natural convection is observed but the overall peak and average values for HRR and MLR are higher.

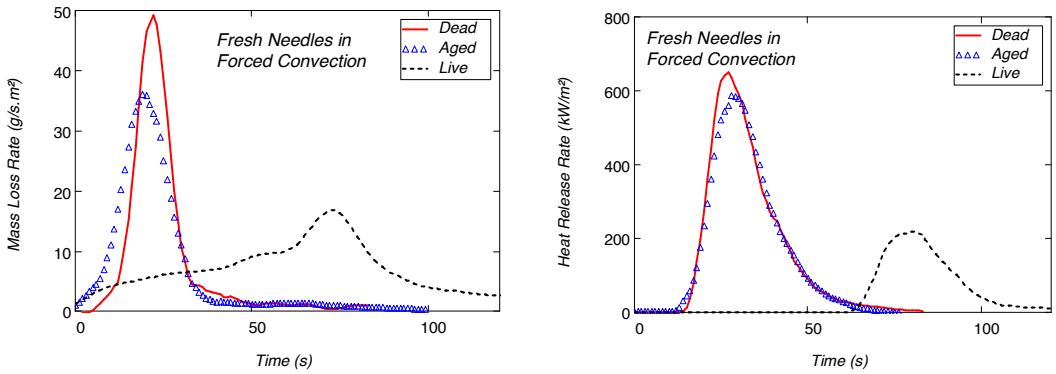

Figure 2.6 ***a) Mass loss b) Heat Release Rate***
for fresh *Pinus halepensis* needles under forced convection

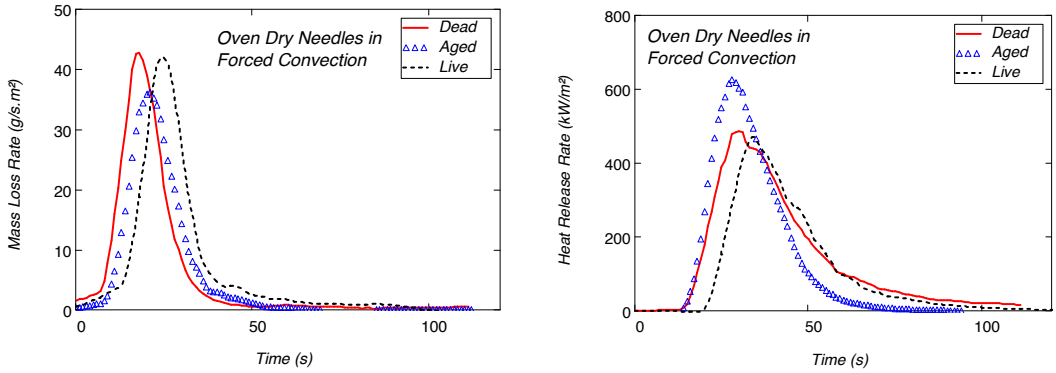

Figure 2.7 ***a) Mass loss b) Heat Release Rate***
for oven-dry ***Pinus halepensis*** **needles under forced convection**

Analysis of flammability measurements

The individual parameters in Table 2.1 were extracted from these transient measurements to understand the combustion behavior. Table 2.2 shows values from repeated experiments averaged to obtain a repeatability error in the measurements taken from heat release rate and mass flux curve of the above mentioned conditions.

Table 2.2 Summary of experiments: average ± standard deviation for ***Pinus halepensis*** **needles**

	Natural Convection					
	Fresh			*Oven-dry*		
Flammability Parameter	Live	Aged	Dead	Live	Aged	Dead
Time to ignition (s)	59 ± 3	13 ± 1	11 ± 2	13 ± 2	11 ± 1	9 ± 0
Flaming Time (s)	30 ± 9	32 ± 2	25 ± 4	24 ± 5	26 ± 5	21 ± 2
Normalized Mass Lost Pre Ignition (g/g)	0.50 ± 0.04	0.06 ± 0.02	0.11 ± 0.05	0.07 ± 0.01	0.08 ± 0.03	0.07 ± 0.03
Normalized Mass Lost Flaming (g/g)	0.39 ± 0.04	0.77 ± 0.04	0.68 ± 0.10	0.51 ± 0.16	0.69 ± 0.07	0.73 ± 0.06
Normalized Mass Lost Post Flaming (g/g)	0.09 ± 0.05	0.15 ± 0.02	0.18 ± 0.07	0.31 ± 0.13	0.21 ± 0.05	0.18 ± 0.03
Peak HRR (kW/m^2)	252 ± 30	457 ± 15	472 ± 51	323 ± 18	483 ± 60	347 ± 25
Effective Heat of Combustion (kJ/g)	11 ± 1	20 ± 1	20 ± 1	19 ± 1	21 ± 2	21 ± 1
Mean CO/CO2 ratio	0.07 ± 0.07	0.15 ± 0.07	0.02 ± 0.01	0.06 ± 0.01	0.12 ± 0.01	0.02 ± 0.01
Peak CO2 Production ($g/s.m^2$)	19 ± 2	35 ± 1	36 ± 4	24 ± 1	37 ± 5	27 ± 2
Radiative Fraction (kW/kW)	0.63 ± 0.07	0.58 ± 0.04	0.53 ± 0.05	0.65 ± 0.07	0.54 ± 0.08	0.65 ± 0.04

	Forced Convection																	
	Fresh									*Oven-dry*								
Flammability Parameter	Live			Aged			Dead			Live			Aged			Dead		
Time to ignition (s)	63	±	3	12	±	1	13	±	2	17	±	3	12	±	1	12	±	1
Flaming Time (s)	34	±	11	16	±	2	18	±	5	14	±	1	18	±	2	13	±	2
Normalized Mass Lost Pre Ignition (g/g)	0.43	±	0.03	0.06	±	0.01	0.08	±	0.04	0.10	±	0.03	0.05	±	0.02	0.08	±	0.01
Normalized Mass Lost Flaming (g/g)	0.36	±	0.03	0.66	±	0.06	0.67	±	0.12	0.65	±	0.05	0.77	±	0.04	0.63	±	0.06
Normalized Mass Lost Post Flaming (g/g)	0.20	±	0.06	0.19	±	0.07	0.22	±	0.08	0.23	±	0.03	0.16	±	0.03	0.30	±	0.07
Peak HRR (kW/m^2)	212	±	15	625	±	29	632	±	34	468	±	24	682	±	40	457	±	23
Effective Heat of Combustion (kJ/g)	9	±	1	21	±	1	21	±	2	20	±	1	23	±	1	24	±	1
Mean CO/CO2 ratio	0.07	±	0.07	0.15	±	0.02	0.04	±	0.02	0.06	±	0.01	0.12	±	0.08	0.02	±	0.01
Peak CO2 Production ($g/s.m^2$)	16	±	1	47	±	2	48	±	3	34	±	2	51	±	3	35	±	2
Radiative Fraction (kW/kW)	0.50	±	0.04	0.59	±	0.05	0.57	±	0.04	0.62	±	0.07	0.58	±	0.06	0.64	±	0.05

Figure 2.8 a) shows time to ignition for the three different needle groups as both fresh and oven dry samples in natural and forced convection. For ignition times, forced convection increases ignition times slightly overall most like due to air flow blowing some of the pyrolysis gases away. Oven-drying only affects the live samples. Most notable are the higher times to ignition for fresh live samples. Moisture is a dominant behaviour on ignition time because during the first phase of thermal decomposition, most of the water will have evaporated before ignition.

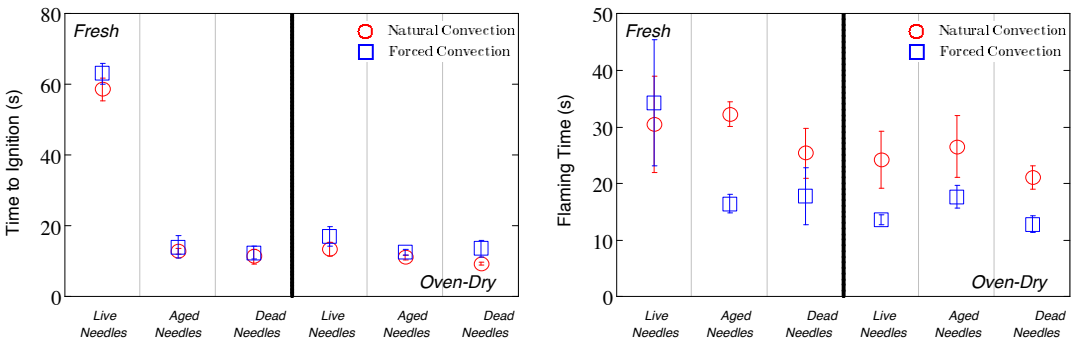

Figure 2.8 ***a) Time to Ignition b) Flaming Time*** **for** ***Pinus halepensis*** **needles**

Flaming times are shown in Figure 2.8 b). With the exception of the fresh live needles, forced convection decreases overall flaming time. Increased availability of oxygen during forced convection allows for the material to burn faster. Oven drying overall decreases flaming times and dead samples display the lowest values.

Figure 2.9 a) shows peak HRR for the tests. With the exception of the fresh live sample, forced convection increases overall peak HRR. This again relates to the increased availability of oxygen allowing for combustion to happen more rapidly. With the exception of the dead needles, oven-drying increases peak HRR values. Aged and dead needles have the highest peak HRR in fresh condition and aged has the highest in the oven-dry state.

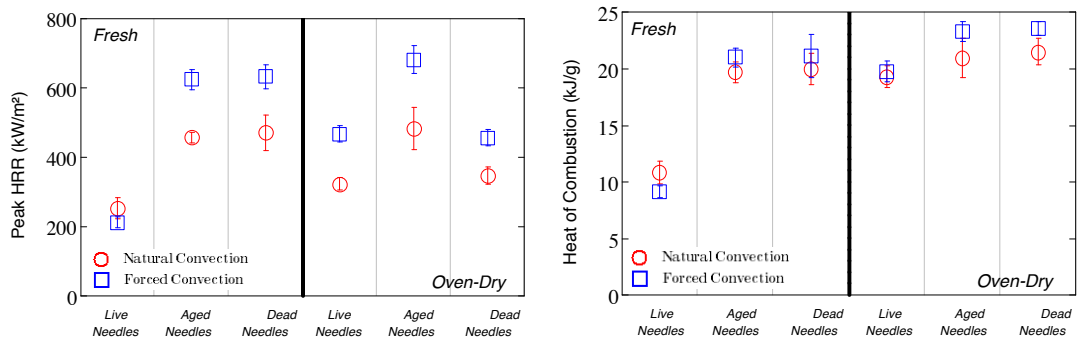

Figure 2.9 ***a) Peak Heat Release Rate b) Effective heat of combustion*** **for** ***Pinus halepensis*** **needles**

Effective heat of combustion values are shown in Figure 2.9 b). With the exception of the fresh live needles, forced convection shows slightly higher values in comparison to natural convection. The increased availability of oxygen allows for the material to be burnt more completely during flaming. Fresh live samples display the lowest at about half the value of the other needles which is almost exactly due to the amount of water content in these needles. In the oven-dry scenario, all needles display higher effective heat of combustion; due to the minimum amount of water in these, all that is left is practically fuel which is why the values are higher.

Figure 2.10 a) shows the normalized mass lost during the pre-ignition stage. Almost all the water evaporates during the pre-ignition stage which is why the fresh live needles show the highest values. Other fuel condition effects are negligible for this parameter.

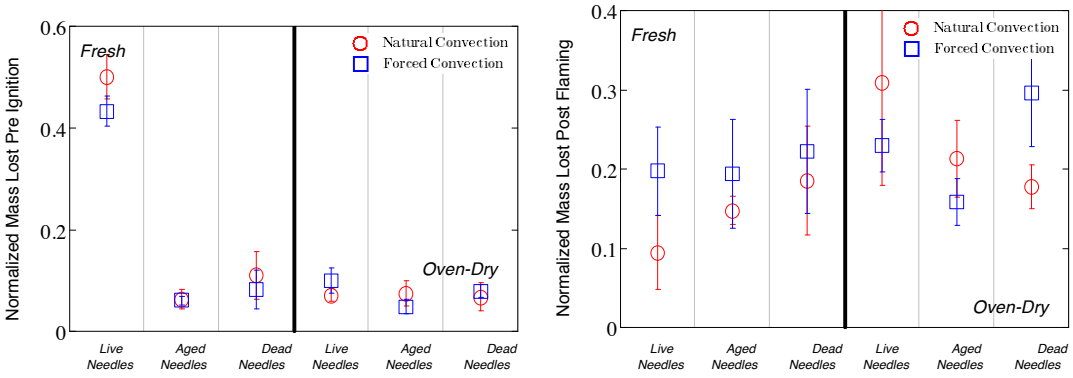

Figure 2.10 Normalized mass lost during *a) Pre Ignition b) Post Flaming regime*

Normalized mass lost during post flaming stage (e.g. during smouldering combustion) is displayed in Figure 2.10 b). A larger percentage of the mass is burnt during forced convection for fresh needles but the opposite seems to be the case in the oven dry state with the exception of oven-dry dead needles. Some differences between the needle groups are visible under natural convection. Live needles have the lowest amount of mass consumed during this stage follow by aged and then dead for fresh sample; however, the opposite happens in the oven-dry state.

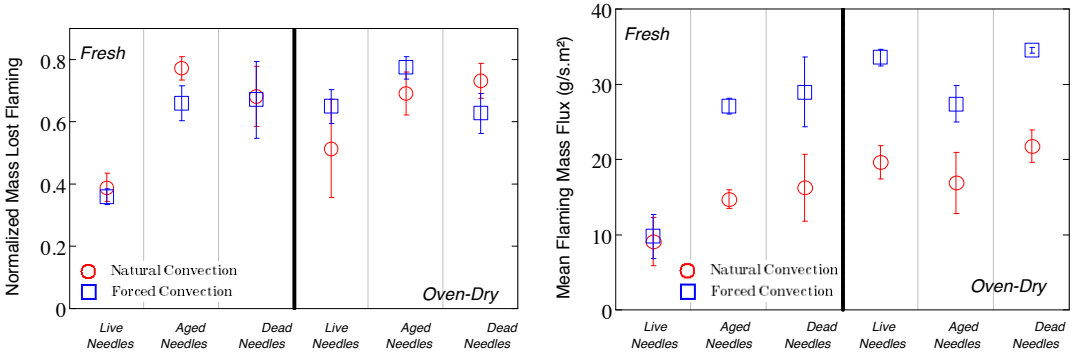

Figure 2.11 *a) Normalized mass lost b) Mean Mass Flux* during flaming

Figure 2.11 shows mass lost and mass flux during the flaming stage. With the exception of live needles, similar amounts of fuel are consumed during the flaming regime. The

effect of flow is more visible with mass flux values. The higher availability of oxygen allows for more mass to be consumed at one point in time with forced convection. This is reflected with flaming times, as we saw earlier, since the mass is consumed faster we obtain shorter flaming times and higher mean values for mass flux. Oven-drying has a similar effect, higher mean mass flux values overall with about the same amount of material burned hence the shorter flaming times.

Mean CO-to-CO_2 ratio and the radiative fraction of HRR during flaming are displayed in Figure 2.12. Aged needles display the highest CO-to-CO_2 ratios especially during natural convection. Flow effect suggests that during forced convection the fuel burns better due to the increased availability of oxygen. Radiative fraction can tell us about differences in combustion chemistry of the fuels during burning. Fresh needles show differences in radiative fraction under natural convection. The highest is for fresh live followed by aged and then dead needles. The effect of flow is negligible on radiative fraction except for fresh live needles where higher values are attained under natural convection. Oven-drying increases radiative fraction overall except for aged needles where it slightly decreases.

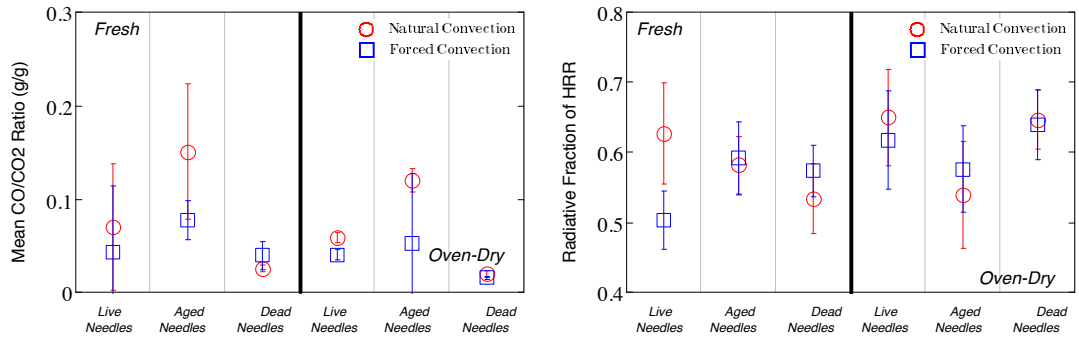

Figure 2.12 ***a) Mean CO/CO2 ratio b) Radiative fracition of HRR*** **during flaming**

Lastly, Figure 2.13 and Figure 2.14 display some of the flammability parameters discussed earlier that were affected by moisture content (the most) graphed in order to

visually observe their effect on the overall combustion process. As stated earlier, most of the water evaporates during the pre-ignition stage. This is the reason behind the increase in time to ignition and mass lost during pre-ignition. Energy is being used to evaporate the water before ignition. The increased water content is also part of the reason behind for changes in heat of combustion and peak HRR. Less flammable fuel is available with increased water content and more energy is required to evaporate the water overall.

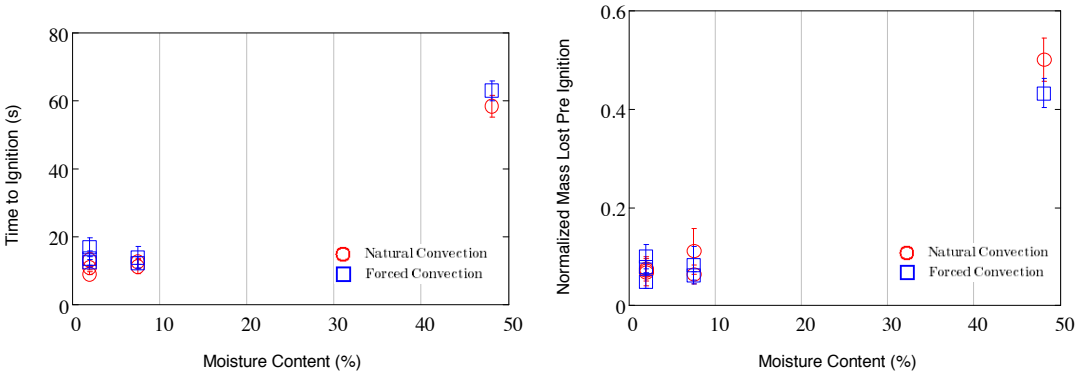

Figure 2.13 Flammability Parameters graphed according to Moisture Content in wet base

a) Time to Ignition b) Normalized Mass lost pre-ignition

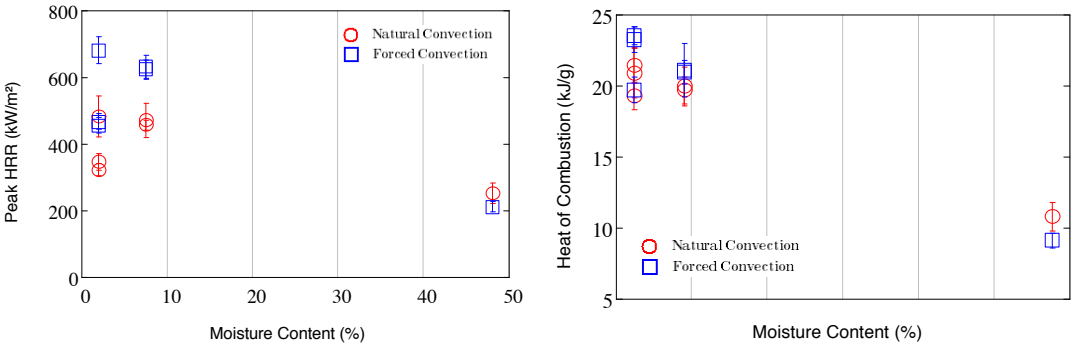

Figure 2.14 Flammability Parameters graphed according to Moisture Content in wet base

a) Peak Heat Release Rate b) Effective heat of combustion

Discussion

Above all, the results show how important moisture content is in the burning dynamics of pine needles. Most notable are the effects seen in ignition times, peak HRR and heat of combustion. Ignition times overall are about six times greater for live needles in comparison to the rest, peak HRR values two to three times smaller and heat of combustion is about half of the value of the rest. Water content of the needles is lost during the pre-ignition stage; this is reflected in the mass lost and the increased ignition times.

Flow inside the fuel bed has different effects on the burning behaviour of each sample. In relation to the three combustion regimes, two dominant effects are observed. During the pre-ignition stage, forced convection hinders ignition slightly as the interaction between flow and the needle bed blow the flammable volatiles away faster than during natural convection. The effect does not seem to be dominant most likely due to the strong heat flux applied to the sample here (50 kW/m^2) but increased ignition times for all samples show this pattern especially for the oven-dry state. During flaming combustion, needles burn for shorter times and more intensely under forced flow compared to natural flow conditions. Mean flaming mass flux and flaming times show this clearly. This is due to the increased availability of oxygen during forced convection allowing for a more intense and complete combustion of the fuel. Between different fuels, fresh live samples are the least affected by imposed flow and oven-dry samples are the most affected. The different effect of flow on each of the samples highlights the important role that transport phenomena play in porous forest fuel, more on this can be seen in chapter 3 of this thesis.

In terms of the different needle groups, the most flammable fuels are fresh dead and fresh aged needles, followed by oven-dry aged, oven dry dead and oven-dry live. The

least flammable fuel is fresh live needles. Although most of the differences observed can be accounted for in terms of the MC, some test series showed fuel internal structure matters as well. For dead needles, oven-dry samples had lower HRR compared to freshly collected ones; whereas, the time to ignition and the mass loss data was almost identical. Oven-dry live samples presented the effects that were expected in comparison to fresh live ones but the peak HRR, as in the oven-dry dead needles was not as high as expected. This suggests that the burning behaviour was affected by the drying process in the oven. The aged needles were set at first as a control means but on the other hand it also gave us another way to look at moisture content effect without the need to expose the needles to higher temperatures. Aged needles closely resembled the behaviour of fresh dead needles with a couple of differences like slightly higher CO/CO2 ratios; however, the biggest difference came when we observed that in the oven-dry state it was not affected like live and dead needles but the peak HRR actually slightly increased.

Upon consideration, these differences could be attributed to chemical changes and loss of volatiles affecting the needles during the drying process. Pappa et al. [20] and Statheropoulous et al. [21] both present work on differential scanning calorimetry and thermobalance results on thermal decomposition of pinus halepensis needles. They both arrive to the same conclusion that for mass loss in the range of 50 – 150 ºC, specifically a peak endotherm at 88 ºC, might be attributed to "desorption of high volatility compounds, moisture and/or softerning, melting of some of the waxy constituents of the pine-needles." [21] The needles for these studies are dried dead needles at 40ºC for 24 hours for Pappa et al [20] and dried needles of both live and dead at 35ºC for 24 hours for Statherpoulous et al [21], needles were dired at 60°C in this study. In the latter, he mentions minor changes between the green needles but does not go into this in detail. The reason believed in this study for the reduction in peak HRR are the evaporation of these high volatility constituents occurring with the live and dead samples. For the aged samples, it might mean water is allowed to evaporate naturally and the constituents bond better because of this. More investigation on thermal degradation of the needles in a similar procedure would be needed to tell for certain for the reason of these differences.

Several studies have highlighted the importance moisture content as noted before. Weise et al [9], presents calorimetry work with the cone on varied ornamental vegetation. Similar effects are seen, like the linear relationship between ignition times and moisture content and increases in peak HRR with oven-dry sample. His study highlights the importance of seasonal difference can have on moisture content. These types of calorimetry experiments help highlight and quantify differences in combustion dynamics with these kinds of duels. This study is the first to quantify differences of moisture content in pine needles but also, more importantly, highlights a big problem on the assumption that oven-drying vegetation samples will only affect the water content in these fuels. Aged samples presented an improvement as water loss happens at lower temperatures; composition seems less likely to be affected. Important differences can sometimes be missed with oven dry samples and the composition of the sample can change with live and dead fuels but it is something that has to be looked at more carefully if we want to be able to explain their burning behaviour.

Conclusions

The burning behavior of live and dead needle samples are studied here for the first time. The fire calorimetry results show good repeatability and demonstrated that the difference in burning dynamics of live and dead pine needles are significant and can be quantified and understood. Dead needles are more flammable. They ignite six times faster, burn faster with two to three times higher intensity than live needles. Moisture content was not as important for dead needles but very important for live needles. Once live needles were oven-dried, its fire behavior resembled more that of dead needles rather than fresh live ones. It is shown that increased airflow inside the needle bed hinders ignition a little but enhances combustion during flaming. Behavior of fresh live needles was not significantly affected by bed flow conditions.

Many of the observations could be explained in terms of moisture content. However, the loss of volatiles and other physicochemical changes to the needles produced during the oven drying process lead to significant differences in the burning behavior. Aged samples presented an improvement as water loss happens at lower temperatures; composition seems less likely to be affected. Overall, the results show that fire physics and chemistry vary for each of the samples, justifying the need for more fundamental understanding of the burning of forest fuels in order to better tackle wildfires.

Acknowledgements

The needle samples were provided by Jean-Luc Dupuy and his team at INRA (Avignon, France). The BRE Trust, UK and EU-FP6 Fire Paradox Project provided financial support for this work. Thanks also to FM Global for the donation of the Fire Propagation Apparatus where these tests were carried out.

References

[1] R.C. Rothermel, 1972: A mathematical model for predicting fire spread in wildland fuels. USDA Forest Service Res. Paper INT-115, Ogden, UT.

[2] W.R. Catchpole, E.A. Catchpole, R.C. Rothermel, G.A. Morris, B.W. Butler, D.J. Latham. Rate of spread of free-burning fires in woody fuels in a wind tunnel. Combustion Science and technology, 1998, 131: 1-37.

[3] Charles W. McHugh, Thomas E. Kolb, and Jill L. Wilson, 2003, Bark Beetle Attacks on Ponderosa Pine Following Fire in Northern Arizona, Environmental Entomology 32 (3), pg 510-522 doi: 10.1603/0046-225X-32.3.510

[4] G Xanthopoulos, C Calfapietra and P Fernandes, Fire Hazard and Flammability of European Forest Types, Chapter 4 in: Post-Fire Management and Restoration

of Southern European Forests, Managing Forest Ecosystems, Volume 24, 2012, doi:10.1007/978-94-007-2208-8_4.

[5] Van Wagner, C. E. Flammability of Christmas Trees, Ministry of Forestry, Ottawa (1963).

[6] Weise DR, Zhou X, Sun L, Mahalingam S. Fire spread in chaparral – 'go or no go?'. International Journal of Wildland Fire, 2005, 14: 99-106.

[7] Finney, M. A., Cohen, J. D., McAllister, S. S. On the need for a theory of fire spread, Internation Journal of Wildland Fire (submitted) (2012).

[8] D Drysdale, An Introduction to Fire Dynamics, 3rd Edition, John Wiley and Sons, Chichester, 2011.

[9] Weise, D. R., White, R. H., Beall, F. C., Etlinger, M., Use of the cone calorimeter to detect seasonal differences in selected combustion characteristics of ornamental vegetation, International Journal of Wildland Fire, 14, 321-338 (2005).

[10] DibbleA,C, Robert H. WhiteB and Patricia K. LebowB, Combustion characteristics of north-eastern USA vegetation tested in the cone calorimeter: invasive versus non-invasive plants, Alison C. International Journal of Wildland Fire, 2007, 16, 426–443

[11] Schemel, A. Simeoni, H. Biteau, J. Rivera, J.L. Torero, Experimental Thermal and Fluid Science, 2008, 32(7): 1381-1389.

[12] P. Bartoli, A. Simeoni, H. Biteau, J.L. Torero, P.A. Santoni, Determination of the main parameters influencing forest fuel combustion dynamics, Fire Safety Journal 46, 2011, pp 27-33, DOI: 10.1016/j.firesaf.2010.05.002.

[13] Tewarson, JS Newman, Scale effects on Fire Properties of Materials, Fire Safety Science 1, pp. 451-462, 1986. doi

[14] ASTM E 2058, Standard Methods of Test for Measurement of Synthetic Polymer Material Flammability Using a Fire Propagation Apparatus (FPA), American Society for Testing Materials, Philadelphia, 2003.

[15] A.P. Dimitrakopoulos. Mediterranean fuel models and potential fire behaviour in Greece. International Journal of Wildland Fire, 2002, 11 (2): 127-130.

[16] M.G. Cruz, M.E. Alexander, R.H. Wakimoto. Assessing canopy fuel stratum characteristics in crown fire prone fuel types of western North America. International Journal of Wildland Fire, 2003, 12(1): 39-50.

[17] T. Marcelli, P.A. Santoni, A. Simeoni, E. Leoni, B. Porterie, Fire spread across pine needle fuel beds: Characterisation of temperature and velocity distributions within the fire plume, International Journal of Wildland Fire, 2004, 13:37-48.

[18] Tewarson, A. Generation of Heat and Chemical Compounds in Fires, SFPE Handbook of Fire protection Engineering, The National Fire Protection Association Presss, 2002, pp. 3-82-3-161.

[19] Parametric Technology Corporation. (2007) Users's Guide Mathcad 14.0, from http://www.ptc.com/products/mathcad/

[20] Pappa, A. A., Tzamtzi, N. E., Statheropoulous, M. K., Parissakis, G. K., Thermal analysis of Pinus halepensis pine-needles and their main components in the presence of (NH4)2HPO4 and (NH4)2SO4, Thermochimica Acta, 1995, 261:165-173.

[21] Statheropoulous, M., Liodakis, S., Pappa, A., Kyriakou, A., Thermal degradation of Pinus halepensis pine-needles using various analystical methods, Journal of analytical and applied pyrolysis, 199, 43:115-123.

Chapter 3

Calorimetric study on the effect of fuel and flow conditions on burning dynamics of dead forest needles

Abstract

A variety of factors can influence flammability of wildland vegetation. In order to predict fire behaviour in forests, a better understanding of burning dynamics is needed. Wildland fire models rely on material flammability properties taken form experimentation. Therefore, if different ambient conditions can affect the flammability of wildland fuels, these properties must be made to reflect such reactions. A study is presented on flammability of wildland fuels in pine forest litter with three Mediterranean species: *Pinus halepensis*, *Pinus nigra* and *Pinus pinaster*. These fuels, chosen due to their importance in wildfire in southern Europe and northern Africa, are studied using FM Global's Fire Propagation Apparatus (FPA) under different moisture and flow conditions. The FPA allows for various measurements to be taken under a controlled environment. Several parameters of interest are extracted from heat release rate and mass loss rate curves that can be used for fire understanding and modelling. Species, flow, moisture, fuel load and imposed heat flux are quantified and shown to have a significant and varied effect on heat release rate, mass flux and time to ignition.

Introduction

Wildland fire research has become increasingly important in the last few decades. [1] With the growth of urban and wildland interface, the dangers these fires can cause

has become evident; including loss of life, property and heavy financial cost in order to suppress these. Consequently, understanding of fire dynamics has become an essential tool in order to tackle these fires. However, fire behaviour depends on various conditions and interrelated physical and chemical mechanisms. As these are all not completely understood yet, experimental data is needed to further our understanding of this complex phenomenon.

Laboratory small scale experiments provide scientists with necessary data for learning and quantifying the importance of different parameters involved in a fire. Fuel species, moisture content, fuel load, and flow velocities are just a few of the parameters involved in affecting the ignition, propagation and intensity of these fires. As previous studies have shown [1][2][3], calorimetric experiments can be used to gain better insight into the burning of wildland fuels. Schemel's study provided the shows the applicability and importance of having sound calorimetric data of wildland fuels. Many of the problems with wildland fuels arise from lack of repeatable data. This becomes inherent, due to the many parameters involved in the combustion process.

The fuels used in this study are pine needles from the Mediterranean region. As fires in this area have become an increasing concern, pine needles present a clear fire hazard. Calorimetric data is collected in this paper with varying species, flow, moisture content, fuel load and imposed heat flux in order to observe the effect and interrelation with each other.

Experimental Device and Protocol

The experiments presented in this paper were conducted using the FM-Global Fire Propagation Apparatus (FPA) following ASTM E 2058 combustion test [4]. Like the cone calorimeter, from which it has kept its operating principle, the FPA allows, among others things, to measure the energy released by the combustion of a material. [5]

The fuel sample is submitted to a radiative heat flux, and a pilot ignition source is provided. For this study, three radiative heat insults have been imposed to the sample: 25, 35 and 50 $kW.m^{-2}$. The infrared heaters were not shut down after ignition but remained on during the whole test. The mass loss rate was measured and the exhaust gases were analysed for composition, temperature, optical obscuration and flow speed with a Pitot tube. The FPA allows natural convection or forced gas flow rate through the fuel bed. FPA basic layout is presented in Figure 3.1 a).

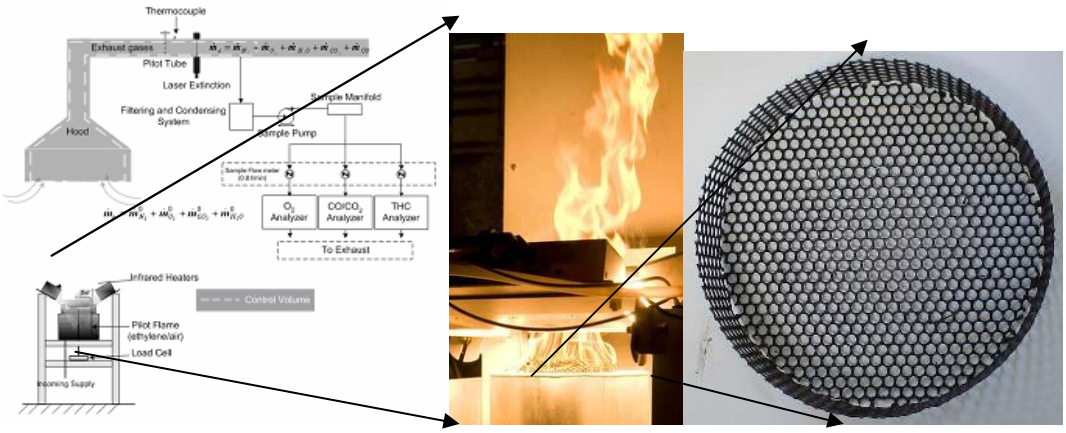

Figure 3.1 a) Schematic of the Fire Propagation Apparatus (FPA)
b) Burning pine needles c) Porous sample holder

Figure 3.1 c) shows the specific porous sample holder used for the experiments noted in [1]. The sample holder is a circular basket, made of stainless steel, with holes on all the surfaces (sides and bottom), to allow flow to pass through the bed of pine needles measuring 13 ± 0.01cm in diameter and 30 ± 0.5mm in depth. The percentage opening of the basket is 63% and its measurements are thirteen centimetres in diameter and thirty millimetres in height. It fits inside the combustion chamber, which is cylindrical, and lies on a load cell.

The species used in this study are dead *Pinus halepensis*, *Pinus nigra* and *Pinus pinaster* seen in Figure 3.2. Random samples of needles were measured to obtain the dimension measurements presented in Table 3.1. These fuels were chosen because they are representative of the Mediterranean ecosystem. The needles can be found in

pine forests litter. Dimension measurements for these are presented in Table 3.1. Different densities are studied ranging from 8 to 52 kg/m^3. Two flow conditions (natural convection, and forced flow) and two moisture conditions have been tested. The forced inflow at the bottom of the combustion chamber was 200 $l.min^{-1}$. Using a hot wire anemometer, the free stream gas velocity was measured to be 0.4 $m.s^{-1}$. The gas velocity through the holder, with and without the needles, was also measured to be 0.1 and 0.2 $m.s^{-1}$ correspondingly with a variability of 0.1 $m.s^{-1}$ on all measurements. Moisture conditions include needles maintained at standard condition of 25 C and 50 % air humidity before testing, after drying these were observed to contain between 7 to 8 % water content; and oven dried needles (assumed zero water content inside oven and between 1 to 3 % once removed as they reach an equilibrium very quickly under atmospheric conditions). [9] Each test conditions were repeated between three and six times.

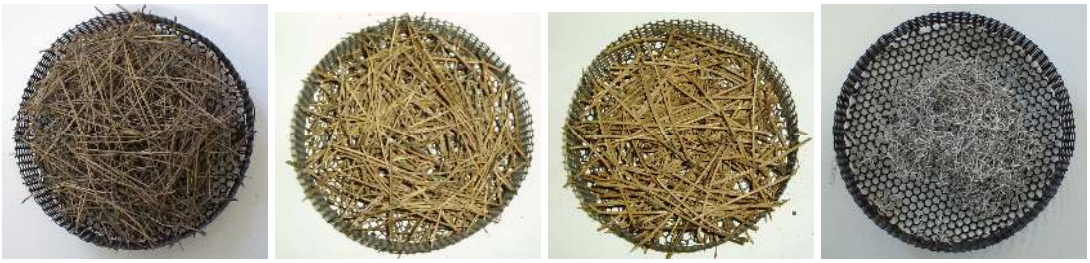

Figure 3.2 a) *Pinus halepensis* b) *Pinus nigra* c) *Pinus pinaster* d) Residue left after burn

Table 3.1 Pine needle dimensions

Species	Average Length (cm)	Average Diameter (mm)
Pinus halepensis	5.7 ± 1.8	0.7 ± 0.1
Pinus nigra	7.6 ± 1.3	0.8 ± 0.1
Pinus pinaster	16.3 ± 5.7	1.2 ± 0.5

Experimental calculations and parameter estimation

Measurements are obtained following ASTM E 2058, standard practice for using the FPA, combustion test. All other calculations outside this scope are described here. In order to describe these in detail, different terminology is used to indicate the set of

measurements and calculations that were used. The main sets of data obtained from the FPA are Heat Release Rate (HRR) and Mass Flux. Mass loss is obtained by deriving mass over time. Due to variability in the load cell, a smoothing algorithm called the supsmooth algorithm is used. [10] Values for energetic constants are obtained from average values described by Tewarson in [5]. From these, parameters are obtained and are explained in the figures and equations below:

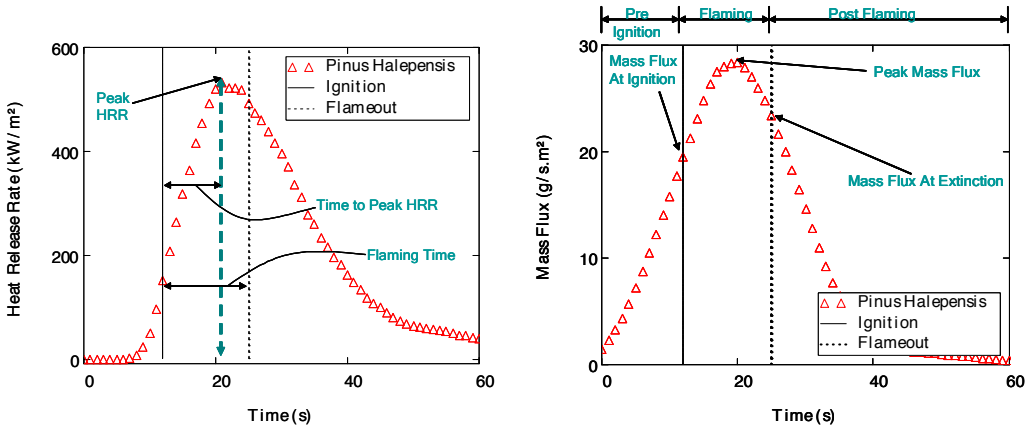

Figure 3.3 ***a) Heat Release Rate b) Mass loss*** **for dead** ***Pinus halepensis*** **needles**

Heat release rate (HRR) is determined using carbon dioxide and carbon monoxide generation (CDG) to obtain total energy released from the combustion process calculated here as, [5]

$$\dot{Q} = \Delta H_{CO_2}\left(\dot{G}_{CO_2} - \dot{G}^0_{CO_2}\right) + \Delta H_{CO}\left(\dot{G}_{CO} - \dot{G}^0_{CO}\right) \qquad \textbf{Equation 3.1}$$

where $\dot{Q}$ is HRR, ΔH is the net heat of complete combustion per mass generated, $\dot{G}$ is the generation rate, $\dot{G}^0$ is the generation rate at time zero, and CO and CO_2 are carbon monoxide and carbon dioxide respectively. Effective heat of Combustion (ΔH_c) for these experiments is obtained by integrating the HRR and then dividing by the initial mass, as

$$\Delta H_c = \frac{\int \dot{Q}\, dt}{m_o} \qquad \textbf{Equation 3.2}$$

where m_o is the initial mass of the sample.

Figure 3.3 a and b are representative of the combustion dynamics for these kinds of experiments. The process can be divided into three main stages: pre ignition, flaming and post flaming stage as can be seen in the mass loss curve. Start time at zero seconds is the time at which the heat flux is imposed on the material. As can be seen from the mass loss curve, at this time the material starts to degrade and lose mass therein producing pyrolysis gases. Once the concentration of these gases around the pilot flame directly above the sample is sufficient the material ignites identified by the solid vertical line. The sample will then start to rapidly release heat from the flames until it reaches its value as marked on Figure 3.3a. Less mass will be available for consumption so the heat release rate starts to decrease after its peak and flameout will occur shortly after. Important parameters are highlighted in the figures that are analyzed in the results section that are important to the combustion dynamics of these fires. A description of parameters of interest to this study is presented in Table 3.2.

Table 3.2 Description of flammability parameters

HRR (kW/m^2)	Heat release rate (HRR) per unit area of sample free surface
Effective Heat of Combustion (kJ/g)	Calculated as the integral of the HRR from ignition to flame out divided by the intial mass (time zero)
Time to Ignition (s)	Time for sample to ignite from when it is first subjected to the heat insult (time zero)
Flaming Time (s)	Duration for which a flame is sustained from ignition to flameout
Mass Flux at Ignition ($g/s.m^2$)	Mass loss rate per unit area of sample free surface at ignition
Mass Flux at Extinction ($g/s.m^2$)	Mass loss rate per unit area of sample free surface at extinction
Normalized Mass Lost Pre-Ignition (g/g)	Total mass lost during the pre-ignition phase divided by the initial mass

Flammability parameters of importance to wildland fires can be derived from these measurements, such as flame spread rate, depth of the flame front, fire intensity and total heat release. For example, the flame spread rate in wild fires is inversely proportional to the time to ignition [11]; so the faster a fuel ignites the faster the flame spread rate. The depth of the fire front is proportional to the peak mass flux, flaming time and fuel load; and the fire intensity per unit length of fire front is proportional to the peak HRR and the depth of the front. Note that we report the effective heat of combustion measured in a fire calorimeter. This is the energy per unit fuel mass that is effectively released in fire conditions. Compared this to the value most reported in the literature, the maximum heat of combustion, which is typically measured in bomb calorimeters and that is only released in ideal combustion conditions (resembling those inside combustion engines) and far from those encountered in real fires.

Results and Discussion

Transient results

Statistical analysis of the tests was done using the direct and calculated values of various parameters. Five different conditions were looked at in this study: natural convection vs forced convection, species, moisture (dead needles and oven dry dead needles), fuel mass load and imposed heat flux effect. Representative Heat Release Rate and Mass Flux curves for a given experiment for all these conditions can be seen in the figures below. Statistical analysis is given under the parameter discussion for each case:

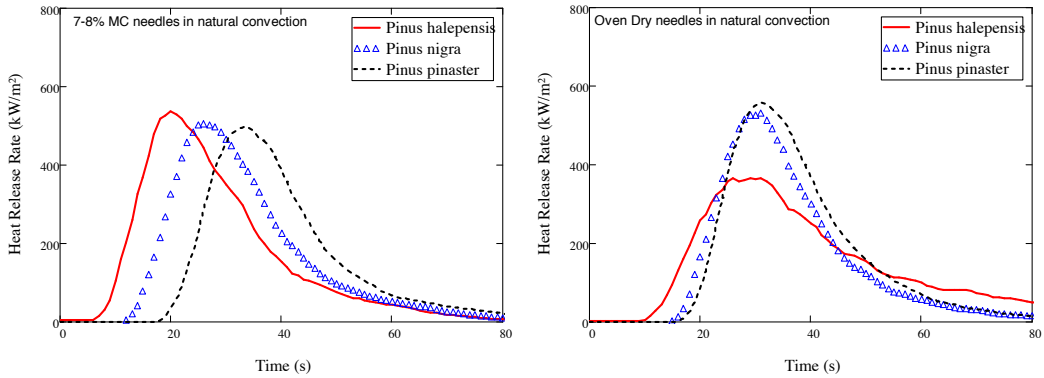

Figure 3.4 HRR for needles in natural convection at a) 7-8% MC b) Oven Dry condition

Figure 3.1 shows HRR for needles under natural convection at different moistures. *Pinus halepensis* needles had the highest peak HRR followed by *Pinus nigra* and then *Pinus pinaster* but the opposite happens during the oven-dry case.

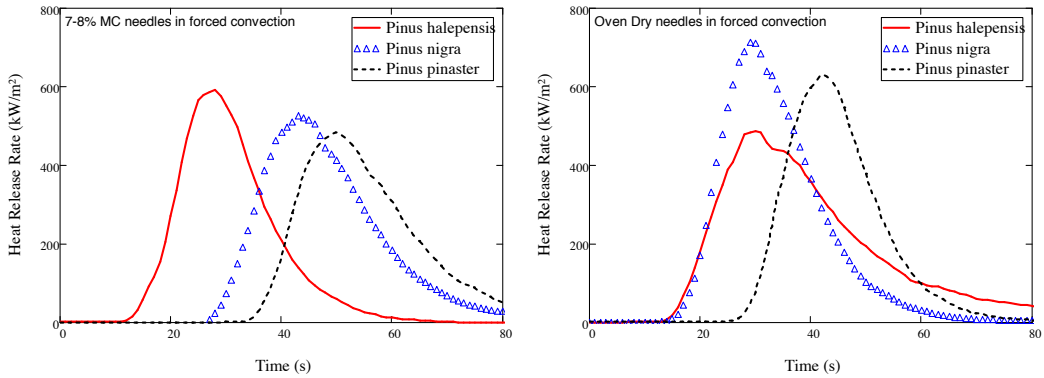

Figure 3.5 HRR for needles in forced convection at a) 7-8% MC b) Oven Dry condition

Figure 3.5 shows HRR for needles under forced convection at different moistures. If we compare between the two MCs, an increase in peak HRR for *Pinus nigra* and *Pinus pinaster* can be observed, *Pinus halepensis* seems to have the opposite effect. If we compare the two flow conditions, overall we can observe an increase in Peak HRR and an increase in time to ignition under forced flow. The effect of sample mass can be seen in the Figures below:

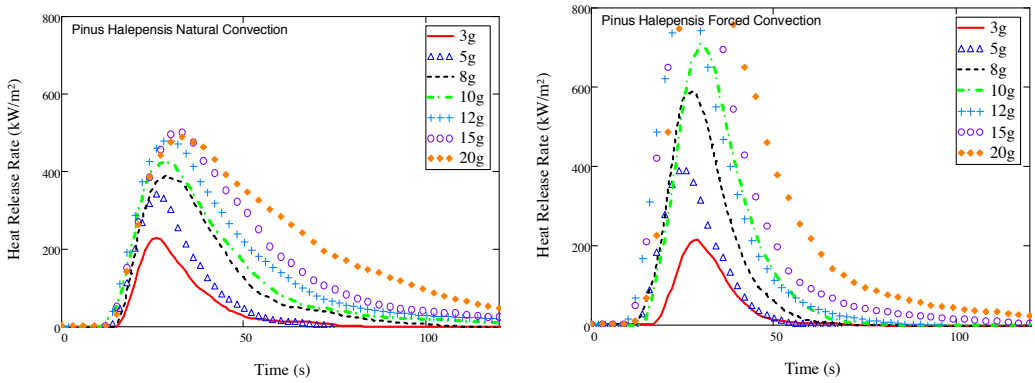

Figure 3.6 Effect of fuel load on HRR for *Pinus halepensis* under a) natural b) forced convection

Fuel load of natural fuels has an important effect as seen in Figure 3.6. The sample mass of 8g is the equivalent density of 20 kg.m^{-3} used for the previous experiments. Unless noted it should be assumed this is the density used. As one can see from the graph; however, this is midway between the highest and lowest of our measurements. Peak HRR can be greatly affected depending on how the fuel is laid out. Flow is also seen to have a greater impact with increasing fuel load. *Pinus nigra* and *Pinus pinaster* are shown to have similar effects as Halenpensis as can be seen in Figure 3.7. Higher peaks overall are seen for *Pinus pinaster* and *Pinus nigra*.

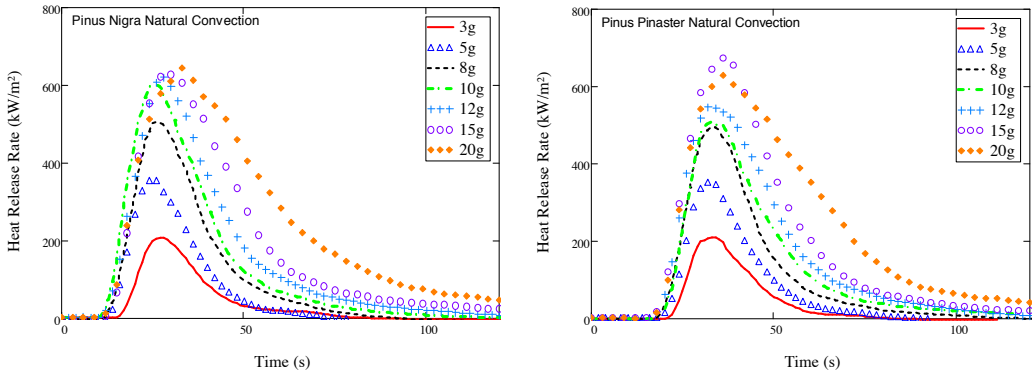

Figure 3.7 Effect of fuel load on HRR under natural convection for a) *Pinus nigra* b) *Pinus pinaster*

Figure 3.8 shows the effect of the applied heat insult on the sample. Time to ignition is seen to increase as the heat insult applied on the sample decreases. This is to be expected as the material degrades faster and releases volatiles faster with the increased heat allowing for ignition.[11] Difference in heat release rate here is most

apparent on *Pinus halepensis*. The sample burns with a higher intensity under forced convection for *Pinus halepensis*. For more information on the effect of heat flux levels refer to Appendix D.

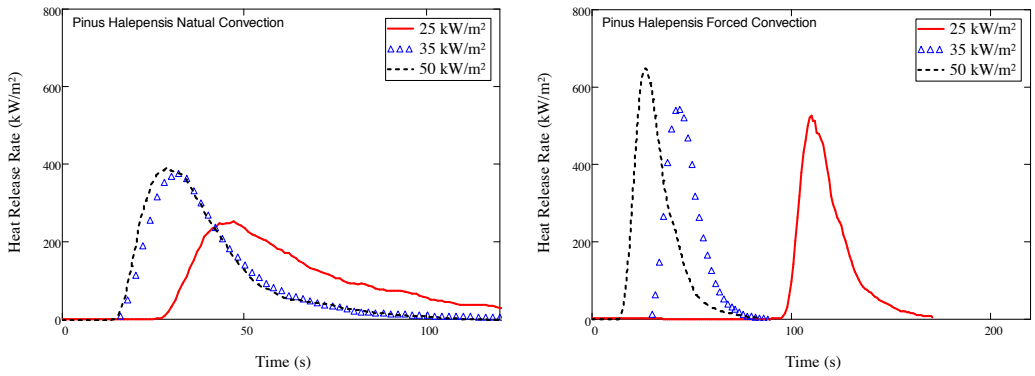

Figure 3.8 HRR for *Pinus halepensis* at various heat insults at a) natural b) forced convection

Similarly, the same analysis was done for mass flux. Due to the low mass in samples used, mass flux measurements are more uncertain; nonetheless, they do give a good representation of the fuel burning dynamics. Figure 3.9 and Figure 3.10 show mass flux curves under varying species, air flow and moisture content. Overall we do see faster ignition according to species size from smallest to largest and dryer pine needles also seem to ignite faster. Increase in air flow seems to accentuate these changes but it is still not clear what exactly is happening solely judging on these curves.

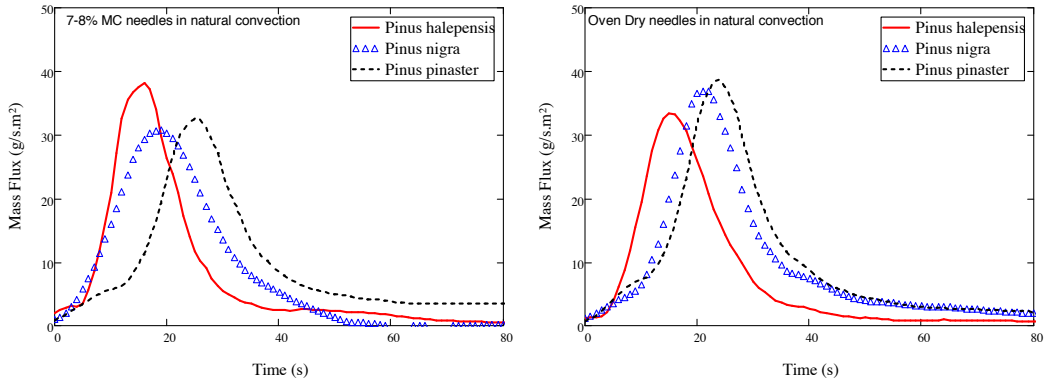

Figure 3.9 Mass flux for needles in natural convection at a) 7-8% MC b) Oven Dry condition

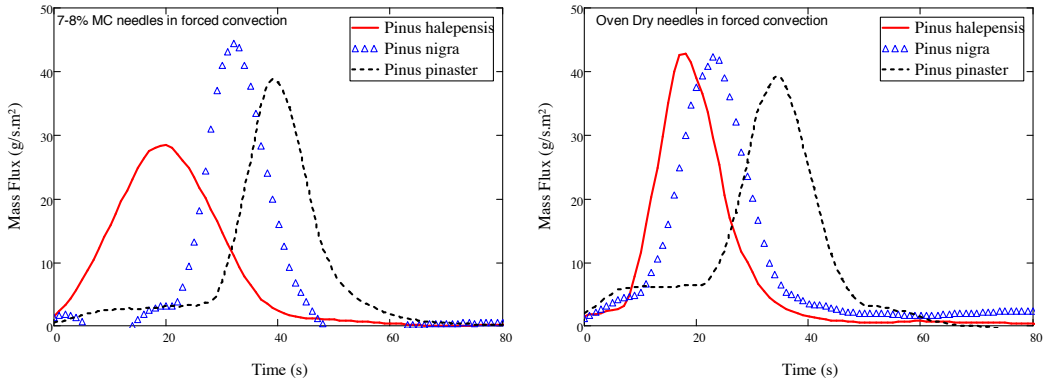

Figure 3.10 Mass flux for needles in forced convection at a) 7-8% MC b) Oven Dry condition

Figure 3.11 and Figure 3.12 show mass flux curves under varying fuel load, species and flow conditions. Most significantly, mass flux is seen to increase with increasing fuel load and forced flow. Some differences are observed between species but not as significant as the fuel load and flow. Ignition times are unaffected in this regard.

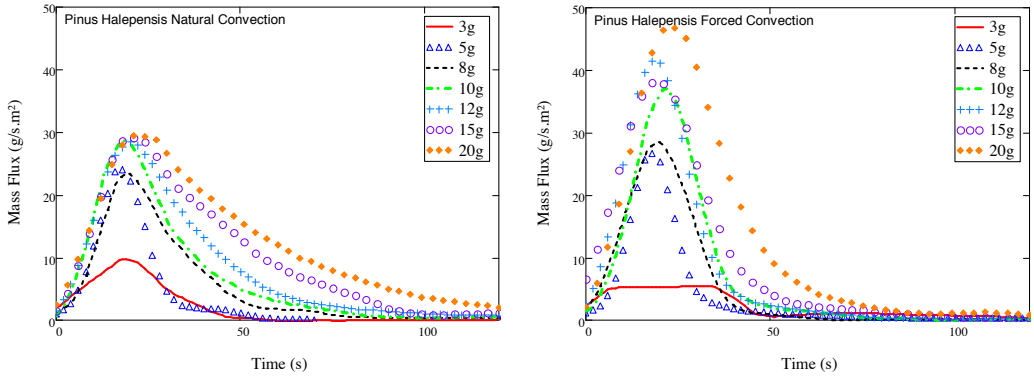

Figure 3.11 Effect of fuel load on mass flux for *Pinus halepensis* under a) natural b) forced convection

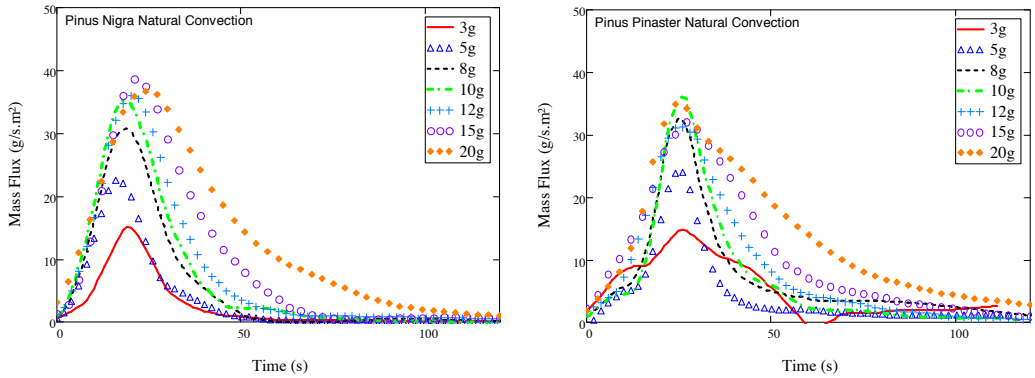

Figure 3.12 Effect of fuel load on mass flux under natural convection for a) *Pinus nigra* b) *Pinus pinaster*

Figure 3.13 shows mass flux curves under varying imposed heat flux for *Pinus halepensis*. Overall, the effect of the imposed heat insult is as expected, lower times to ignition and mostly higher peak mass flux values. Flow for the most part, accentuate this most notably on *Pinus halepensis*. Differences between species are not observed in this regard.

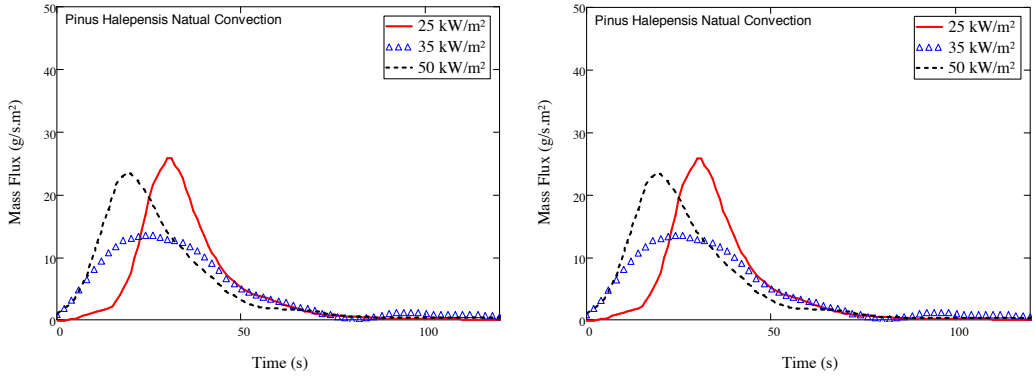

Figure 3.13 Mass flux for *Pinus halepensis* at various heat insults at a) natural b) forced convection

Parameter analysis

Individual parameters were extracted from data to analyze the burning behaviour. Values from repeated experiments are considered to assess repeatability in the

measurements taken from heat release rate and mass flux curve of the above mentioned conditions.

Time to Ignition

Figure 3.14 shows time to ignition for pine needles varying fuel load. Given these conditions, as can be seen in Figure 3.8 a) and b), time to ignition decreases slightly for smaller loads but is stable from 8g (20 kg.m^{-3}) on for all the species. Slight differences can be seen between species mainly *Pinus pinaster* having higher times to ignition than the other two, most likely due to physical size differences. Flow is seen to have little effect at this stage.

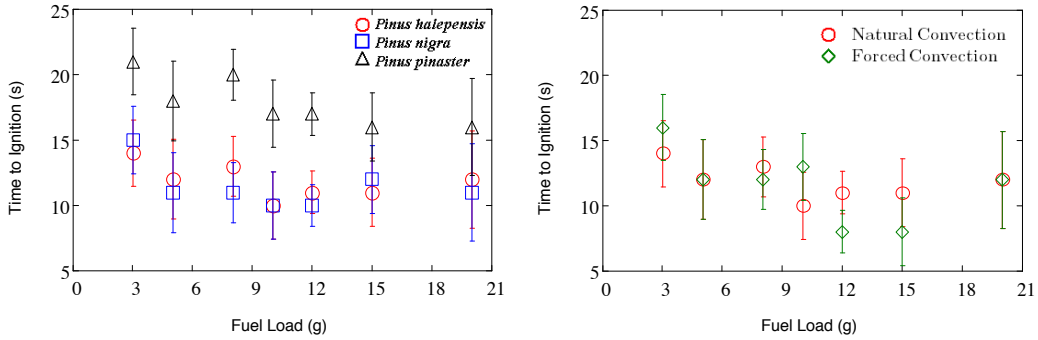

Figure 3.14 Time to ignition varying fuel load and a) species b) flow condition (*Pinus halepensis*)

Figure 3.15 shows time to ignition varying species, air flow and moisture content. Overall, species differences seem to indicate that with a larger physical size of pine needles there is an increase in time to ignition. Also, increased air flow slightly increases time to ignition on all species and MC conditions. Little difference is observed from the two MC condtions.

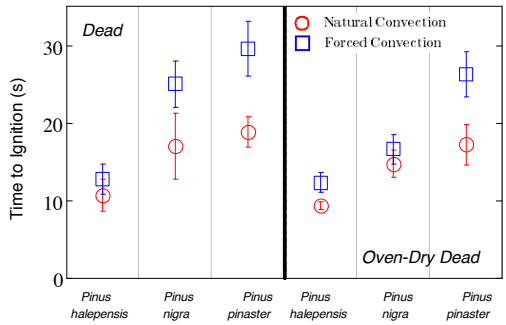

Figure 3.15 Time to ignition under varying species, air flow and moisture content

Flaming Time

Figure 3.16 a) and b) show flaming time for pine needles under varying fuel load. Overall, flaming time is seen to increase linearly under increasing fuel load. Species differences seem to indicate with a larger physical size of pine needles there is a decrease in flaming time; this becomes more apparent at the higher fuel loads. Also, increase in air flow shortens flaming time. This is expected as an increase in air flow allow for ready available oxygen for the burning of the fuel.

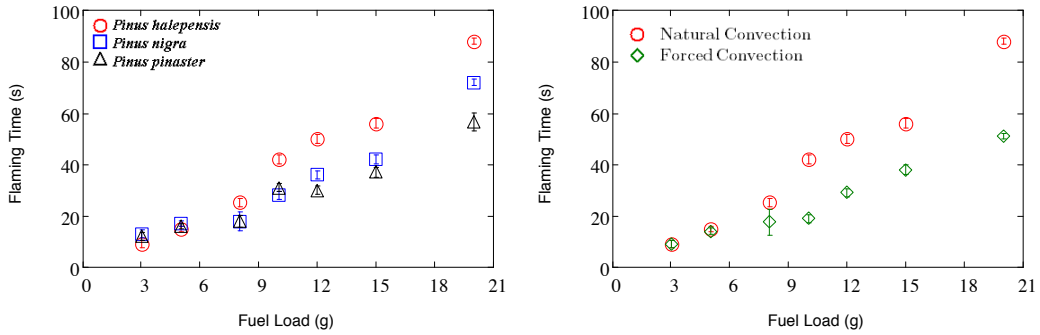

Figure 3.16 Flaming time varying fuel load for different a) species b) flow conditions (*Pinus halepensis*)

Figure 3.17 shows flaming time for pine needles under varying species, air flow and moisture content. Overall, a small decrease in flaming time is observed at oven dry conditions. *Pinus halepensis* needles are seen to have slightly higher flaming times at natural convection but all needles behave almost the same at forced convection.

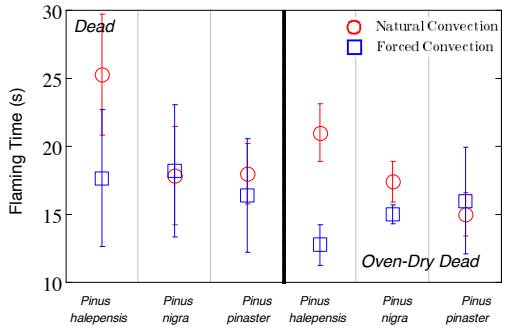

Figure 3.17 Flaming time under varying species, air flow and moisture content

Peak Heat Release Rate

Figure 3.18 a) and b) show peak heat release rate for needles under varying fuel load. Peak HRR increases as fuel load increases. Peak HRR seems to level out for all needles somewhere close to 15g (39 kg.m^{-3}). Some differences in species can be observed mainly *Pinus halepensis* having the lowest peak HRR of all three. The greatest difference for peak HRR becomes apparent with the change in flow at high fuel load. The higher the fuel load, the higher the difference in peak HRR levelling out once again somewhere close to 15g (39 kg.m^{-3}).

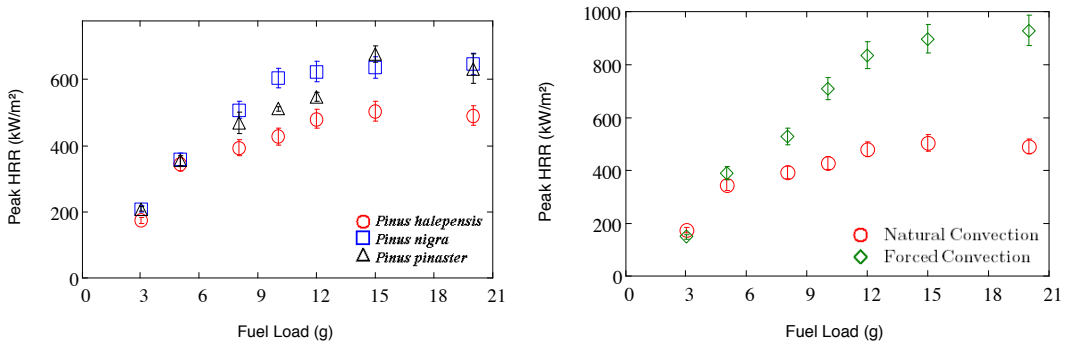

Figure 3.18 Peak HRR varying fuel load for different a) species b) flow conditions (*Pinus halepensis*)

Figure 3.19 shows peak HRR for pine needles under varying species, air flow and moisture content. With the exception of *Pinus halepensis* needles, peak HRR

increase for oven dry conditions. Due to differences in chemical and physical composition, *Pinus halepensis* needles seem to lose some volatiles during the drying process which could explains this behaviour. For the most part, forced convection increases except for one case: *Pinus nigra* at natural convection. Given there is a greater delay in ignition time with these needle and due to its composition, this could be due to more volatiles being lost at the early stages of combustion due to the increase air flow.

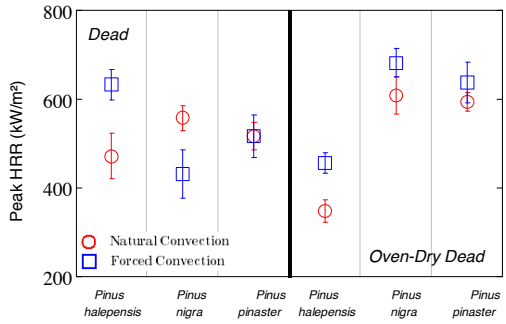

Figure 3.19 Peak HRR under varying species, air flow and moisture content

Mean flaming mass flux

Figure 3.20 a) and b) show mean flaming mass flux for needles under varying fuel load. From the results, mass flux stays constant at higher densities but starts dropping somewhere around 8g. *Pinus halepensis*, has the lowest mean flaming mass flux. Also forced convection increases mean flaming mass flux. This is to be expected as a readily available supply of air will increase the burning of the fuel. Earlier we also saw flaming times to be shorter under forced convection sinceas we see here the fuel is being consumed much faster.

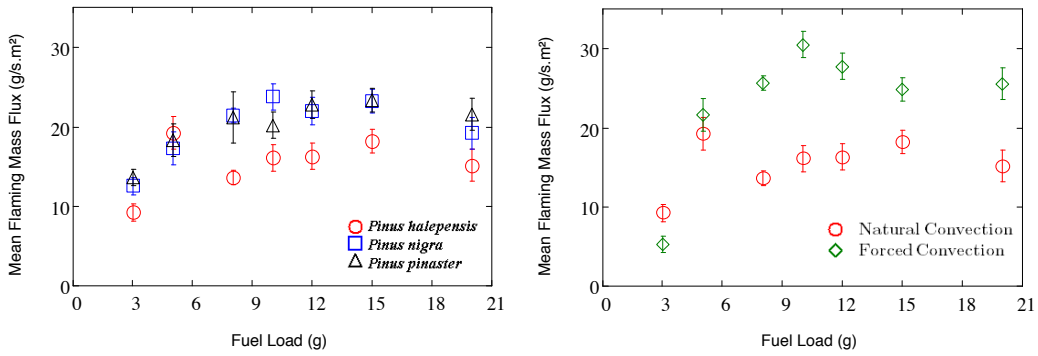

Figure 3.20 Mean flaming mass flux varying fuel load for different a) species b) flow conditions (*Pinus halepensis*)

Figure 3.21 shows mean flaming mass flux for pine needles under varying species, air flow and moisture content. If we look at the effect of increase flow on the combustion, for the most part we see a clear increase in mass flux. Once again, more air flow allows for oxygen to be more readily available for combustion, which increasing burning therefore increasing mass flux. Drying the samples also seems to increase mass flux. Physically, if there is less water to be evaporate before combustion, more fuel will readily burn, this is more a case of more fuel being available to burn because water is lost during pre ignition phase. If we look at species differences, mass flux is seen to increase with the larger physical size of the species during natural convection. During forced convection, we see it remains constant at 7-8% MC and a decreasing trend in oven dry condition. Physical interaction between the flow and the fuel could be the cause of this.

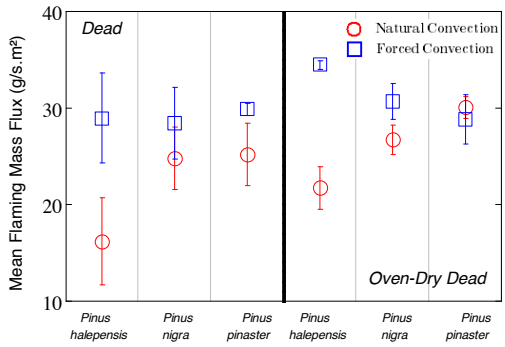

Figure 3.21 Mean flaming mass flux under varying species, air flow and moisture content

Mass lost during pre-ignition phase

Figure 3.22 a) and b) show mass lost during the pre-ignition phase normalized for the total mass for needles under varying fuel load. As we can see, with increasing fuel load there is an overall decrease in the mass lost at this stage. This levels out to a constant value at the higher ends of fuel load. Since is certain concentration of flammable gas is necessary for ignition, this is to be expected as when not enough is produced as is the case for the low fuel load, more material needs to degrade to allow for this concentration to be reached. Flow and species does not seem to affect mass lost during this stage.

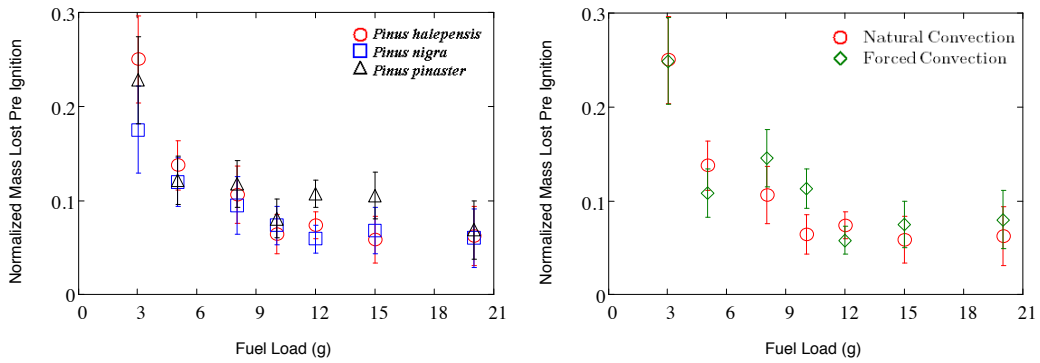

Figure 3.22 Mass lost pre-ignition varying fuel load for different a) species b) flow conditions (*Pinus halepensis*)

Figure 3.23 shows mass lost during pre-ignition for pine needles under varying species, air flow and moisture content. Overall, differences in species seem to indicate physical size increases the overall mass lost at this stage. This difference is accentuated with forced convection; furthermore, *Pinus pinaster* seems to lose more mass with this increased flow. No significant change is seen with varying moisture content.

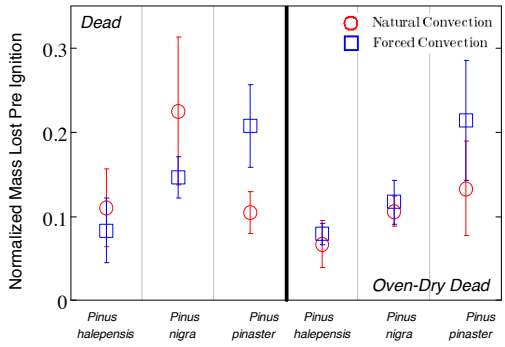

Figure 3.23 Mass lost pre-ignition under varying species, air flow and moisture content

Mass flux at ignition

Figure 3.24 a) and b) show mass flux at ignition for needles under varying fuel load. For all needles, mass flux seems to increase with increasing fuel load. The trend seems to level out towards a constant value towards the end. Not much difference is observed between the needles in this aspect. Imposed flow does increase mass flux at ignition due to more availability of air for when the fuel ignites.

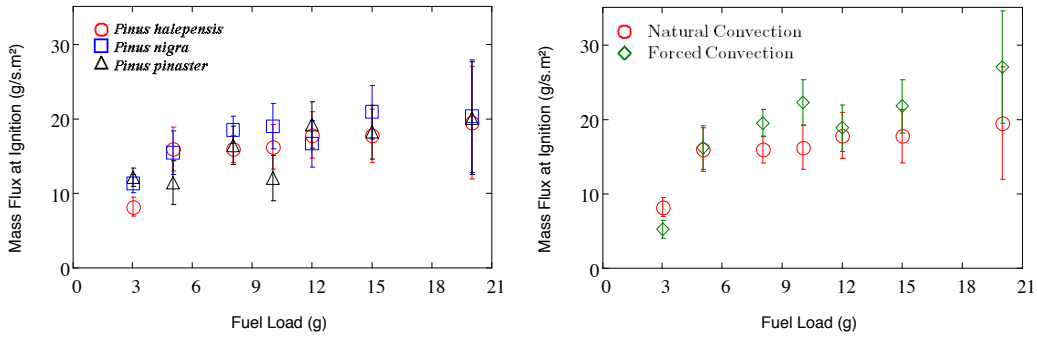

Figure 3.24 Mass flux at ignition varying fuel load for different a) species b) flow conditions (*Pinus halepensis*)

Figure 3.25 shows mass flux at ignition for pine needles under varying species, air flow and moisture content. Drying seems to increase mass flux at ignition. Due to the short times for ignition, since there is less water to evaporate, this could explain why more fuel is being consumed at this time. Flow and species do not show a clear

relation between each other so we can assume under these condition these differences are maybe just due to instability of mass measurements.

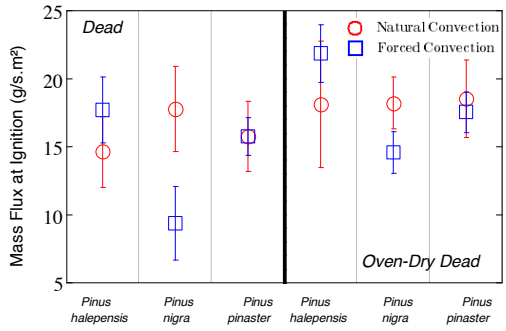

Figure 3.25 Mass flux at ignition under varying species, air flow and moisture content

Mass flux at extinction

Figure 3.26 a) and b) show mass flux at flameout for needles under varying fuel load. *Pinus pinaster* is shown to have a higher mass flux at this point. Other than that, no clear relation is shown for other variabilities.

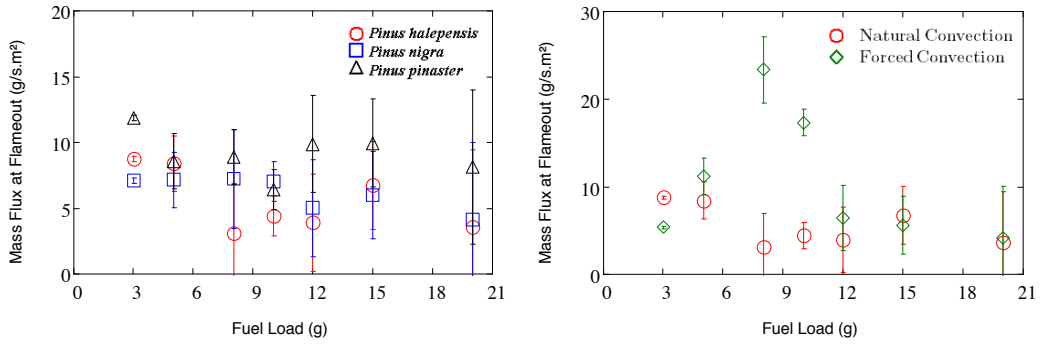

Figure 3.26 Mass flux at flameout varying fuel load for different a) species b) flow conditions (*Pinus halepensis*)

Figure 3.27 shows mass flux at extinction for pine needles under varying species, air flow and moisture content. Overall, imposed flow is seen to increase mass flux. Species differences also seem to indicate increasing physical size increases mass flux as well. There is a slight increase in mass flux with decrease in MC however the relation is not as clear.

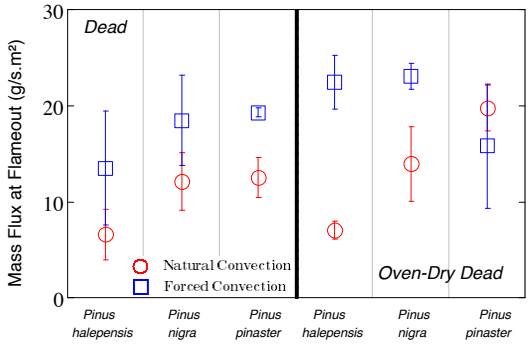

Figure 3.27 Mass flux at flameout under varying species, air flow and moisture content

Effective Heat of Combustion

Figure 3.28 a) and b) show effective heat of combustion for needles under varying fuel load. *Pinus halepensis* shows the lowest values overall; nonetheless, the needles have very similar energy content overall, and is not significantly affected by species or flow which makes sense since energy content of the needles shouldn't be affected by combustion conditions.

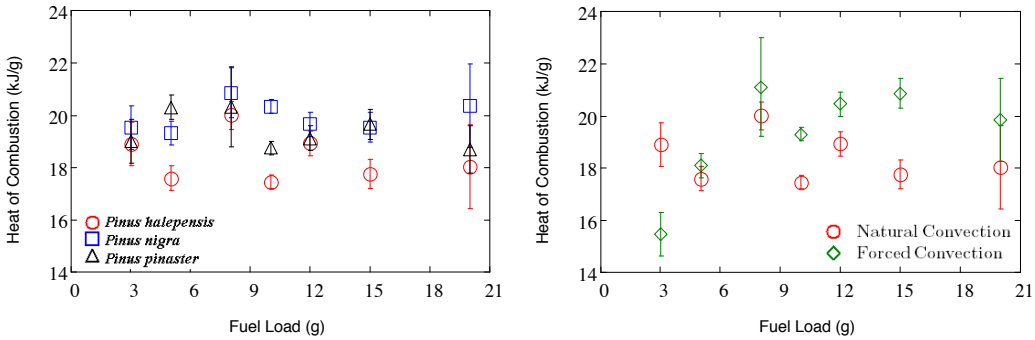

Figure 3.28 Effective Heat of combustion varying fuel load for different a) species b) flow conditions (*Pinus halepensis*)

Figure 3.29 show heat of combustion for pine needles under varying species, air flow and moisture content. Moisture content is seen to increase heat of combustion which makes sense since lower MC content would mean more fuel is available for burning.

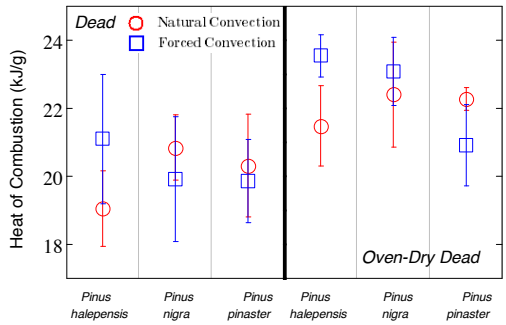

Figure 3.29 Effective Heat of combustion under varying species, air flow and moisture content

Summary

Various combustion parameters are reviewed in the results. Due to the large number of variables studied, a summary is presented on each fuel condition studied and some of the effects observed of interrelationships between these conditions.

Fuel Load

By varying the initial mass of the sample, we were able to observe the effects of fuel load on the combustion of different pine needles. Time to ignition, mean flaming mass flux, mass flux at ignition, mass flux at extinction, mass lost during pre ignition, and effective heat combustion were mostly unaffected by fuel load of 8g (~20kg/m^3) and above. Below this density, changes were seen due to the small amount of fuel available for combustion and the higher error attributed due to our measurement accuracy. Rise in flaming time with greater fuel load was attributed to the increased fuel content. Given more mass was available; more flammable gases were emitted and readily available to maintain flaming for a longer time. The greatest difference was seen in peak heat release rate. As the fuel load increased, the peak heat release rate rose. Peak HRR seem to reach a steady value around 15g (~40kg/m^3).

Flow

Flow of air is important because it can change the oxygen available for combustion and therefore change the combustion dynamics during burning. The effects observed were varied but what became predominant were the changes observed with the interrelationship between the other variables studied such as applied heat flux, fuel load and species. With respect to mass lost during pre-ignition, it was mostly unaffected; nonetheless, as stated previously on the imposed heat insult summary, a small change was seen between *Pinus pinaster* and *Pinus halepensis* between natural and forced convection, most likely due to a flow, heat and size interaction during combustion. Heat of combustion was also mostly unaffected except for slightly higher values for *Pinus halepensis* needles with forced convection. Mass flux at extinction, ignition and flaming had higher values overall with increased flow. This is tied to more oxygen being available during flaming combustion. Flaming time was seen to decrease with forced convection especially with increased fuel load. The faster combustion during flaming was the reason for this. The most important changes were observed with respect to peak HRR and time to ignition. Higher peak values for HRR were seen throughout with forced convection and this difference is seen to increase with increasing fuel load. Times to ignition were slower with forced convection; the difference becomes much more important with lower heat insults.

Moisture Content

Two low moisture contents (2 and 8% wet base) are studied here for three different pine needles; for an analysis on a wider range of moisture content of pine needles refer to chapter 2 of this thesis. Moisture can vary combustion dynamics because energy will need to be inputted in order to evaporate the water. The rise in heat of combustion at oven dry conditions shows this quite well. Since less water is present, there is more fuel in dry needles to burn. Mass flux values at ignition, extinction and during flaming slightly increase at the lower moisture content. Mass lost during pre ignition, times to ignition and flaming time is overall slightly lower. Peak HRR, with

the exception of *Pinus halepensis* needles, have a significant rise at oven dry conditions. All these effects relate, to less heat needed for water evaporation and more fuel content available for burning.

Species

Differences in species can affect combustion because of varying fuel content and or varying heat transfer due to size differences. This becomes apparent as differences are accentuated depending on the interrelationship with other variables. In regards to time to ignition, mass lost during pre-ignition and mass flux at extinction, higher values were seen in this order: *Pinus pinaster*, *Pinus nigra* and then *Pinus halepensis*. Overall, this becomes more important at lower heat fluxes. Flaming time had a varied effect. In natural convection, in order values highest to lowest were from *Pinus halepensis*, *Pinus nigra* and *Pinus pinaster* while the opposite occurred under forced convection. Peak HRR, flaming mass flux and heat of combustion had a similar behaviour. *Pinus pinaster* and *Pinus nigra* had higher values at natural convection, but the opposite was true under forced convection. This was accentuated at lower heat fluxes as well. Mass flux at ignition was mostly unaffected by species differences. During flaming, *Pinus halepensis* needles were the ones to benefit more from the increased air flow. *Pinus pinaster* and *Pinus nigra* were seen to combust better than *Pinus halepensis* during natural convection.

Imposed Heat Insult

The effects of varying heat insults tells us about changes in the combustion process that could happen due to changes in flame radiation or the initial heat applied before ignition. Flaming time, mass flux at extinction and effective heat of combustion were mostly unaffected by this. For peak HRR, only *Pinus halepensis* showed a direct relationship with applied heat flux. Mass flux at ignition showed a direct relationship with applied heat flux for all needles. At higher heat fluxes, the mass loss will be higher because of more flammable gases being produced with increased energy

input. With respect to mass lost during pre-ignition, *Pinus halepensis* needles have an inverse relationship with applied heat flux in natural convection and *Pinus pinaster* needles have an inverse relationship during forced condition. Changes here are attributed to flow and heat interaction with the different sized needles. Needles also show a direct relationship with respect to mean flaming mass flux and applied heat flux in forced convection but not in natural convection. This difference is attributed to more oxygen being available for combustion with forced convection but not present with natural convection. Lastly, applied heat flux had the greatest effect on time to ignition, as expected, since flammable gases are produced more rapidly with higher heat insults due to the increased energy input and therefore faster time to ignition are observed.

Discussion

The results have shown us how many different fuel conditions can have diverse effects on the combustion of pine needles. Fuel load, flow and moisture content are the conditions seen to affect peak HRR the most. Up until a fuel load of ~40kg/m^3, peak HRR is seen to vastly change from about 200 at ~8kg/m^3 to 600 kW/m^2 under natural convection and 900 kW/m^2 under forced convection at ~40kg/m^3. With the exception of *Pinus halepensis* needles, at ~20kg/m^3, moisture content is also seen to have a pronounced effect on peak HRR with values ranging from about 400 to 500 kW/m^2 for fresh needles and values ranging from 600 to 700 kW/m^2 for oven dry needles.

Time to ignition was greatly affected by imposed heat flux and flow conditions the most. Lower heat insults produced longer times to ignition, as we expected; furthermore, this effect was enhanced under forced convection. Flow of air through the bed before ignition was blowing away the pyrolysis gas too fast and therefore a delayed ignition was observed. Although moisture content is considered quite important during the pre-ignition stage because most of the water is evaporated before flaming, due to the high heat flux applied for most of this study (50kW/m^2)

and the low moisture contents studied (2 and 8% wet base), it did not play a significant role during the combustion of these needles.

In comparison of the different species, *Pinus halepensis* needles were seen as the most easily ignitable reflected in the lowest times to ignition followed by *Pinus nigra* and then *Pinus pinaster*. Under natural convection, *Pinus halepensis* needles produced the lowest peak HRR, however, under natural convection it produced the highest.

Similar results are presented by Schemel et al.[1], Simeoni et al. [12] and Bartoli et al. [2] Schemel et al. [1], the first to present repeatable calorimetry data for these kinds of fuels, describes more into detail on flow transport using different porosity of holders with *Pinus pinaster* and *Pinus halepensis* needles. The work is done at the higher densities (eg ~40kg/m^3) and at 25 kW/m^2 and dealing mostly with peak HRR and time to ignition. Bartoli et al. [2], goes into more detail by adding a mid flow condition and *Pinus nigra* data but still dealing at the same density and heat flux. Simeoni et al. [11], presents some more analysis by adding some new data on *Pinus halepensis* needles fuel load mean HRR with varying porosity. The study here complements these studies as it looks into moisture and also studies these variables at different density, heat fluxes and fuel loads with various other flammability parameters. As we have seen from the data, many of the fuel conditions effects can sometimes be enhanced by the interactions between each other and the study here compiles all of these to see the effect much more clearly.

An anomaly was presented when *Pinus halepensis* needles produced lower peak HRR results under oven dry conditions. Upon consideration, this behaviour was attributed to two possible reasons . Given the other two species did not show this behaviour, differences would have to be attributed either to chemical composition or physical size difference affecting the needles during the drying process. Pappa et al. [13] and Statheropoulous et al. [14] both present work on differential scanning calorimetry and thermobalance results on thermal decomposition of *Pinus halepensis* needles. They both arrive to the same conclusion that for mass loss in the range of 50

– 150 ºC, specifically a peak endotherm at 88 ºC, might be attributed to "desorption of high volatility compounds, moisture and/or softerning, melting of some of the waxy constituents of the pine-needles." [14] The two possible reasons believed in this study for the reduction in peak HRR are the evaporation of these high volatility constituents occur at higher temperatures for *Pinus nigra* and *Pinus pinaster* or is much more important with *Pinus halepensis* needles and/or the size difference actually allow for higher temperature to be reached by *Pinus halepensis* needles during the drying process. More investigation on thermal degradation of the needles in a similar procedure would be needed to be looked at to tell for certain if it is one or the other or both.

Acknowledgements

The needle samples were provided by Jean-Luc Dupuy and his team at INRA (Avignon, France). The BRE Trust, UK provided financial support for this work. Thanks also to Alberto Ponce for his help with experiments, Professor Jose Torero for access to the Fire Science Laboratory and FM Global for the donation of the Fire Propagation Apparatus where these tests were carried out.

Conclusions

Various environmental and physical conditions were studied to observe the effect on the burning dynamics of pine needles. It is important that we know what affects the combustion of natural fuels as they can be a key to understanding wild land fire behaviour. Interrelation between varying conditions sometimes also proves to be important during burning; most notably, the relation between fuel load and flow conditions. Fuel load, as shown is the results, is likely to be the most essential condition to know as it gives and a direct indication of the intensity of the fire followed by flow and moisture content. At higher fuel loads, flow conditions become much more important in regards to intensity of the fire. Given the relation between flow and density of the fuel; however, flow can either aid or determent ignition times

which most likely will mean the same relation will hold if we were to look at flame spread in this regard. Fuel condition interactions shown indicate it is very important to know what density, heat insult, moisture and flow conditions the burn is taking place as changing one of these can mean the effect of the other rendered unimportant or accentuated. With this taken into account, we still must be cautious of applying this knowledge to large scale fires as other large scale effects can also undermine or enhance these relations.

References

[1] C. Schemel, A. Simeoni, H. Biteau, J. Rivera, J.L. Torero, Experimental Thermal and Fluid Science, 2008, 32(7): 1381-1389.

[2] P. Bartoli, A. Simeoni, H. Biteau, J.L. Torero, P.A. Santoni, Fire Safety Journal, 2011, 46: 27-33.

[3] Weise, D. R., White, R. H., Beall, F. C., Etlinger, M., Use of the cone calorimeter to detect seasonal differences in selected combustion characteristics of ornamental vegetation, International Journal of Wildland Fire, 14, 321-338 (2005).

[4] ASTM E 2058, Standard Methods of Test for Measurement of Synthetic Polymer Material Flammability Using a Fire Propagation Apparatus (FPA), American Society for Testing Materials, Philadelphia, 2003.

[5] A. Tewarson, in: Generation of Heat and Chemical Compounds in Fires, SFPE Handbook of Fire protection Engineering, The National Fire Protection Association Presss, 2002, pp. 3-82-3-161.

[6] M. Hille, J. den Ouden. Fuel load, humus consumption and humus moisture dynamics in Central European Scots pine stands. International Journal of Wildland Fire, 2005, 14(2): 153-159.

[7] A.P. Dimitrakopoulos. Mediterranean fuel models and potential fire behaviour in Greece. International Journal of Wildland Fire, 2002, 11 (2): 127-130.

[8] M.G. Cruz, M.E. Alexander, R.H. Wakimoto. Assessing canopy fuel stratum characteristics in crown fire prone fuel types of western North America. International Journal of Wildland Fire, 2003, 12(1): 39-50.

[9] T. Marcelli, P.A. Santoni, A. Simeoni, E. Leoni, B. Porterie, Fire spread across pine needle fuel beds: Characterisation of temperature and velocity distributions within the fire plume, International Journal of Wildland Fire, 2004, 13:37-48.

[10] Parametric Technology Corporation. (2007) Users's Guide Mathcad 14.0, from http://www.ptc.com/products/mathcad/

[11] D Drysdale, An Introduction to Fire Dynamics, 3rd Edition, John Wiley and Sons, Chichester, 2011.

[12] Simeoni, A., Bartoli, P., Torero, J. L., Santoni, P., On the Role of Bluk Properties and Fuel Species on the Burning Dynamics of Pine Forest Litters. International Association of Fire Safety Science, 2011.

[13] Pappa, A. A., Tzamtzi, N. E., Statheropoulous, M. K., Parissakis, G. K., Thermal analysis of *Pinus halepensis* pine-needles and their main components in the presence of (NH4)2HPO4 and (NH4)2SO4, *Thermochimica Acta*, 1995, **261**:165-173.

[14] Statheropoulous, M., Liodakis, S., Pappa, A., Kyriakou, A., Thermal degradation of *Pinus halepensis* pine-needles using various analystical methods, *Journal of analytical and applied pyrolysis*, 199, **43**:115-123.

Chapter 4

Experimental Investigation of the relationship between leaf morphology and flammability using fire calorimetry

Abstract

Leaf morphology, typically divided into broad or narrow taxa has been suggested as a mayor flammability fuel property. The Triassic/Jurassic Boundary marked a time period of major environmental changes on Earth in which increased fire activity has been shown to been a major contributing factor. The changes were attributed to climate-driven shift from broad leaved taxa to a predominantly narrow leaved assemblage. In this study, we use state-of-the-art fire calorimetry on a wide range of leaf types representative from that time period to understand how leaf morphology affects flammability, time to ignition, etc. The results show that smaller leaf area and larger surface area to volume ratio show a strong correlation to an increase in flammability of these fuels for all variables measured. This is an extension to the previous paper by Belcher et al Nature Geoscience (2010).

Introduction

Many studies have shown fires to be a major influence to global ecosystem patterns and processes throughout time. [1][2] Throughout the years, variations in CO_2 and CO have been linked to biomass burning around the globe. [3] Fire activity has also been linked to changes in vegetation composition throughout time. [4] Given these indications, it is not surprising that researchers have tried to study the relationship between fire activity and global climate as a whole in the present and in the past.

The Triassic/Jurassic Boundary (TJB) marked a time period of major environmental changes. A rise from 600 to 2100-2400 ppmv in atmospheric carbon dioxide concentration suggesting an associated rise of 3 to 4 degrees Celsius of greenhouse warming gives us an idea of the changes in this time period. The boundary marked a major floral and faunal turnover linked to the increase in carbon dioxide levels. [5] Using paleontological reconstructions of the fossil flora from East Greenland and records of fossil charcoal preserved in rocks, a strong correlation was observed linking a marked increase in fire activity across the Triassic/Jurassic Boundary. These changes were attributed to climate-driven shift from broad leaved taxa to a predominantly narrow leaved assemblage. [1] This study shows how the fire calorimetry used in Belcher et al. [1] is used in detail to assess the leaf flammability between the leaf morphologies that were representative of this time period.

Morphology will delineate the structure and configuration of leaves. This configuration will affect how heat is transferred into the material and will therefore affect its burning behavior. As many studies have shown [6], thickness of materials plays a key role into solid burning. Thermally thick and thermally thin materials will behave very differently. Most plants will fall into the thermally thin category in which thickness will directly affect flammability. [6]

Calorimetric tools such as laboratory small scale experiments have provided scientists with necessary data for understanding fire combustion dynamics and the importance of different parameters involved in a fire. Fuel species, moisture content, fuel load, and flow velocities are just a few of the parameters involved in affecting the ignition, propagation and intensity of these fires. As previous studies have shown [7][8], calorimetric tools can be used to better understand the burning of wildland fuels. Schemel's study provided the basis to show the applicability and importance of having sound calorimetric data of wildland fuels. In this study we study the effect of leaf

morphology of specific leaves representative of the Triassic/Jurassic Boundary in order to assess how this will affect the combustion process.

Experimental Device and Protocol

The experiments presented in this paper were conducted using the FM-Global Fire Propagation Apparatus (FPA) following ASTM E 2058 combustion test [9]. Like the cone calorimeter, from which it has kept its operating principle, the FPA allows, among others things, to measure the energy released by the combustion of a material. [10]
The fuel sample is submitted to a radiative heat flux, and a pilot ignition source is provided. For this study, a radiative heat insults has been imposed to the sample of 40 $kW.m^{-2}$. The infrared heaters were not shut down after ignition but remained on during the whole test. The mass loss rate was measured and the exhaust gases were analyzed for composition, temperature, optical obscuration and flow speed with a Pitot tube. The FPA allows natural convection or forced gas flow rate through the fuel bed of which only the former is used here. FPA basic layout is presented in Figure 4.1 a).

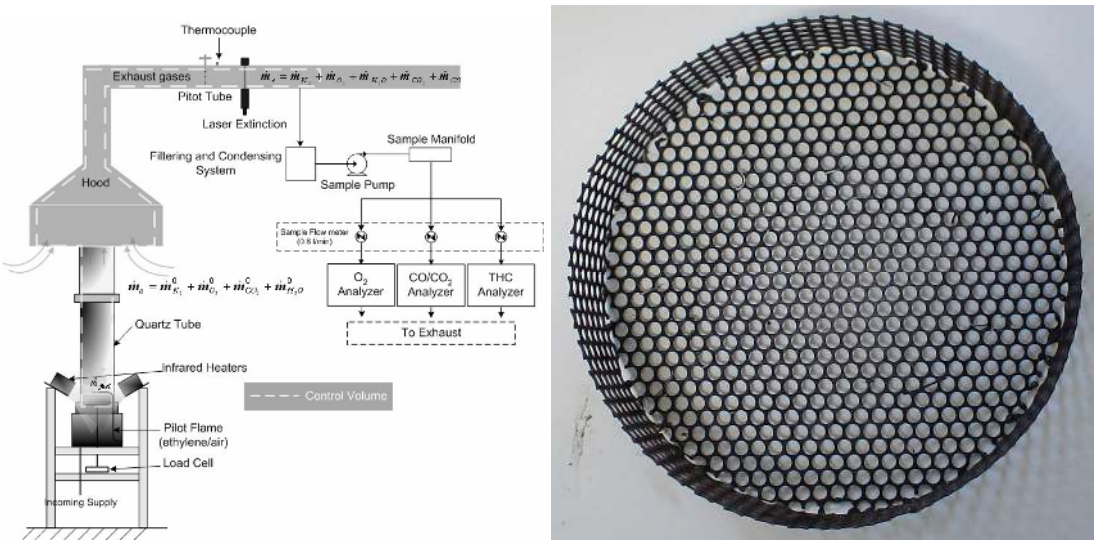

Figure 4.1 a) Schematic of the Fire Propagation Apparatus (FPA) b) Porous sample holder

Figure 4.1 b) shows the specific sample holder used for the experiments noted in [7]. The aim of this work is to study the effect of leaf morphology on the combustion dynamics. The sample holder is a circular basket, made of stainless steel, with holes on all the surfaces (sides and bottom), to allow flow to pass through the fuel bed measuring 13 ± 0.01cm in diameter and 30 ± 0.5mm in depth (see Figure 4.1 b). The percentage opening of the basket is 63%. It fits inside the combustion chamber, which is cylindrical, and lies on a load cell.

Extant conifer species that share morphological and ecological similarity to the fossil collections from East Greenland were selected. Branches of the plants were collected from the Royal Botanical Garden of Edinburgh. Six species were selected: Metasequoia glyptostroboides (MS) and Glyptostrobus pensilis (GS) (narrow leaved), Wollemia nobilis (WN) and Afrocarpus sp. (AF) (slim broad leaved) and Agathis australis (AA) and Nageia naga (NN) (broad-leaved). Three samples of each were tested to ensure repeatability. Figure 4.2 a), b) and c) show representative picture of the leaves in each group used in this study.

Figure 4.2 Leaf images for a) Agathis Australis b) Metasequoia glyptostroboides c) Afrocarpus sp.

Experimental calculations and parameter estimation

Measurements are obtained following ASTM E 2058, standard practice for using the FPA, combustion test. All other calculations outside this scope are described here. In order to describe these in detail, different terminology is used to indicate the set of measurements and calculations that were used. The main sets of data obtained from the FPA are Heat Release Rate (HRR) and Mass Flux. Chemical HRR is obtained through carbon dioxide and carbon monoxide generation (CDG) calorimetry and convective HRR is obtained using gas temperature rise as described by Tewarson. [10] Mass flux is obtained by deriving mass over time. Due to variability in the load cell, a smoothing algorithm called the supsmooth algorithm is used. [11] Values for energetic constants are obtained from average values described by Tewarson in [10] From these, parameters are obtained and are explained in the figures and equations below:

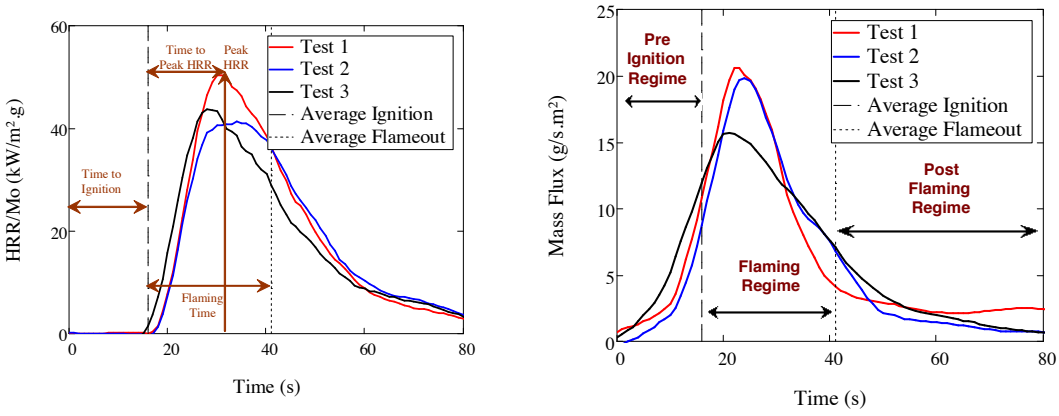

Figure 4.3 a) Heat Release Rate/Initial Mass and b) Mass Flux of Metasequoia glyptostroboides

Heat release rate (HRR) is determined using carbon dioxide and carbon monoxide generation to obtain total energy released from the combustion process calculated here as, [10]

$$\dot{Q} = \Delta H_{CO_2}\left(\dot{G}_{CO_2} - \dot{G}^0_{CO_2}\right) + \Delta H_{CO}\left(\dot{G}_{CO} - \dot{G}^0_{CO}\right) \quad \textbf{Equation 4.1}$$

where $\dot{Q}$ is HRR, ΔH is the net heat of complete combustion per mass generated, $\dot{G}$ is the generation rate, $\dot{G}^0$ is the generation rate at time zero, and CO and CO_2 are carbon monoxide and carbon dioxide respectively. Effective heat of Combustion (ΔH_c) for these experiments is obtained by integrating the HRR and then dividing by the initial mass, as

$$\Delta H_c = \frac{\int \dot{Q}\, dt}{m_o} \quad \textbf{Equation 4.2}$$

where m_o is the initial mass of the sample. Leaf area was measured by flattening the leaf on a film to obtain an image and then using Matlab's image processing software. The area for one side of the leaf is measured. Surface area to volume ratio is calculated using Equation 4.3, where A_L is leaf area, SA_L is the surface area of a leaf, V is the volume and τ is the thickness of the leaf measured using a micrometer (0.001mm resolution).

$$\frac{SA_L}{V} = \frac{2 \cdot A_L}{A_L \cdot \tau} \quad \textbf{Equation 4.3}$$

Figure 4.3 a and b are representative of the combustion dynamics for these kinds of experiments. The process can be divided into three main stages: pre ignition, flaming and post flaming stage as can be seen in the mass flux curve. Each stage is important in its own right as they give different indication of what kind of fire can be achieved from the given material and conditions. Start time at zero seconds is the time at which the heat flux is imposed on the material. As can be seen from the mass flux curve, at this time the material starts to degrade and lose mass therein producing pyrolysis gases. Once the concentration of these gases around the pilot flame directly above the sample is sufficient the material will ignite as can be seen identified by the solid vertical line. The sample will then start to rapidly release heat from the flames until it reaches its peak heat

release rate as marked on Figure 4.3a. Due to a limited mass of the sample, less and less mass will be available for consumption so the heat release rate starts to decrease at this point and flameout will occur shortly after this. Some uncertainty does exist due to the rapid accumulation of gases as it is being analyzed so the delay time is also affected by this but this is harder to get a measure of. Important parameters are highlighted in the figures that are analyzed in detail in the results section such as the mass flux at certain points, different record of time for events among others that are important to the combustion dynamics of these fires. A description of parameters of interest to this study is presented in Table 4.1.

Table 4.1 Description of flammability parameters

HRR (kW/m^2)	Heat release rate (HRR) per unit area of sample free surface
Effective Heat of Combustion (kJ/g)	Calculated as the integral of the HRR from ignition to flame out divided by the initial mass (time zero)
Time to Ignition (s)	Time for sample to ignite from when it is first subjected to the heat insult (time zero)
Time to Peak HRR (s)	Time from ignition to the peak HRR
Flaming Time (s)	Duration for which a flame is sustained from ignition to flameout
Pre-Ignition Mass Flux ($g/s.m^2$)	Mass loss rate per unit area of sample free surface during pre-ignition stage
Mass Flux during flaming ($g/s.m^2$)	Mass loss rate per unit area of sample free surface flux during flaming stage
Total Hydrocarbon Flux ($g/s.m^2$)	Flux of total unburnt hydrocarbon emitted
Leaf Area (cm^2)	Area of one leaf on one side

Parameters of great importance to wildland fires can be derived from these measurements, such as flame spread rate, depth of the flame front, fire intensity and total heat release. For example, the flame spread rate in real-scale fires is inversely proportional to the time to ignition [6]; so the faster a fuel ignites the faster the flame spread rate. The depth of the fire front is proportional to the flaming time (and the bulk density); and the fire intensity per unit length of fire front is proportional to the HRR and the depth of the front. Note that we report the effective heat of combustion measured in a fire calorimeter. This is the energy per unit fuel mass that is effectively released in fire conditions. Compared this to the value most reported in the literature, the maximum heat of combustion, which is typically measured in bomb calorimeters and that is only released in ideal combustion conditions (resembling those inside combustion engines) and far from those encountered in real fires.

Results

Transient Results

Statistical analysis of the tests was done using the direct and calculated values of various parameters. Discrete and continuous variables are described below. Representative Heat Release Rate and Mass Flux curves for a given experiment for all species can be seen in the figures below; however, representation of statistical reliability is given under the parameter discussion for each case:

Overall a spread of differences can be observed through these curves in the dynamics of combustion of these leaves like ignition time, fire growth and dynamics of volatile formation. For example, if we look at MS classified as a narrow leaf compared to AA classified as a broad leaf. The process though, is similar for all in that when the material is exposed to a heat insult it will start to degrade and produce flammable volatile gases,

once these gases reach a flammable mixture known as the firepoint, the fuel will ignite and we start to observe the rapid rise in HRR; as the material is rapidly consumed it reaches a peak energy release which will start to decrease as less and less fuel becomes available for combustion until the flame extinguishes due to lack of fuel. It becomes hard to differentiate these important differences here, however, which is why we extract certain parameters that give us an indication of the combustion process.

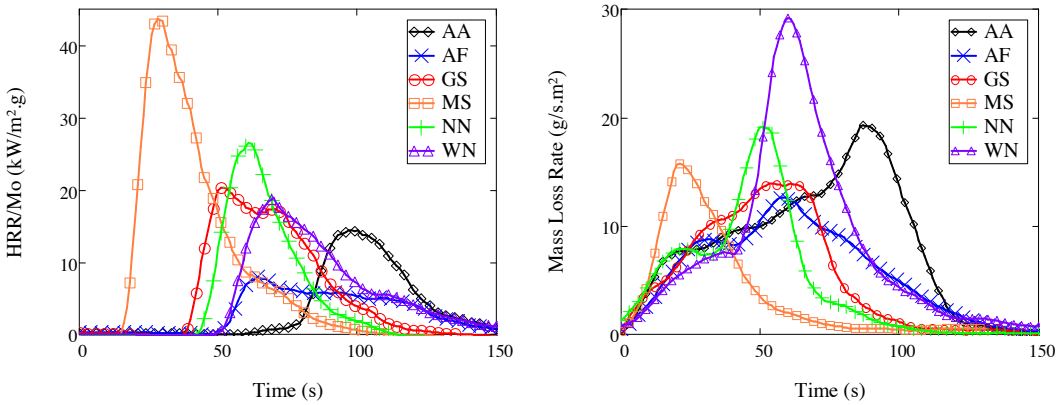

Figure 4.4 a) Heat Release Rate/Initial Mass and b) Mass Flux for all species

Parameter analysis on flammability variables

The individual parameters in Table 4.1 were extracted from these transient measurements to understand the combustion behavior. Values from repeated experiments are averaged to obtain a repeatability error in the measurements taken from heat release rate and mass flux curve of the above mentioned conditions and compared to two different leaf morphology variables: area and surface-area-to-volume ratio as seen in Table 4.2.

Table 4.2 Summary of experiments: average ± standard deviation for different leaf species

Flammability Parameter	Leaf Species																	
	GS			*MS*			*AF*			*WN*			*AA*			*NN*		
Time to ignition (s)	56	±	20	16	±	1	50	±	1	60	±	8	83	±	2	44	±	2
Heat of combustion (kJ/g)	8.6	±	1.7	16.7	±	0.6	5.7	±	0.2	11.0	±	0.9	6.9	±	0.0	9.9	±	1.2
Time to peak HRR (s)	14	±	2	15	±	1	17	±	1	17	±	0	17	±	1	20	±	1
Mean pre-ignition mass flux (g/sm^2)	6.7	±	0.6	3.1	±	0.6	6.4	±	0.6	6.4	±	0.7	9.2	±	0.5	6.2	±	0.3
Mean mass flux during flaming (g/sm^2)	10.2	±	1.1	13.2	±	0.5	12.2	±	0.5	16.7	±	0.9	17.3	±	2.5	13.5	±	0.7
Flaming time (s)	12	±	5	25	±	2	20	±	18	51	±	5	19	±	0	32	±	7
Peak THC Flux/Initial mass (g/sm^2.g)	0.0067	±	0.0003	0.0086	±	0.0017	0.0067	±	0.0012	0.0025	±	0.0002	0.0017	±	0.0010	0.0029	±	0.0010
Peak CO Flux/ Initial mass (g/sm^2.g)	0.0830	±	0.0007	0.1610	±	0.0140	0.0580	±	0.0110	0.0500	±	0.0045	0.0410	±	0.0140	0.0640	±	0.0140
Leaf area (cm^2)	0.09	±	0.04	0.17	±	0.04	2.46	±	0.97	2.66	±	1.49	8.46	±	1.67	9.82	±	1.78
Surface area-to-volume ratio (1/mm)	5.59	±	0.13	6.53	±	0.64	4.75	±	0.26	3.64	±	0.95	3.66	±	0.17	4.11	±	0.26
Average Initial Mass (g)	15.0	±	0.5	16.1	±	0.4	12.3	±	1.6	5.9	±	0.2	8.5	±	1.1	17.4	±	1.2

Figure 4.5 shows time to ignition for the various leaves. Time to ignition quantifies ease of ignitability. Lower time to ignitions, will tend to indicate fires will spread more rapidly and easier overall. Figure 4.5 shows us a direct relationship between time to ignition and an inverse relationship with surface area to volume ratio.

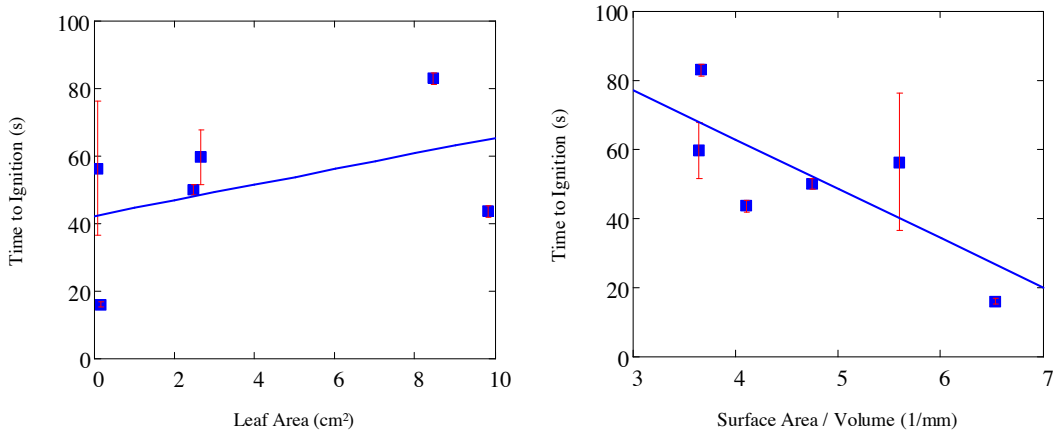

Figure 4.5 Time to Ignition vs a) leaf area b) Surface Area / Volume

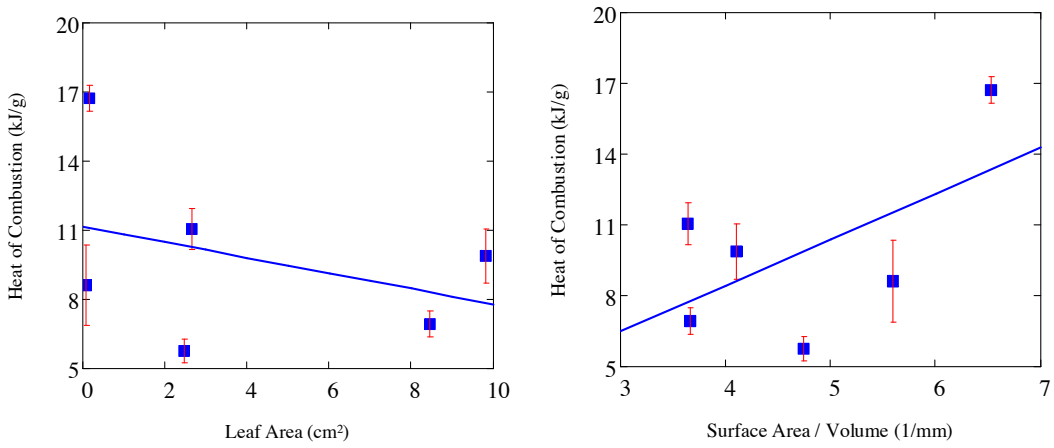

Figure 4.6 Heat of Combustion vs a) leaf area b) Surface Area / Volume

The effective heat of combustion presented in Figure 4.6, provides information about the amount of energy realeased in the fire per mass of fuel. A higher heat of combustion will mean more energy will be available for combustion. These two graphs show us an inverse relationship between leaf area and heat of combustion and a direct relationship between heat of combustion and surface to volume ratio.

Time to peak HRR is regarded as a measurement of fire growth. Lower times to peak HRR will be an indicator fast growing fires which tend to be a greater threat overall. The relationships we see in Figure 4.7 are a direct relationship between leaf area and time to peak HRR and an inverse relationship with surface area to volume ratio.

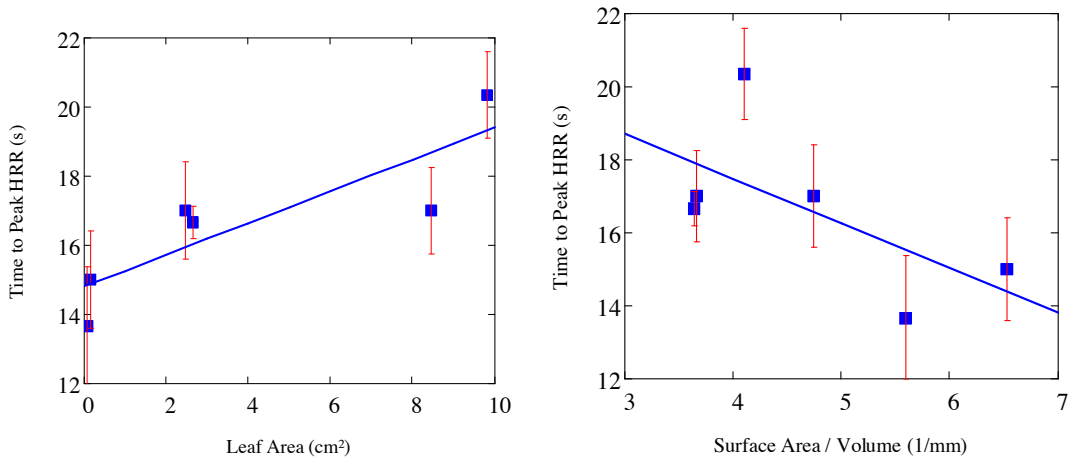

Figure 4.7 Time to peak HRR vs a) leaf area b) Surface Area / Volume

Figure 4.8 shows the average mass flux during the pre ignition stage. Lower fluxes, in this case, could mean less material is needed before ignition to start the combustion process, an overall ease of ignitability. If we couple this with shorter times to ignition, it would tend to indicate less energy input is required to ignite the material; therefore, it is an indirect indication of flame speeds and fire growth. Figure 4.8 shows a direct relationship between leaf are and these fluxes and an indirect relationship with respect to surface area to volume ratio.

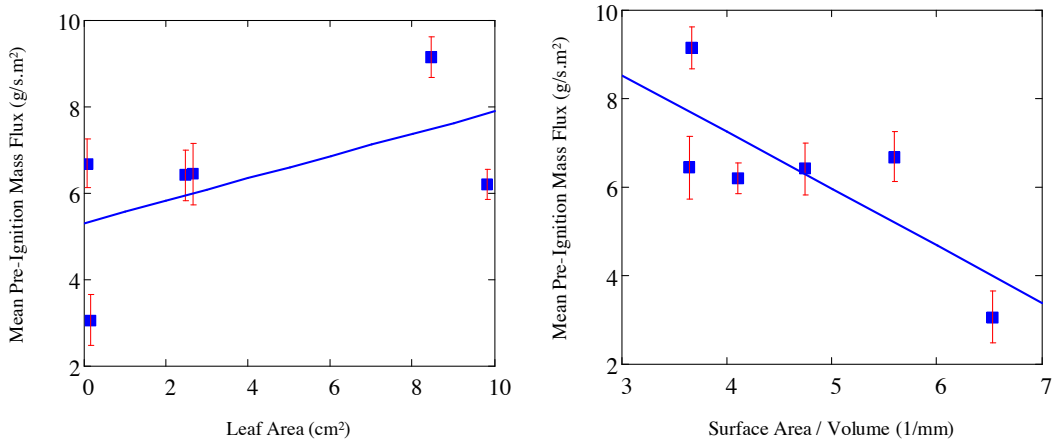

Figure 4.8 Mean Pre-Ignition Mass Flux vs a) leaf area b) Surface Area / Volume

Lower mass fluxes during the flaming process given that the heat input remains constant for all these tests (ie 40 kW/m^2 insult), can indicate less fuel is required to maintain combustion overall. If we also look at the time during which flaming takes place, a shorter overall time for similar fuel content could also be an indicator of a fast growing fire. Figure 4.9 and Figure 4.10 show a direct relationship of these variables for leaf area and an inverse relationship for surface area to volume ratio.

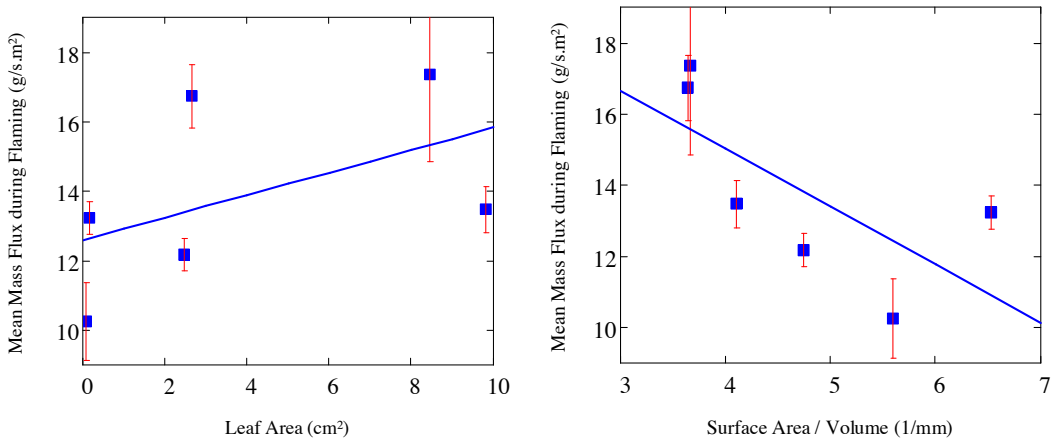

Figure 4.9 Mean mass flux during flaming vs a) leaf area b) Surface Area / Volume

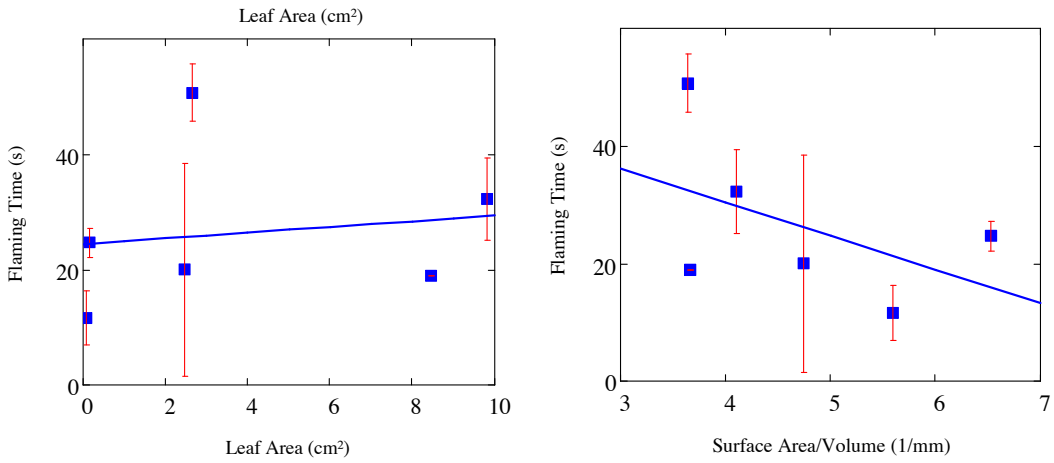

Figure 4.10 Flaming Time vs a) leaf area b) Surface Area / Volume

Figure 4.11 and Figure 4.12 are both representation of peak gas production for total unburnt hydrocarbons and carbon monoxide concentration. These measurements tend to be associated with incompleteness in the combustion process; given that the total hydrocarbon flux is a measure of the amount of hydrocarbons that were not burned during the reaction and carbon monoxide is generally more abundant when there is not enough air to fully consume the fuel. Similarly, they are both indicators of the same phenomena here. Natural fuels tend to have a higher ignitability overall mainly due to their high cellulose composition and ease of ignitability. These measurements here, therefore, tell us more about the growth of the fire. The faster the fire grows, the less immediate air will be available for combustion; therefore, higher fluxes of these measurements will tend to indicate faster growing fires.

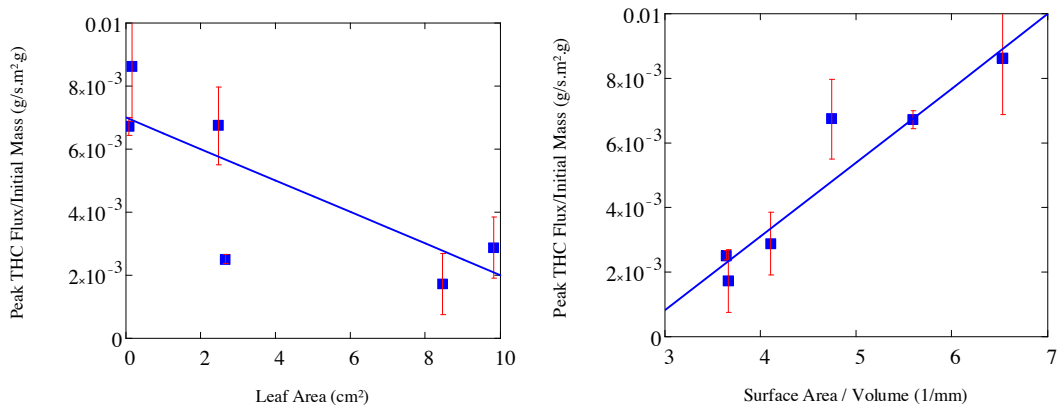

Figure 4.11 Peak Total Hydrocarbon flux/Initial Mass vs a) leaf area b) Surface Area / Volume

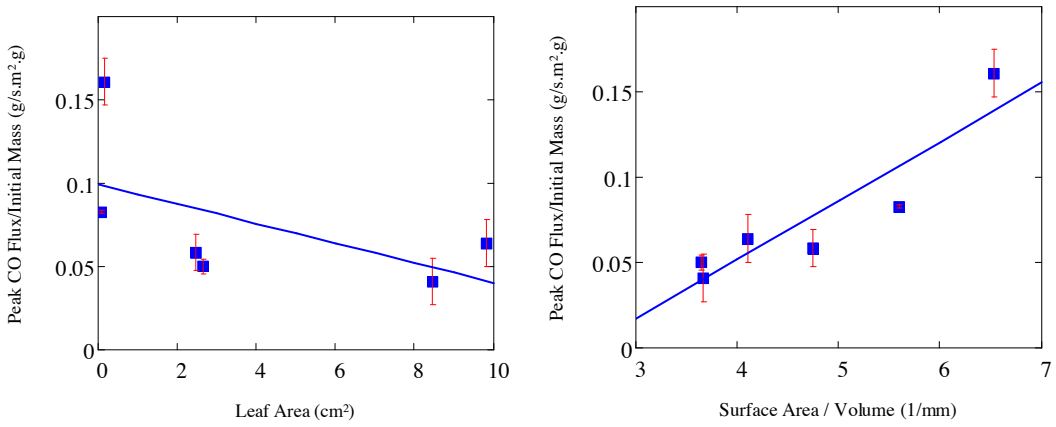

Figure 4.12 Peak Carbon Monoxide flux / Initial Mass vs a) leaf area b) Surface Area / Volume

Lastly, Figure 4.13 presents the relationship between surface area to volume ratio vs leaf area. The two variables are shown throughout compared to various fire parameters. The original study was focused on the leaf area which was of interest to geoscientists due to their classification system for leaves. As fire safety scientists, surface area to volume ratio, tends to mean more in the combustion sense since this relates to the area available for burning and thickness of the fuel, two variables that are important in calorimetry. Surface-area-to-volume ratio presents the greater fit overall. Higher slopes within the same measured flammability variable are seen throughout meaning a greater change is observed with this morphology measurement. Nonetheless, the inverse relationship here would seem to indicate that for this specific study either measure would give us an indication of the flammability of these fuels.

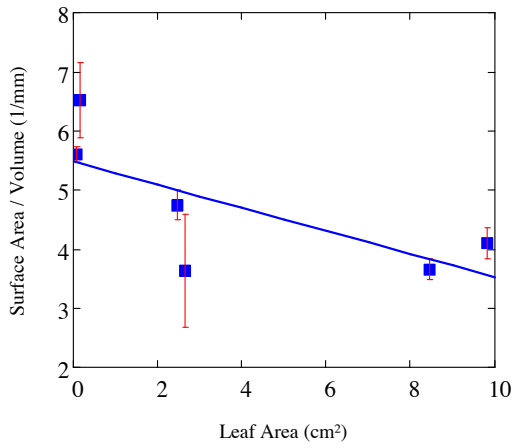

Figure 4.13 Leaf area vs Surface Area / Volume for measured species

Discussion

Data presented in Belcher et al. [1], presents times to ignition, heat of combustion and THC flux measurements. The data there is presented divided into groupings of narrow, slim-broad and broad leaves. The same behavior described there is observed here with the added investigation of how to quantify morphology on leaf area and measurement comparisons to surface-area-to-volume ratio as well. Five other flammability variables are presented here to support the increased flammability with decreased area hypothesis.

Decreasing leaf area has been shown to have a strong correlation with an increase in overall flammability of leaves. As the measured leaf area decreased, higher heats of combustion, lower times to ignition, lower times to peak HRR, lower mean pre ignition and flaming mass flux and higher flux measurements of peak total unburnt hydrocarbons were observed and measured. All these measures show indications of different aspects of the fire such as time to ignition for ignitability or heat of combustion on overall heat content. There is not one measure that can give us flammability of vegetation or a

universally accepted method of flammability rating for vegetation [12]; nonetheless, the conjunction of all these flammability variables here seem to suggest leaf area can be used as a means to assess relative vegetation flammability for this given range.

Much of the same behavior is observed with increasing surface-area-to-volume ratio. Higher heats of combustion, lower times to ignition, lower times to peak HRR, lower mean pre ignition and flaming mass flux and higher flux measurements of peak total unburnt hydrocarbons were observed and measured with increased surface area-to-volume ratio. Moreover, between the two morphologies, surface area-to-volume ratio presents a stronger fit with the data. Higher slopes indicating a greater change over the same range of the flammability variable are seen on most flammability variables and a better fit overall.

Surface area-to-volume ratio and leaf area are shown to have an inverse relationship as we would expect given the behavior observed with the flammability parameters. What we cannot ascertain is whether this is an innate characteristic of the vegetation or if statistically this has grown to be a dominant behavior. Heat of combustion values give us an idea of the flammable content present in the fuel. Given that this measure also varied with leaf morphology, this could indicate vegetation composition will also affect structure and configuration of the plant. The limitation we have is that given the wide variety of species, our sampling size is small. Many factors will affect the combustion as pointed out before and this can vary throughout species but with a larger sampling size we should be able to tell at least if these relations will hold. The reason behind leaf morphology and vegetation composition will most likely require more investigation in physical and chemical composition to be able to tell us why we predominantly find decreased flammability in leaves with larger leaf area and smaller surface area to volume ratio.

Fire scientists will give more weight to surface area to volume ratio presented herein. [6] Surface area to volume ratio is known to control combustion dynamics of solid fuels

since it relates to the area available for burning and thickness of the fuel. The ratio for the leaf samples presented here, due to their configuration, is inversely related to the thickness of the sample. Leaves, for the most part, are thermally thin fuels. The thin slab approximation is therefore a valid approach to the combustion process. [6] Thickness of the sample will be directly proportional to ignition time and hence present a greater fire risk.

Weise et al. [12] presents work for different species of ornamental vegetation. Similarly he presents study of flammability on different species but his focus is more on moisture content and seasonal variation of the vegetation fuels. Surface area to volume ratios are presented for the species studied. On analysis on some of the reported values and comparison to their peak heat release rate ranking, similarly to values here, species with reported higher surface area to volume ratio are generally categorized as more flammable such as Olea europea and species with lower ratios such as Aloe sp. are ranked as less flammable. Dimitrakopoulous [13] has also reported a flammability ranking in which vegetation with higher flammability will have low foliage heat content, low surface area to volume ratio and high ash content.

Conclusions

In order to study differences in flammability between different leaf species, calorimetric tools have been used to analyze and characterize these species against leaf morphology. Various combustion parameters can give us indication and understanding of fire growth, speed and intensity. Ignition time and time to peak HRR tells us about ignitability, fire growth and speed. Gas combustion and mass flux measurements also tell us about fire growth, energy content of the fuel and sustainability of the fire. All the parameters here have contributed to telling us there is a correlation between increased flammability and smaller leaf area (ie narrow leaved plants) and increased flammability with larger surface area-to-volume ratios. Between the two morphologies, surface area-to-volume

ratio presents a stronger fit with the data. It is suggested study on vegetation composition and its relation to leaf morphology will give us a better understanding of these relations to ascertain whether this change in flammability is only due to a change in morphology configuration or if because different compositions will affect the structure of the plant and leaves this will also partake in the reason behind the increased combustion behavior.

Acknowledgements

Thanks to P. Thomas (Royal Botanic Gardens, Edinburgh) for providing modern vegetation samples and the BRE Trust, UK for financial support for this work. Thanks also to Professor Jose Torero for access to the Fire Science Laboratory and FM Global for the donation of the Fire Propagation Apparatus where these tests were carried out.

References

[1] Belcher, C. M., Mander, L., Rein, G., Jervis, F. X., Haworth, M., Hesselbo, S. P., Glasspool, I. J. and McElwain, J. C. Increased fire activity at the Triassic/Jurassic boundary in Greenland due to climate-driven floral change. *Nature Geoscience*, ***3****(6),* doi: 10.1038/NGEO871, (2010).

[2] Bowman, D., Balch, J., Artaxo, P., Bond, W., Carlson, J., Cochrane, A., D'Antonio, C., Defries, R., Doyle, J., Harrison, S., Johnston, F., Keeley, J., Krawchuk, M., Kull, C., Marston, J., Moritx, M., Prentice, C., Roos, C., Scott, A., Swetnam, T., van de Werf, G. and Pyne, S. Fire in the Earth System. *Science* **324**, 481-484 (2009).

[3] Langenfelds, R. L., R. J. Francey, B. C. Pak, L. P. Steele, J. Lloyd, C. M. Trudinger, and C. E. Allison, Interannual growth rate variations of atmospheric CO_2 and its $\delta^{13}C$,H_2,CH_4, and CO between 1992 and 1999 linked to biomass

burning, *Global Biogeochem. Cycles,* ***16***(3), 1048, doi:10.1029/2001GB001466, (2002).

[4] Carcaillet, C. et al. Change of fire frequency in the eastern Canadian boreal forests during the Holocene: Does vegetation composition or climate trigger the fire regime? *J. Ecol.* **89**, 930-946 (2001).

[5] McElwain, J. C., Beerling, D. J. & Woodward, F. I. Fossil plants and global warming at the Triassic-Jurassic boundary. *Science* **285**, 1386-1390 (1999).

[6] Drysdale, D. An Introduction to Fire Dynamics (Wiley, 1998)

[7] C. Schemel, A. Simeoni, H. Biteau, J. Rivera, J.L. Torero, *Experimental Thermal and Fluid Science,* 2008, **32**(7): 1381-1389l

[8] P. Bartoli, A. Simeoni, H. Biteau, J.L. Torero, P.A. Santoni, *Fire Safety Journal*, 2011, **46**: 27-33.

[9] ASTM E 2058, Standard Methods of Test for Measurement of Synthetic Polymer Material Flammability Using a Fire Propagation Apparatus (FPA), American Society for Testing Materials, Philadelphia, 2003.

[10] A. Tewarson, in: Generation of Heat and Chemical Compounds in Fires, SFPE Handbook of Fire protection Engineering, The National Fire Protection Association Presss, 2002, pp. 3-82-3-161.

[11] Parametric Technology Corporation. (2007) Users's Guide Mathcad 14.0, from http://www.ptc.com/products/mathcad/

[12] Weise, D. R., White, R. H., Beall, F. C., Etlinger, M., Use of the cone calorimeter to detect seasonal differences in selected combustion characteristics of ornamental vegetation, *International Journal of Wildland Fire*, **14**, 321-338 (2005).

[13] Dimitrakopoulos, A.P. A Statistical classification of Mediterannean species based on their flammability components, *International Journal of Wildland Fire*, **10**,113-118, doi:10.1071/WF01004 (2001).

Chapter 5

Effect of varying O_2 concentration and applied heat flux on the burning dynamics of low and high density chipboard using calorimetry

Abstract

Calorimetric experiments are used to analyze the effects of varying oxygen levels, heat insults, material thicknesses and densities on the process of chipboard burning. Applied heat flux and varying oxygen concentration have been shown to produce important changes on the burning of chipboard mostly on the flame but also on the solid burning as well. For a thermally thick sample, the two densities studied, standard grade chipboard and industry grade MDP is shown to have little effect on the combustion process as a whole. Chipboard is also shown to steadily burn once the first char formation has been established on the surface of the solid.

Introduction

Wood has always been widely used for construction. In these days, interior wood surfaces, furniture and timber constructions are examples where industry has used this material due to its vast flexibility of use. Wood is readily available, renewable and it is relatively a low cost construction material. Overall its advantages allow for lower energy usage and less pollution which presents a wide appeal for consumers in a variety of sectors. [1] It therefore presents a substantial fraction of the fuel load for building fires. For this reason it is important to understand its behavior while undergoing burning as fire presents one the leading risks of combustible materials such as wood.

Wood being a heterogeneous, non-isotropic material is a complex mixture of natural polymers largely composed of cellulose. Under heating, wood undergoes thermal decomposition producing volatile, water vapor and char. This process has been widely studied but still not fully understood. [2] The char formation is key to understand the burning dynamics of wood, as it presents the most complex interaction of chemistry, heat and mass transfer. Char layer formation, as it accumulates, has shown to increase the thermal resistance between the exposed surface and the pyrolysis front. [3] Most fire retardants in wood act by promoting the char formation process to slow down the heating of the material.[2] More in detail studies of char behavior can be found in works of Atreya such as [4].

Changes in combustion behavior can be seen through the burning rate. Calorimetric experiments allow for this term to be measured. For solids, as described by Drysdale [2], burning rate can be calculated as,

$$\dot{m}'' = \frac{\dot{Q}''_F + \dot{Q}''_E - \dot{Q}''_L}{L_V} \qquad \textbf{Equation 1[2]}$$

where $\dot{Q}''_F$ is the heat flux supplied by the flame, $\dot{Q}''_E$ is the external heat flux applied, $\dot{Q}''_L$ represents the loss expressed as a heat flux through the fuel surface and L_V is heat required to produce the volatiles. Heat supplied by the flame is affected by environment in which the burning is taking place. Increased rate of spread, intensity and faster ignitions are some of the behavior we see as we increase levels of oxygen in the environment. [2] During compartment fires, oxygen concentrations can range from ambient (21%) to almost zero. The largest effect is seen on the flame itself; given a lower oxygen environment, this will affect the flame heat feed back to the solid and the flame radiation but it is one of the least known variables. Increased oxygen levels allows

for the more volatiles to readily combust and hence give off more heat and therefore increase the burning rate. Beaulieu has shown this effect in her work measuring flame heat flux in enhanced oxygen environments for some plastics. [5] Volatile formation in wood pyrolysis can also be affected under a change in oxygen environment as seen on Kashiwagi's work. Results for his work in a non-flaming scenario showed ambient oxygen significantly increases the gasification mass flux, sample temperatures and char depth. [6]

It is because of this complexity that laboratory small scale experiments become essential in order to understand the burning dynamics of materials under different conditions. This study aims to experimentally study the burning behavior of wood using calorimetric data under varying oxygen environments and imposed heat flux under controlled conditions. The fuels used in this study are standard grade chipboard (European standard) [7] of two different thicknesses: 12 and 18 mm (Figure 5.1 a) and industry grade medium density particleboard (MDP) [8] of three different thicknesses: 6, 15 and 25 mm (Figure 5.1 b). In this study standard grade chipboard will be referred to as chipboard low density (LD) and MDP will be referred to as chipboard medium density (MD). Both of these fuels are widely used in construction specifically furniture, wood linings among other commodities; hence, they are representative materials encountered inside buildings.

Figure 5.1 a) 12 and 18 mm thick Chipboard LD b) 6, 15, and 25 mm thick Chipboard MD

Experimental Device and Protocol

The experiments were conducted using the FM-Global Fire Propagation Apparatus (FPA) following ASTM E 2058 combustion test unless otherwise noted. [9] Like the cone calorimeter, from which it has kept its operating principle, the FPA allows, among others things, to modify the flow rate and composition of the environment surrounding the sample. [10]

The fuel sample is exposed to a radiative heat flux, and a pilot ignition source is provided above its free surface. For this study, a range of radiative heat insults are imposed ranging from 10 to 70 $kW.m^{-2}$. The infrared heaters were not shut down after ignition but remained on during the whole test. The mass loss rate was measured and the exhaust gases were analyzed for composition, temperature, and flow rate. The ambient condition was controlled through an imposed flow through the sample through which oxygen environments ranging from 0 to 21% O_2 were studied. The flow is set in all experiments to 200 L/min, the recommended flow for these tests according to the standard. FPA basic layout is presented in Figure 5.2a.

Figure 5.2 b) shows the sample placed inside the FPA chamber. The sample size is 8 by 8 cm with different thicknesses. Similarly to the holder design in Ris and Khan in [11], the sample is surrounded with 3 layers of thick cotronics ceramic paper (3mm) in the back and sides in order to leave only one side exposed the heat applied and minimize heat losses in the sample. It is then pushed into a metallic holder and placed on the stand of the mass balance.

Figure 5.2 a) Schematic of the Fire Propagation Apparatus (FPA)
b) Sample of chipboard LD inside FPA chamber
c) Chipboard LD burning at 20 kW/m^2 in air

Measurements are obtained following ASTM E 2058, standard practice for using the FPA, combustion test. All other calculations outside the standard are described here. In order to describe these in detail, different terminology is used to indicate the set of measurements and calculations that were used. The main sets of data obtained from the FPA are Heat Release Rate (HRR) and Mass Loss Rate (MLR). HRR is obtained through the carbon dioxide and carbon monoxide generation method as described by Tewarson. [10] Mass flux is obtained by deriving mass over time. Due to variability in the load cell data, a smoothing algorithm called the supsmooth algorithm is used. [12] Due to the combustion dynamics of the experiments, different regimes are established in order to show the different burning dynamics and understand the behavior of each. From these, parameters are obtained and are explained in the figures and equations following.

Heat release rate (HRR) is determined using carbon dioxide and carbon monoxide generation to obtain total energy released from the combustion process calculated here as, [10]

$$\dot{Q} = \Delta H_{CO_2}\left(\dot{G}_{CO_2} - \dot{G}^0_{CO_2}\right) + \Delta H_{CO}\left(\dot{G}_{CO} - \dot{G}^0_{CO}\right) \qquad \textbf{Equation 5.2 [10]}$$

where $\dot{Q}$ is HRR, ΔH is the net heat of complete combustion per mass generated, $\dot{G}$ is the generation rate, $\dot{G}^0$ is the generation rate at time zero, and CO and CO_2 are carbon monoxide and carbon dioxide respectively.

HRR is shown in Figure 5.3 a) for a series of tests for 15mm chipboard MD subjected to a 30 kW/m^2 heat insult at 18% oxygen flow and Figure 5.3 b) shows a representative mass loss curve for this same test. The sample is subjected to the heat insult at start time zero seconds. From this moment, as can be seen from the mass flux curve, the sample starts to degrade and produce volatiles. These gases accumulate and once the fire point is reached the sample will ignite due to the pilot flame right above it. At this point, as can be seen in the HRR curve, the flame rapidly starts to release energy until it reaches a peak HRR. During this process, the sample forms a char layer on the surface. The peak is reached due to a balance between the char forming rate and heat transfer (char forms a barrier to the rest of the material underneath). As the char layer fully forms, the sample reaches a near steady state of burning. The material continues to burn and once the thermal front reaches the back face of the sample a second peak is reached due to the effect of the insulating barrier at the back as Carvel et al has described in his study. [13]. Once most of the material has burned away, less flammable volatile will be available to maintain flaming combustion, at which point the flame will extinguish. The material continues to slowly smoulder until the end of the test at which point the FPA lamps are shut off.

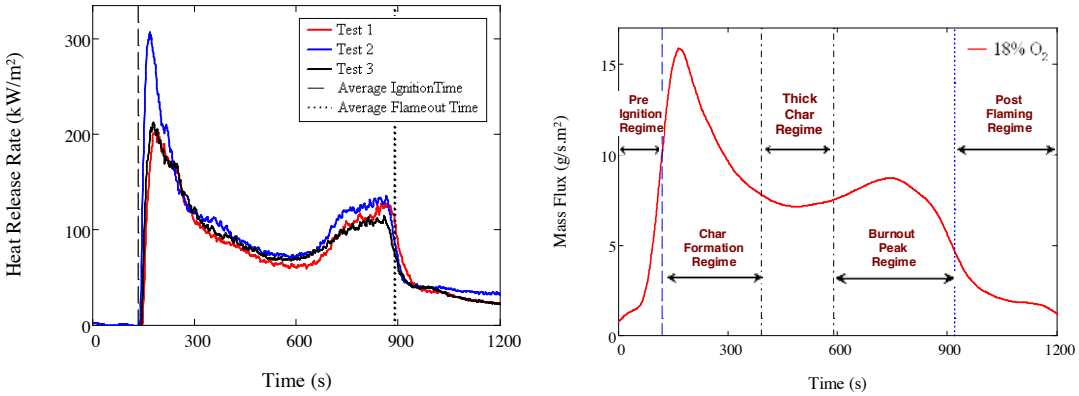

Figure 5.3 a) HRR for chipboard MD 15mm in air at 30 kW/m^2

b) Mass flux for chipboard MD 15mm at 18% O_2

As can be seen in Figure 5.3 b), an experiment is subdivided into five different regimes that outline the burning behaviour representative of these tests. The first is the pre-ignition regime where the material starts to thermally degrade and pyrolyze until it reaches ignition. From ignition until a thick layer of char is formed to allow for steady state burning is referred as the char formation regime. The thick char regime is where the char layer has been full formed and a steady state burning regime is established. A similar effect is seen in Wichman and Atreya's study for wood pyrolysis. [4] We refer to this regime as the burnout peak regime until the flame is extinguished. From when the flame extinguishes till the end of the test the material slowly smoulders away until mostly mineral content is left, we refer to as the post flaming regime.

Results and Discussion

Four different variables were looked at in this study: varying oxygen concentration, imposed heat insult, thickness and material density. Representative Heat Release Rate and Mass Flux curves for a given experiment for all these condition can be seen in the figures below; however, representation of statistical reliability is given under the regime discussion for specific cases:

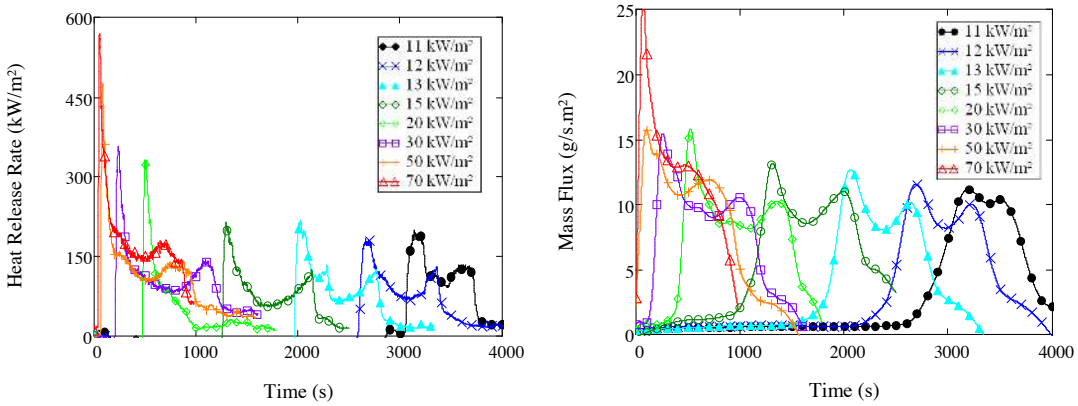

Figure 5.4 18 mm Chipboard LD at 21% O2 with varying heat insults *a) HRR b) Mass Flux*

Varying heat insults are studied on Figure 5.4. Most notable are the increasing ignition times and decreasing peak values of MLR and HRR with decreasing heat insult. It should be noted that we did not obtain ignition for samples subjected to a heat flux of 10 kW/m^2, the critical heat flux for ignition of this material.

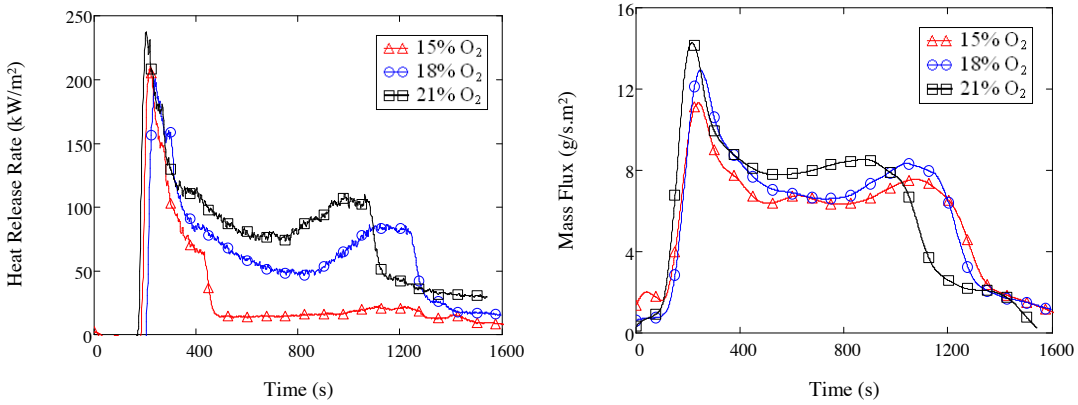

Figure 5.5 18 mm Chipboard LD at 30 kW/m^2 in varying O_2 environments *a) HRR b) Mass Flux*

Figure 5.5 shows a representation of HRR and mass flux for chipboard LD under different oxygen environments. Most notably is the reduction in HRR and MLR specifically in the thick char regime. This will be more visible in the parameter

estimation section of this work. We did not obtain ignition for any sample at 14 % O_2, the critical oxygen concentration for flaming ignition.

Different densities and thicknesses effects are illustrated in Figure 5.6. Overall an increase in peak for HRR is observed with smaller thicknesses as observed by Babrauskas with PMMA. [14] The material sample thicknesses that are tested the most in this study: (15mm Chipboard MD and 18mm Chipboard LD), behave as thermally thick. Apart from this, longer flaming times are observed for increased thickness due to more fuel available during the test. The density does not show a significant effect but a direct comparison was not possible due to the differing thicknesses. More on this will be seen on the extrapolated parameters from this data.

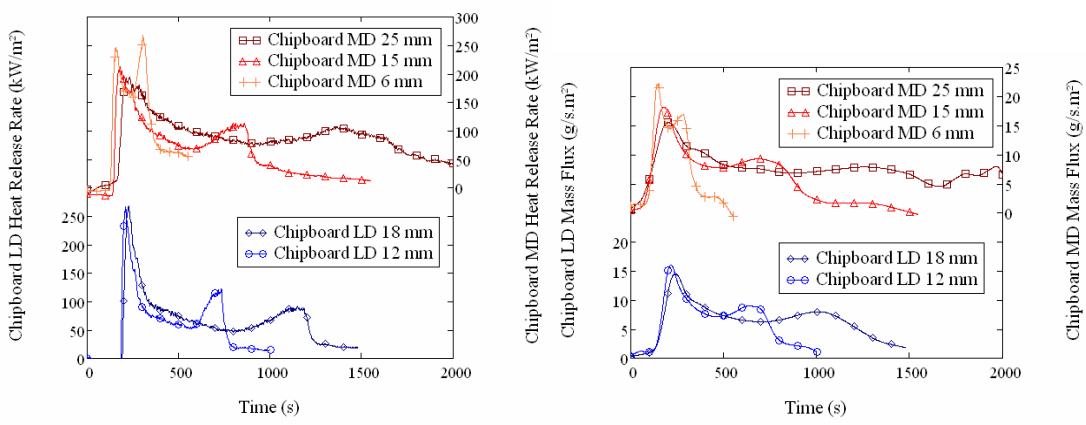

Figure 5.6 *a) HRR* and *b) Mass Flux* under 21 % O2 and 30 kW/m2 varying thicknesses and densities

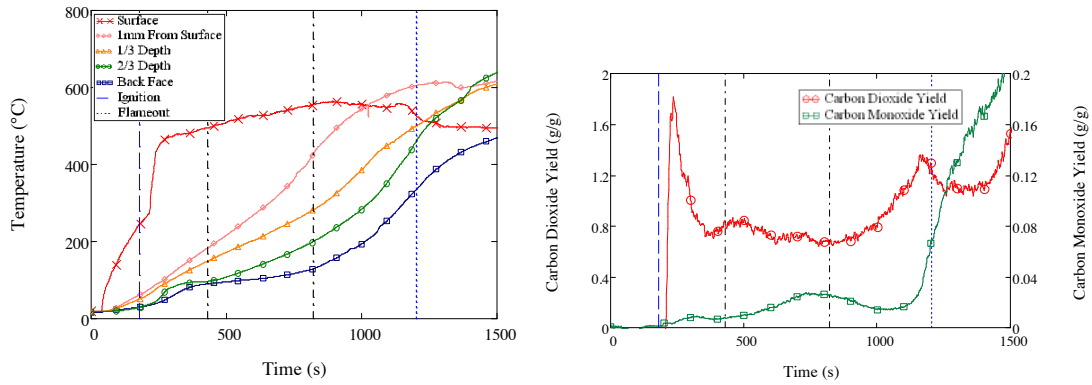

Figure 5.7 ***a) Material temperature profile*** **and** ***b) Carbon Dioxide and Carbon Monoxide Yields*** **for 18 mm Chipboard LD under 21% O_2 and 30 kW/m^2**

One set of temperature measurement for the base case: 18 mm Chipboard LD under 21% oxygen, was taken as a means to get a better understanding of the burning regimes illustrated in Figure 5.7 a). The temperatures are obtained through thermocouples placed inside the sample at various depths as well as on the surface and the back face of the sample. Figure 5.7 b) shows carbon dioxide and carbon monoxide yields for this same test to indicate the burning dynamics taking place. Most notable is the thick char regime where the temperature measurement and gas yields corroborate that for the most part, the burning during this stage is near steady state. Surface temperature seems to have reached a maximum and back face temperature is mostly constant during this regime which means advancement in the thermal decomposition front can be visibly tracked as the in depth temperature measurements show us.

Pre Ignition Regime

In the pre ignition regime the material is first exposed to the heat insult and starts to degrade and pyrolyze until ignition. The time length of this period, otherwise known as the time to ignition, can be seen in Figure 5.8 a) for chipboard MD and Figure 5.8 b) for

chipboard LD. A strong dependence is seen with applied heat flux with both chipboard types as ignition theory predicts. [2]

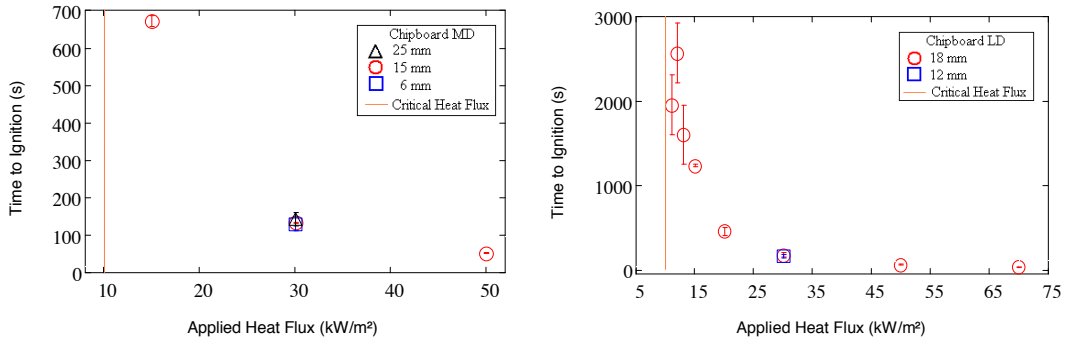

Figure 5.8 Time to ignition under varying heat insults and thicknesses at 21% O_2 for *a) Chipboard MD b) Chipboard LD*

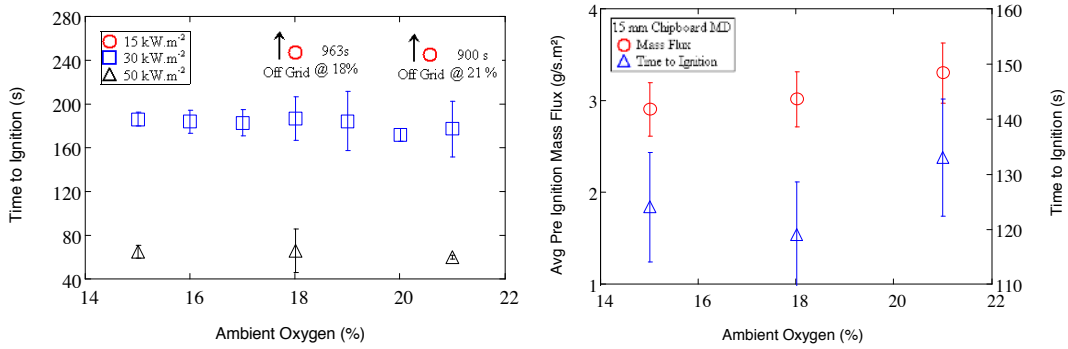

Figure 5.9 ***a) Ignition times for Chipboard 18mm LD under varying O_2 concentrations and heat insults b) Ignition times and Average pre ignition mass flux for 15mm Chipboard MD under varying O_2 concentration***

Figure 5.9 shows ignition times for 18mm chipboard LD and 15 mm chipboard MD. No significant change is seen in ignition times for either chipboard type with varying oxygen concentrations in time to ignition. Ignition times are slightly higher for Chipboard LD in comparison to Chipboard MD as seen on Figure 5.10 a) and increased ignition times are observed with higher thicknesses for both types. Figure 5.9 b), Figure

5.10 and Figure 5.11 show measurements for average pre ignition mass loss. No significant changes are observed with varying O_2 concentrations for either chipboard type. Chipboard MD values increase with increasing thicknesses. Increased heat insults give higher values for both chipboard types as well.

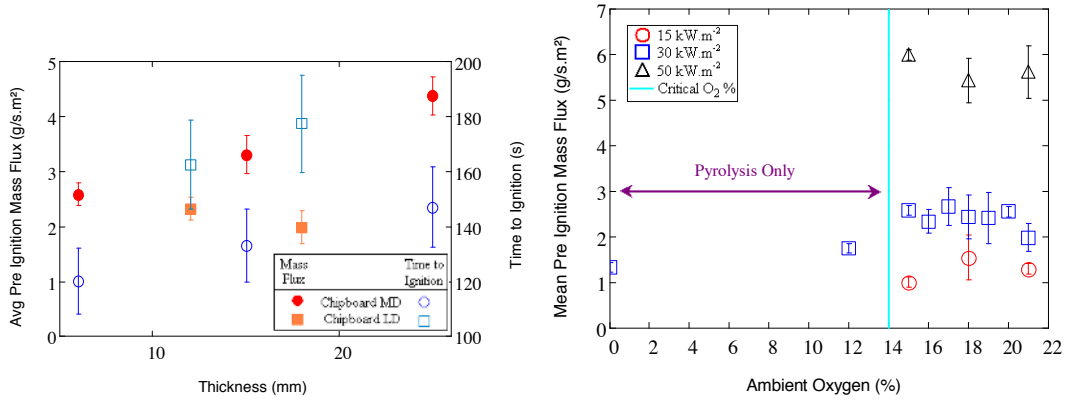

Figure 5.10 ***a) Average pre ignition mass flux and ignition times for varying chipboard thicknesses and densities at 30 kW/m2 and 21% O_2 b) Mean pre ignition mass flux for chipboard LD under varying O_2 concentration and heat insults***

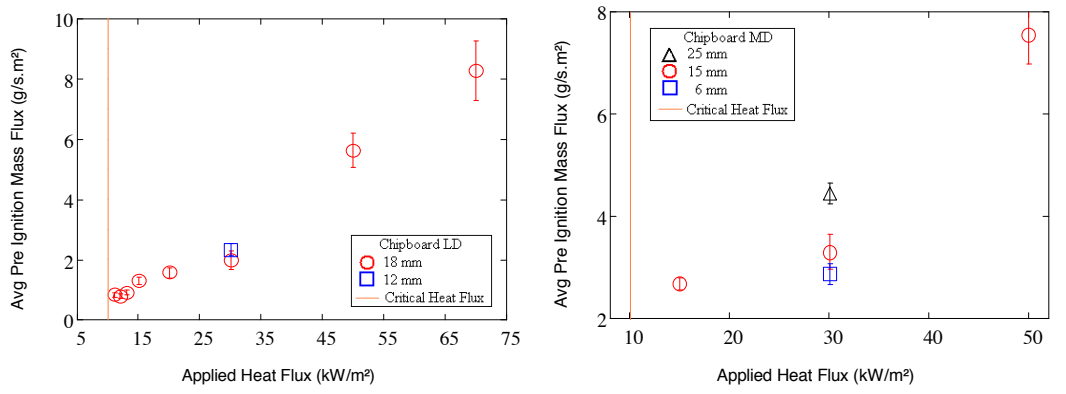

Figure 5.11 Average pre ignition mass flux under varying heat insults at 21% O_2 for ***a) Chipabord LD and b) Chipboard MD***

Char Formation Regime

During the char formation regime, burning reaches its highest peak, shown in both HRR and MLR. Peak values for HRR of chipboard are shown in Figure 5.12, Figure 5.13, and Figure 5.14 a). Both oxygen concentration and heat flux increase peak values for both chipboard types; nonetheless, applied heat flux is more dominant. Oxygen levels become more important at low heat insults and close to the critical oxygen concentration for ignition. Thickness and density do not affect peak HRR significantly.

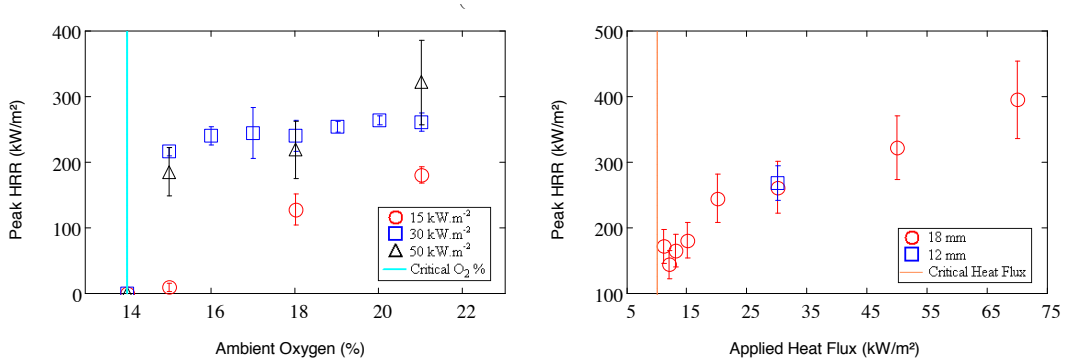

Figure 5.12 Peak HRR during char formation regime for Chipboard LD under *a) varying O_2 concentration and heat insults and b) varying heat insults and thicknesses at 21% O_2*

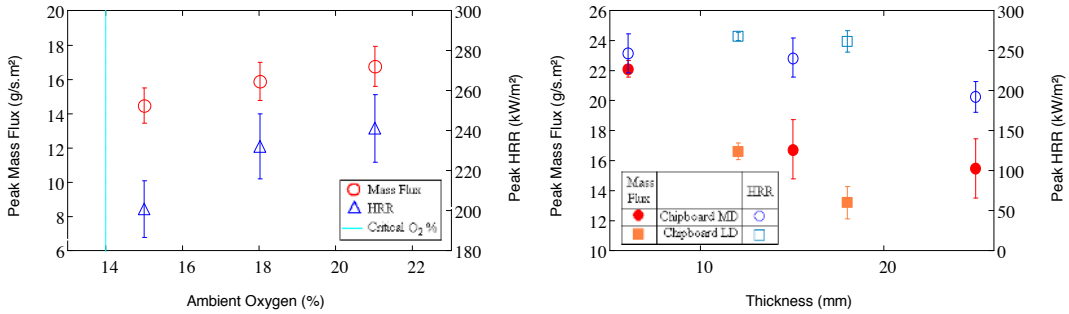

Figure 5.13 Peak HRR and MLR during char formation regime for *a) Chipboard MD under varying O_2 concentration at 30 kW/m^2 b) varying chipboard thicknesses and densities at 30 kW/m^2 and 21% O_2*

Peak MLR values are given in Figure 5.13, Figure 5.14 b), Figure 5.15. Similarly to peak HRR, both increasing oxygen and heat flux levels increase mass flux for both

chipboard types. Oxygen concentration is more important at low heat flux levels and peak mass flux continues to steadily decrease past the critical oxygen concentration for flaming combustion. At low thicknesses, mass flux values rise, but at higher thicknesses they level out most likely because it becomes thermally thick at this point.

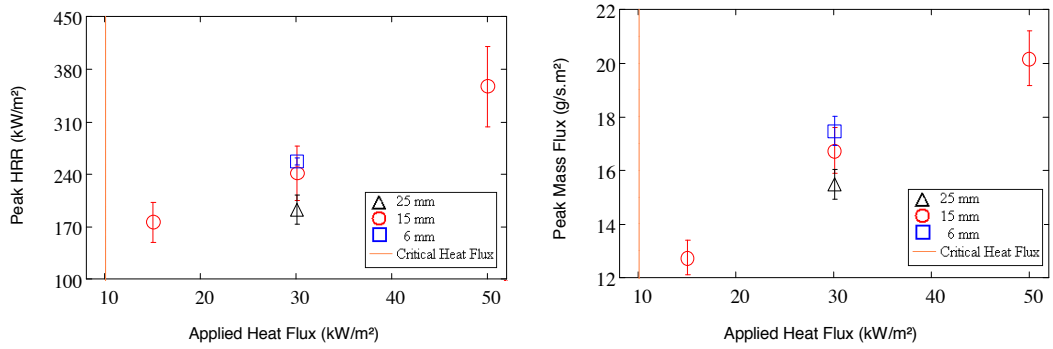

Figure 5.14 Chipboard MD at 21%O2 with varying heat insults ***a) Peak HRR and b) Peak Mass Flux***

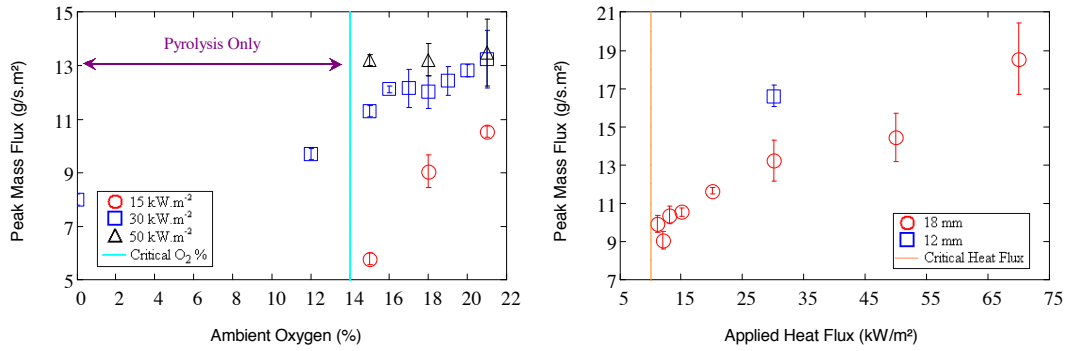

Figure 5.15 Peak mass flux during char formation regime for Chipboard LD under ***a) varying O_2 concentration and heat insults and b) varying heat insults and thicknesses at 21% O_2***

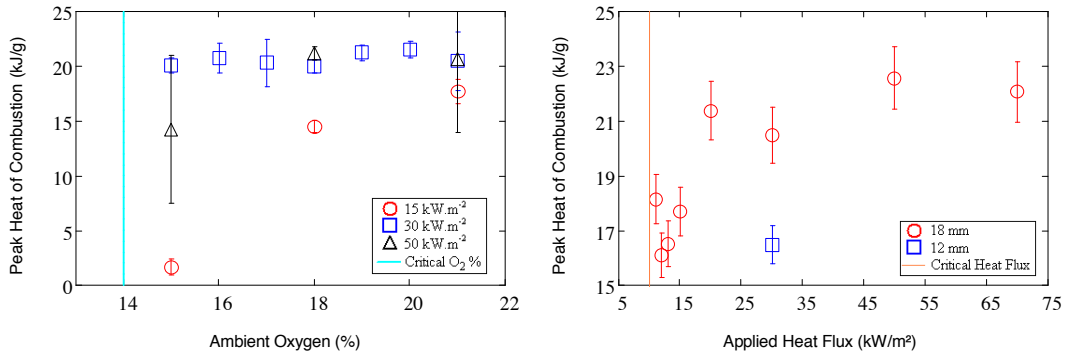

Figure 5.16 Peak instantaneous heat of combustion during char formation regime for Chipboard LD under *a) varying O_2 concentration and heat insults and b) varying heat insults and thicknesses at 21% O_2*

The instantaneous heat of combustion was also calculated. Peak values are shown in Figure 5.16, Figure 5.17, Figure 5.18 b). For chipboard MD, values increase with rising oxygen levels. The effect is less dominant for chipboard LD at high fluxes but becomes important at low fluxes. Close the heat flux ignition limit values decrease rapidly for both chipboard types. Thickness and density do not influences this parameter significantly.

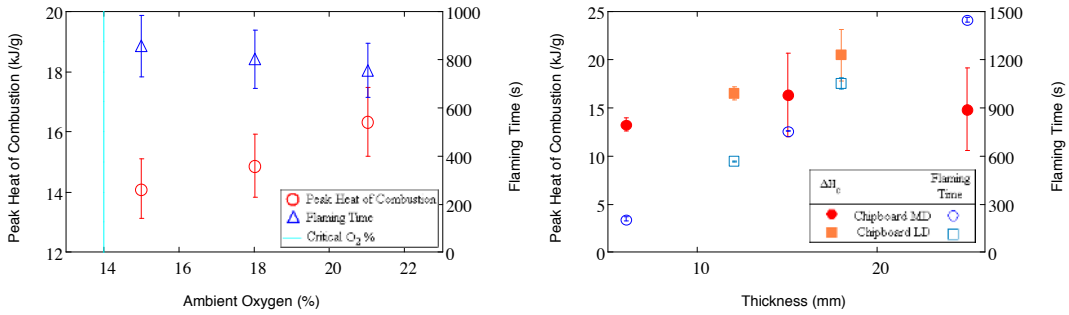

Figure 5.17 Peak instantaneous heat of combustion and flaming time for *a) 15 mm Chipboard MD under varying O_2 concentration at 30 kW/m^2 during char formation regime b) varying chipboard thicknesses and densities at 30 kW/m^2 and 21% O_2*

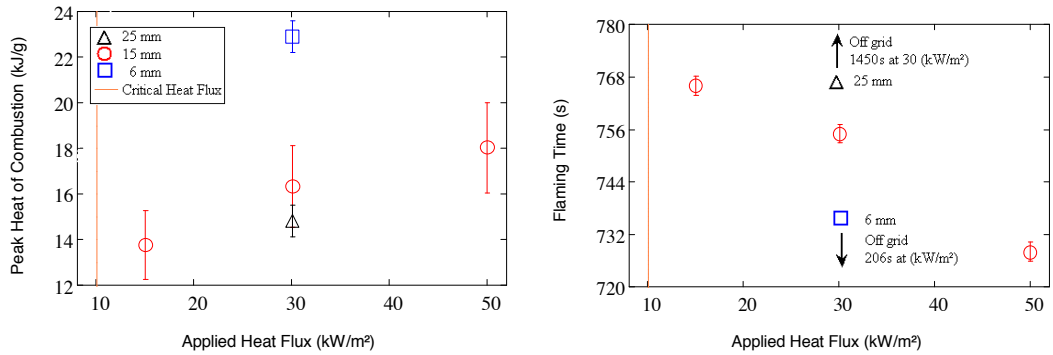

Figure 5.18 Chipboard MD at 21%O2 with varying heat insults ***a) Instantaneous peak heat of combustion and b) Flaming time***

Flaming times are presented on Figure 5.17, Figure 5.18 b), and Figure 5.19. Although not specific to the char formation regime, flaming time takes into account the char forming, thick char and burn out peak regime. Most important are the direct linear effects of thickness and heat insult on flaming time for both chipboard types. Increasing thicknesses and decreasing heat flux levels increase flaming time because more time is required for all the material to burn away. Decreasing oxygen levels is seen to slightly increase the flaming time but is not a dominant effect. Close to the ignition limit for both heat flux and oxygen concentration flaming time rapidly decreases.

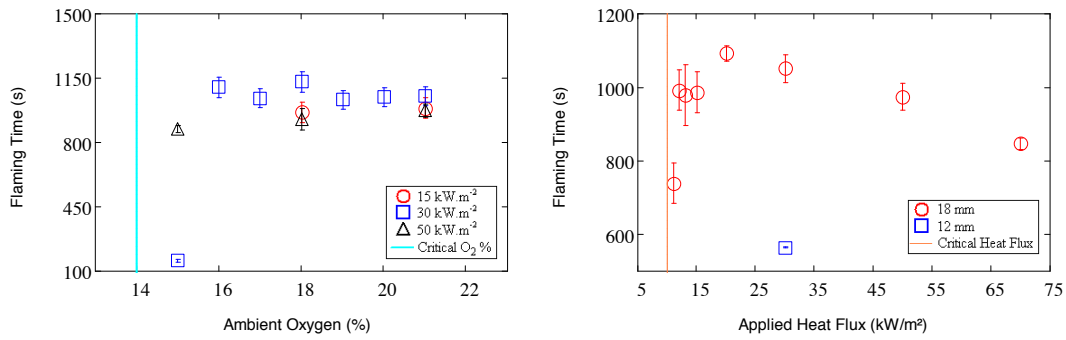

Figure 5.19 Flaming time for Chipboard LD under ***a) varying O_2 concentration and heat insults and b) varying heat insults and thicknesses at 21% O_2***

Thick Char Regime

The thick char regime is characterized by the observation that a near steady state is reached in the mass loss rate. This presents the opportunity to gain a better understanding of the effect of the different experimental conditions based on the dynamics of the char layer. Since the char layer has already been formed, the heat transfer between the unburnt material, the char, the flame and the heat being applied have reached equilibrium at this stage.

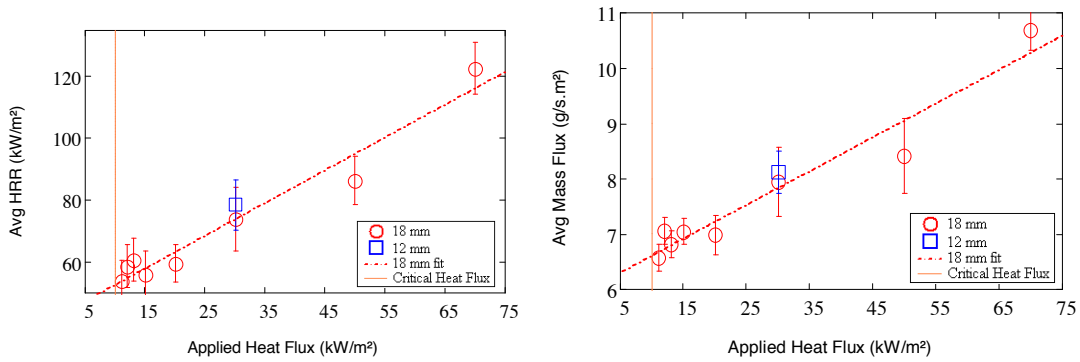

Figure 5.20 ***a) Average HRR and b) Average Mass flux***
for Chipboard LD under 21% O_2 with varying heat insults in thick char regime

Applied heat flux effect for chipboard LD and chipboard MD is seen in Figure 5.20 and Figure 5.21 correspondingly. Similar effects are seen in both. An expected direct linear relationship is seen for both HRR and mass flux against imposed heat insult. The more heat is applied, the faster the material degrades and gives off flammable gases which are burnt. Neither material ignites below 11 kW/m^2. Differences in thicknesses are observed with Chipboard MD which is more visible in Figure 5.23 b).

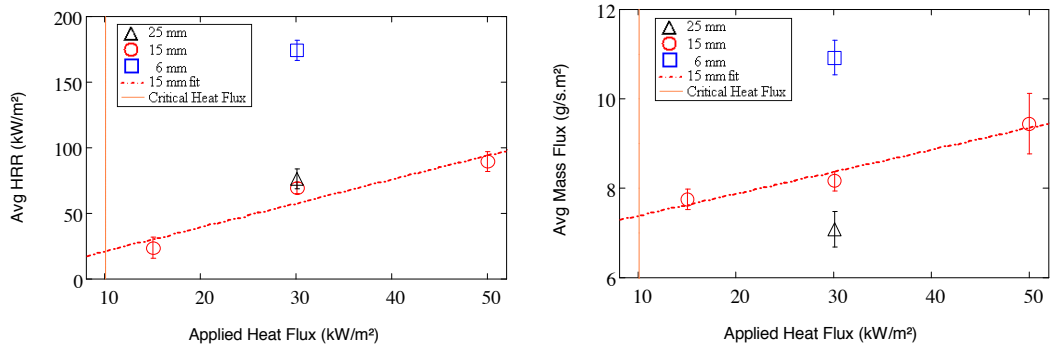

Figure 5.21 ***a) Average HRR*** **and** ***b) Average Mass flux***
for Chipboard MD under 21% O2 with varying heat insults in thick char regime

The effect of increasing oxygen on the material, similarly to increasing heat flux, increases the burning rate by allowing oxygen to be more readily available for combustion; hence, increase the fuel burning. The oxygen level affects the flame more than anything because of this. With more available oxygen the flame grows and radiates more heat which is visible during tests because of the flame colour change. As the oxygen reduces, the flame becomes darker and more sooty due to increased incomplete combustion of the fuel;.at higher oxygen concentration the flame becomes more vividly orange. As the critical oxygen level limit in which we can sustain a flame is approached, what is observed is a rapid decrease in the energy being released. The 15 kW/m^2 sample at 15% O_2 for chipboard LD did not ignite, so the critical limit at this heat flux is approached much sooner.

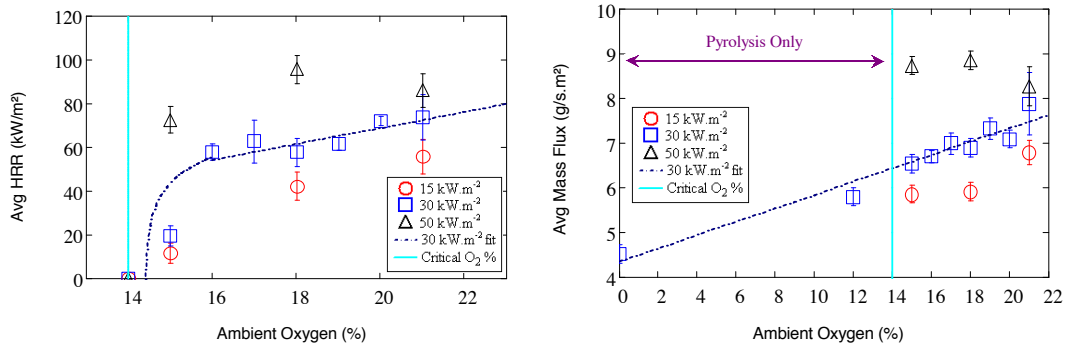

Figure 5.22 ***a) Average HRR*** **and** ***b) Average Mass flux***
for Chipboard LD with varying oxygen concentrations and heat insults in thick char regime

Mass flux, like HRR, is similarly affected by the oxygen levels as can be seen in Figure 5.22 b) for chipboard LD and Figure 5.23 a) for chipboard MD. Values are included for Chipboard LD under the critical oxygen limit (14% O_2) because, although it is not flaming combustion, the smouldering combustion process reaches a similar steady state period. What is most notably observed is that it continues to react because of the applied heat; although the gases are not igniting into a flame.

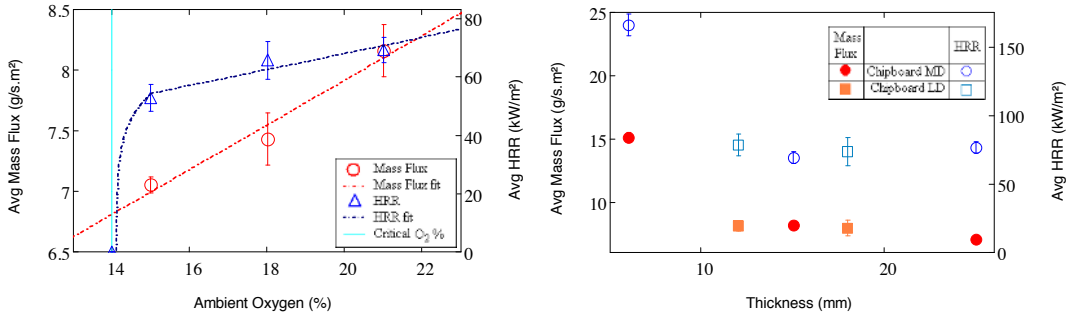

Figure 5.23 Average HRR and Average Mass Flux at 30 kW/m^2 for *a) 15mm Chipboard MD under varying oxygen concentration b) varying chipboard thicknesses and densities at 21% O_2*

Figure 5.23 b) presents the differences between density and thickness of chipboard. Most important is that little difference is actually observed between the two thicknesses at this scale. The two material thicknesses used in this study the most, 15mm Chipboard MD and 18mm Chipboard LD, are already in the thermally thick regime.

Average values during the thick char regime for instantaneous heat of combustion are presented in Figure 5.24 and Figure 5.25. Under varying O2 concentrations, values are fairly constant except close to the ignition limit for both Chipboard types and at low heat fluxes values drop earlier on. With varying thicknesses for both chipboard types the values do not change much. Under increases in heat insults, values of heat of combustion increase linearly.

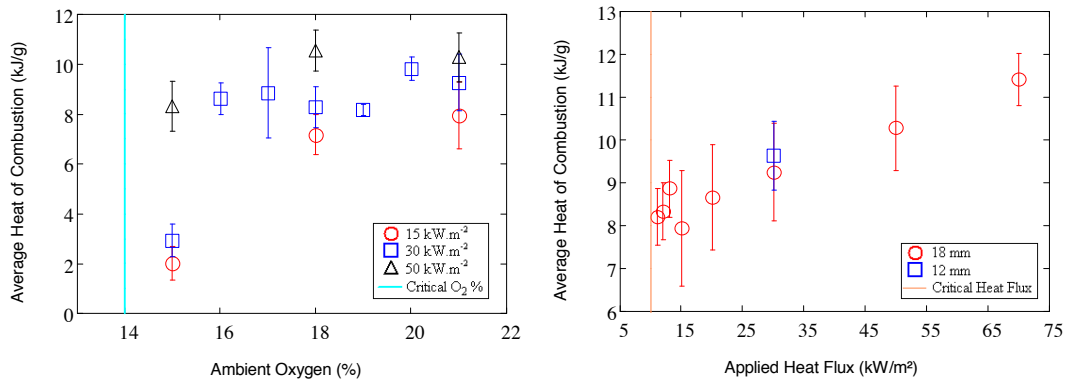

Figure 5.24 Average Instantaneous heat of combustion for Chipboard LD ***a) 18mm varying O_2 concentration and b) varying heat insults at 21% O_2***

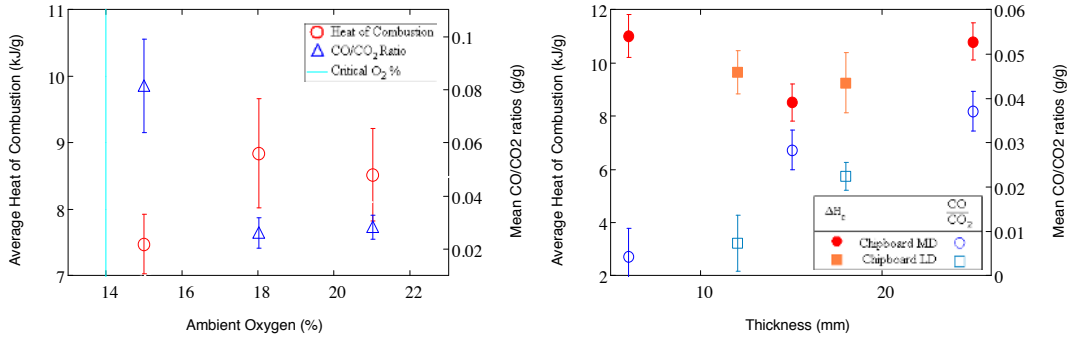

Figure 5.25 Average Instantaneous heat of combustion and Mean CO/CO_2 ratios at 30 kW/m^2 for ***a) 15mm Chipboard MD varying O_2 concentration b) varying chipboard thicknesses and densities***

Figure 5.25 and Figure 5.26 show values for mean CO/CO_2 ratio during the thick char regime. Under increasing oxygen concentrations, values drop steadily for both chipboard types. Values also drop with decreasing thicknesses for both chipboard types with Chipboard LD having slightly smaller values overall. Lastly, with increasing heat insult, mean CO/CO_2 ratios decrease as well.

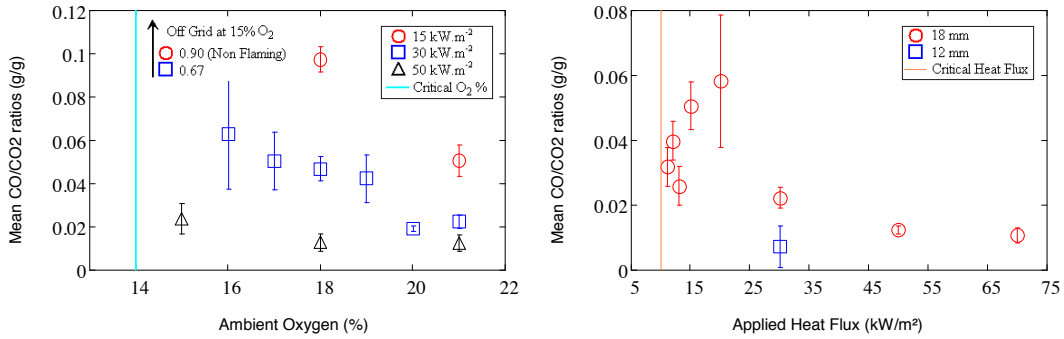

Figure 5.26 Mean CO/CO2 ratio for Chipboard LD under *a) varying oxygen concentration and heat insults (15mm thick) and b) varying heat insults and thicknesses*

Post Flaming Regime

During the post flaming regime the flame has extinguished and the material undergoes smouldering combustion. Average mass flux values for this regime under varying heat insults are shown in Figure 5.27. Values are mostly unaffected by the heat flux level except close to the critical limit where they start to decrease.

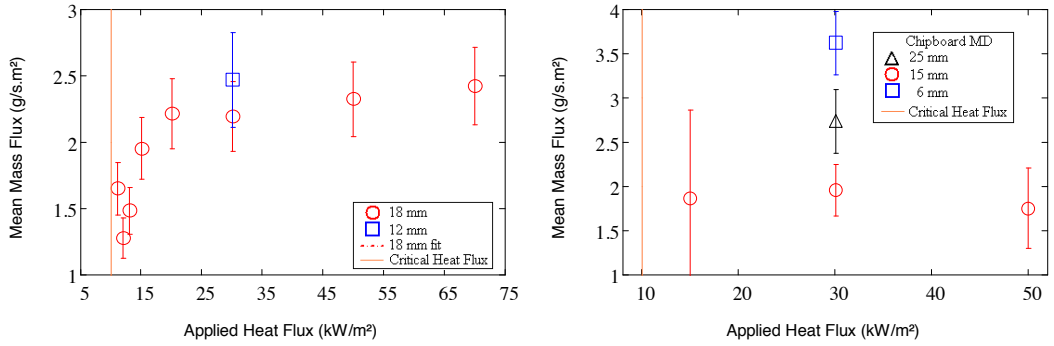

Figure 5.27 Mean mass flux under varying heat insults at 21% O_2 for *a) Chipboard LD and b) Chipboard MD*

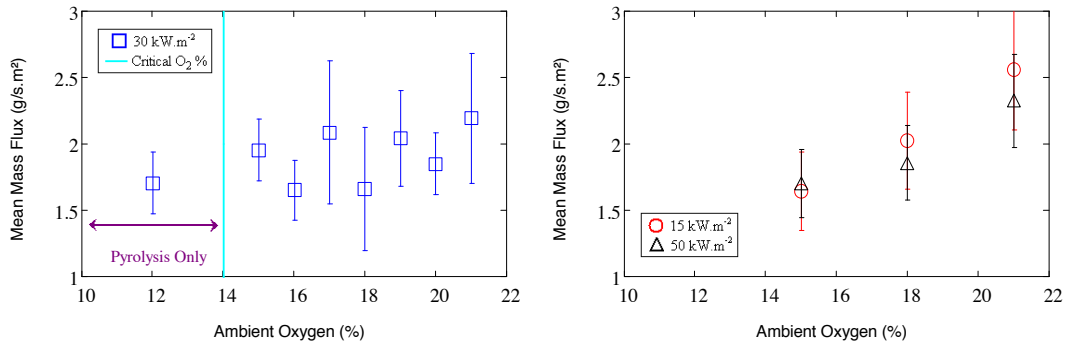

Figure 5.28 Mean mass flux for Chipboard LD under varying oxygen concentrations

The effect of oxygen concentration and thickness on mean mass flux values during this regime can be seen in Figure 5.28 and Figure 5.29. Values decrease slightly with reduced O2 levels. Chipboard thickness and density does not seem to have a significant effect.

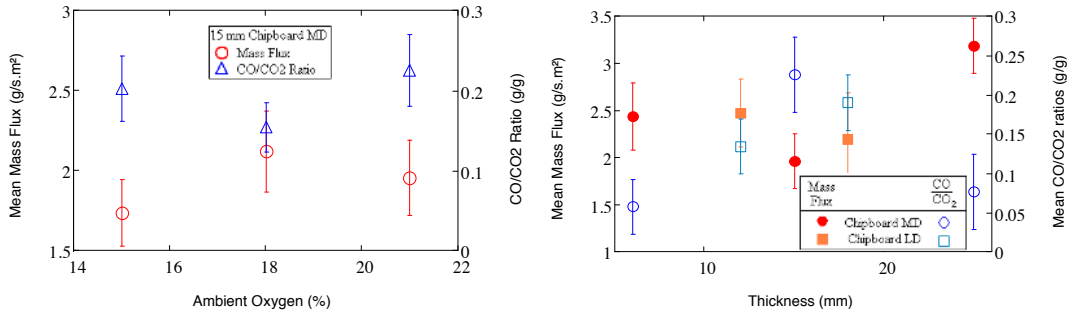

Figure 5.29 Mean mass flux and CO/CO_2 ratio for *a) 15 mm Chipboard MD under varying O_2 concentration at 30 kW/m2 and b) with varying thicknesses and densities at 30 kW/m2 and 21% O_2*

Figure 5.29 and Figure 5.30 show CO/CO2 ratios during this regime. For chipboard LD, greater oxygen levels and heat flux levels decrease CO/CO2 ratios. The effect is not apparent with Chipboard MD. Thickness difference does not show much change either.

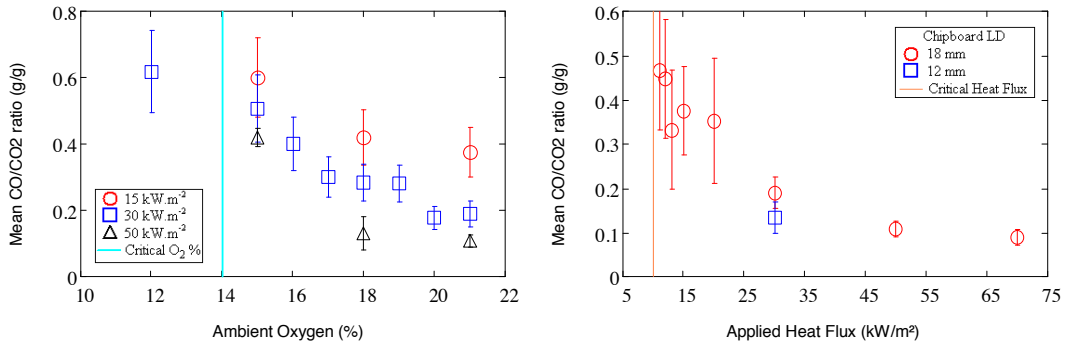

Figure 5.30 Mean CO/CO_2 ratio for Chipboard LD under *a) varying O_2 concentrations and heat insults and b) varying heat insults and thicknesses at 21% O_2*

At Ignition and Flame-Out

Mass flux at ignition values are presented on Figure 5.31, Figure 5.32 and Figure 5.33 b). Overall values do not vary much with varying oxygen levels for both chipboard types. With increasing heat insults, mass flux increases steadily. Values are also higher for the smaller thicknesses and higher density. Mass flux values at flameout are shown on Figure 5.32, Figure 5.33 b) and Figure 5.34. Under varying heat insults oxygen levels, mass flux values do not change significantly for either chipboard type. Values are also higher for the smaller thicknesses and chipboard MD.

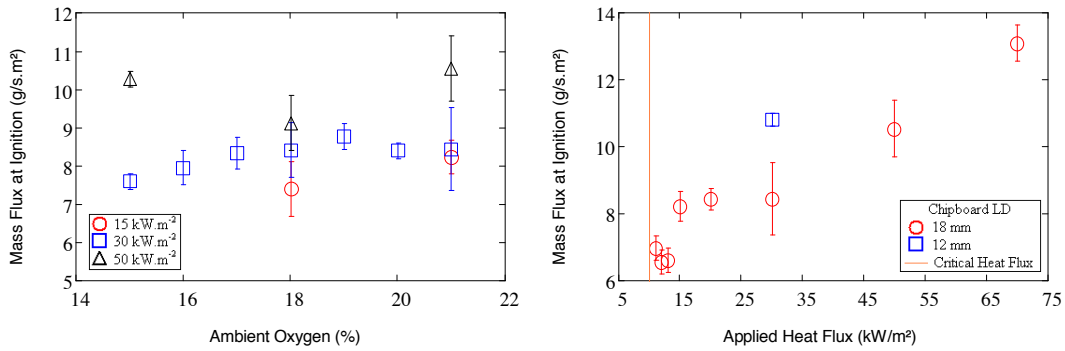

Figure 5.31 Mass flux at ignition for Chipboard LD under *a) varying O_2 concentrations and heat insults and b) varying heat insults and thicknesses at 21% O_2*

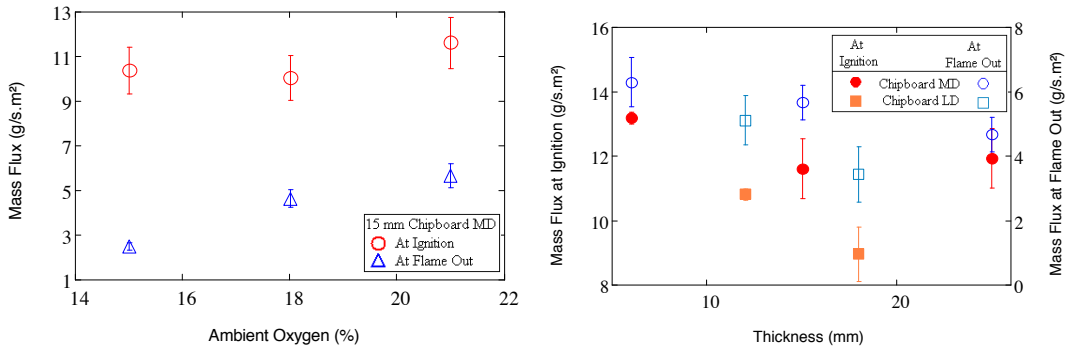

Figure 5.32 Mass flux at ignition and flameout for *a) 15 mm Chipboard MD under varying O_2 concentration at 30 kW/m2 and b) with varying thicknesses and densities at 30 kW/m2 and 21% O_2*

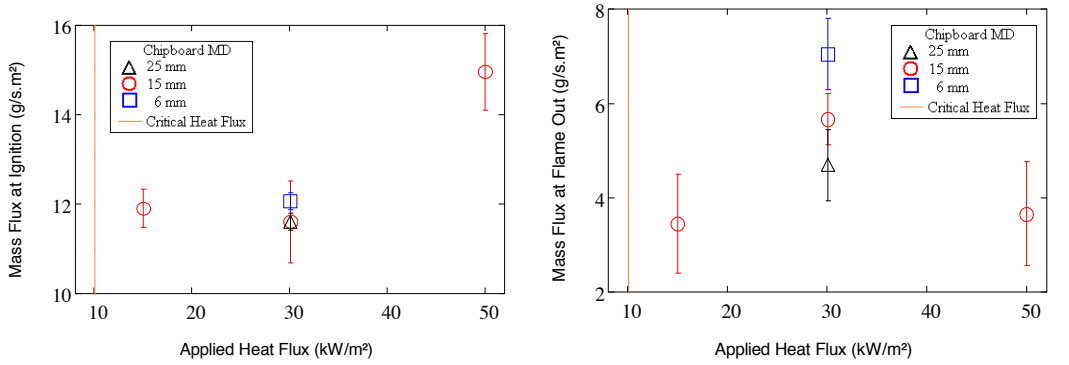

Figure 5.33 *a) Mass flux at ignition and b) Mass flux at flameout* for Chipboard MD under 21% O2 with varying heat insults

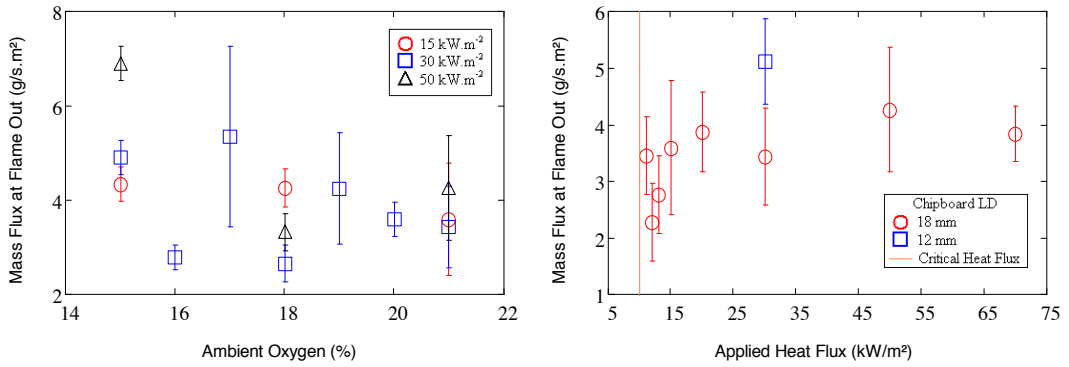

Figure 5.34 Mass flux at flameout for Chipboard LD under *a) varying O_2 concentrations and heat insults and b) varying heat insults and thicknesses at 21% O_2*

Discussion

Heat flux levels affect the solid burning so the effect was seen all throughout, both during flaming and non flaming regimes. With increased heat insults, increase in both MLR and HRR were seen in all regimes, ignition time and flaming time was reduced, and lower CO-to-CO_2 ratios were recorded. An important aspect was with increasing heat insults; the effect of other variables like oxygen level became less and less significant. Thickness and material density did not affect the burning behavior significantly while the material was in the thermally thick regime. Time to ignition and flaming time were the most important changes affected by thickness due to the larger amount of material.

Oxygen concentration is seen to be very important during flaming combustion. Both during the char formation and thick char regime, lowering oxygen levels reduces HRR and MLR steadily and close to the ignition limit the effect is enhanced greatly. With more oxygen readily available, more volatiles combust faster hence releasing more energy and transferring more heat back to the solid. At lower heat fluxes, this effect is seen to be more dominant. CO-to-CO_2 ratios corroborate this behavior as well. With lower oxygen levels, the flame struggles to fully combust all of the volatiles that are being emanated by the fuel hence producing more CO due to incomplete combustion and therefore allowing for higher CO-to-CO_2 ratios. The effect is more pronounced at lower heat insults. The effective heat of combustion reflects this as well especially at low fluxes. Due to fuel not being fully burned, the total amount of energy allowed to be obtained from the fuel is reduced. In the pre ignition regime, during pyrolysis, oxygen effect is seen to be minimal. Time to ignition of the material was unaffected by changes in oxygen levels. The effect is however important in the post flaming regime, during which the material undergoes smouldering combustion. A steady rise is observed in CO-to-CO_2 ratios which increases at low heat fluxes. The effect is reflected in the mass loss however, due the low mass at this point, it is believed that the variability of the load cell does not allow to fully capture this behavior.

Drysdale [2] and Spearpoint et al [15] report average critical heat flux for wood: $12kW.m^{-2}$ and $10kW.m^{-2}$ respectively in ambient conditions. Values of critical oxygen concentration for re-ignition of white maple at $30kW.m^{-2}$ were reported by Xin et al [16] as 15.41% O_2 by volume. The range agrees well with the values encountered here $11kW.m^{-2}$ and 16% O_2 for flaming ignition for chipboard. This suggests that the mechanisms leading to flaming ignition are similar to wood samples in those experiments. Xin et al [16] concludes that external radiant heat flux has a significant effect on the limiting oxygen concentration for ignition (LOC). It is pointed out that above $30kW.m^{-2}$, the LOC appears to be insensitive to further increases of the external radiant heat flux, a behavior observed here as well. The enhanced effects of oxygen concentration at low heat insults here also corroborate the importance oxygen levels have the lower the external applied heat flux is.

Conclusions

Flammability of chipboard has been studied with varying oxygen levels, heat insults, material thickness and density. Critical limits for ignition were found to be 14% O_2 above 30 kW/m^2 and 10 kW/m^2 at 21% O_2. Char formation is seen to have a large effect on the burning dynamics of chipboard. Once the first char formation has been established on the surface of the solid a regime where chipboard steadily burns has been identified. HRR, MLR and CO/CO_2 ratio are seen to be significantly affected by both changes in heat insults and oxygen levels. Material thickness and density do not seem to affect HRR and MLR significantly as long as the material is thermally thick. During pyrolysis, chipboard seems to be mostly unaffected by changes in oxygen concentrations, the effect was significant mostly during flaming showing the importance of the oxygen effect on the flame itself.

Acknowledgements

Thanks to Cesar Alvarez (Pelikano, Ecuador) for providing part of the chipboard samples and the BRE Trust, UK for financial support for this work. Thanks also to Professor Jose Torero for access to the Fire Science Laboratory and FM global for the donation of the Fire Propagation Apparatus were these tests were carried out.

References

[1] Fire safety in timber buildings - Technical guideline for Europe, SP Technical Research Institute of Sweden, SP Report 2010:19.

[2] Drysdale, D. An Introduction to Fire Dynamics (Wiley, 1998)

[3] Yang, L., Chen, X., Zhou, X. and Fan, W. The pyrolysis and ignition of charring materials under an external heat flux. Combustion and Flame, 2003, 133:407-413.

[4] Wichman, I. S., Atreya, A. A simplified model for the pyrolysis of charring materials. Combustion and Flame, 1987, 68: 231-247.

[5] Beaulieu, P. A. and Dembsey, N. A. Effect of oxygen on flame heat flux in horizontal and vertical orientation. Fire Safety Journal, 2008, 43: 410-428.

[6] Kashiwagi, T., Ohlemiller,T., Werner, K. Combust. Flame, 69 (1987), pp. 331–345.

[7] BS EN 312, Particleboards – Specifications, BSI Standards Publication, London,UK, 2010.

[8] MDP Tropical – A new generation of board, Pelikano, from http://www.pelikano.com/index.php

[9] ASTM E 2058, Standard Methods of Test for Measurement of Synthetic Polymer Material Flammability Using a Fire Propagation Apparatus (FPA), American Society for Testing Materials, Philadelphia, 2003.

[10] Tewarson, A. in: Generation of Heat and Chemical Compounds in Fires, SFPE Handbook of Fire protection Engineering, The National Fire Protection Association Presss, 2002, pp. 3-82-3-161.

[11] Ris, J. L. and Khan, M. M. A Sample Holder for Determining Material Properties. Fire and Materials, 2000, 24: 219-226.

[12] Parametric Technology Corporation. (2007) Users's Guide Mathcad 14.0, from http://www.ptc.com/products/mathcad/

[13] Carvel, R., Steinhaus, T., Rein, G. and Torero. Determination of the flammability properties of polymeric materials: A novel method. Polymer Degradation and Stability, 2011, 96:314-319.

[14] Babrauskas, V. in: Heat Release Rates, SFPE Handbook of Fire protection Engineering, The National Fire Protection Association Presss, 2002, Section Three Hazard Calculation: pgs 3-1-3-37.

[15] Spearpoint, M. J., Quintieri, J. G. Predicting the piloted ignition of wood in the cone calorimeter using an integral model – effect of the species, grain orientation and heat flux. Fire Safety Journal, 36 (2001) 391-415.

[16] Xin, Y., Khan, M. M. Flammability of combustible material in reduced oxygen environment. Fire Safety Journal, 42 (2007) 536-547.

Chapter 6

Conclusions

Calorimetric studies are presented that illustrate the use of these devices to study the effect of varying environmental and fuel conditions on the burning of different fuels. The studies presented here are done in order to demonstrate capability and relevance of the state of the art in these small scale tests that enable us to gain a better understanding of the combustion dynamics involved during the burning of some these complex fuels. They also show how repeatable reliable data can be obtained for these. Methodologies are presented in these studies that can help us study the effects of various conditions not just the ones illustrated herein. Using devices such as the Fire Propagation Apparatus (FPA), allows for versatile small scale calorimetric experiments to be performed that help us understand these burning processes.

In Chapter 2, the burning behavior of live and dead needle samples is studied here for the first time. The fire calorimetry results show good repeatability and demonstrated that the difference in burning dynamics of live and dead pine needles are significant and can be quantified and understood. Assumptions commonly made such as the effect of moisture content, adds uncertainty in our results but using these devices were able to ascertain its effect. Moisture content was not as important for dead needles but very important for live needles. It was also only by testing these materials that we could gain understanding how common experimental practices such as oven drying a sample can have a significant effect on the burning dynamics. Once live needles were oven-dried, its fire behavior resembled more that of dead needles rather than fresh live ones; nonetheless, the loss of volatiles and other physicochemical changes to the needles produced during the oven drying process lead to significant differences in the burning

behavior. Aged samples presented an improvement as water loss happens at lower temperatures; composition seems less likely to be affected.

In Chapter 3, fuel load and species effect of pine needles were studied. It was through this study that the importance of interrelation between varying conditions is shown to be important during burning; most notably, the relation between fuel load and flow conditions. Fuel load is likely to be the most essential condition to know as it gives and a direct indication of the intensity of the fire followed by flow and moisture content. At higher fuel loads, flow conditions become much more important in regards to intensity of the fire. Given the relation between flow and density of the fuel; however, flow can either aid or determent ignition times, behavior observed in Chapter 2 as well, which most likely will mean the same relation will hold if we were to look at flame spread in this regard. Fuel condition interactions shown indicate it is very important to know what density, heat insult, moisture and flow conditions the burn is taking place as changing one of these can mean the effect of the other rendered unimportant or accentuated.

In Chapter 4, we were able to test theories that we also do not have full understanding of. In order to study differences in flammability between different leaf species, calorimetric tools were used to analyze and characterize these species against leaf morphology. Various combustion parameters can give us indication and understanding of fire growth, speed and intensity. Ignition time and time to peak HRR tells us about ignitability, fire growth and speed. Gas combustion and mass flux measurements also tell us about fire growth, energy content of the fuel and sustainability of the fire. All the parameters contributed to telling us there is a correlation between increased flammability and smaller leaf area (ie narrow leaved plants) and increased flammability with larger surface area-to-volume ratios. Between the two morphologies, surface area-to-volume ratio presents a stronger fit with the data. Through these results, though, realization of natural behaviors such as different leaf morphology connections to other variables was made. It is suggested study on vegetation composition and its relation to leaf morphology will give us a better understanding of these relations to ascertain whether

this change in flammability is only due to a change in morphology configuration or if because different compositions will affect the structure of the plant and leaves this will also partake in the reason behind the increased combustion behavior.

Effect of oxygen concentration on the burning of fuels, is an environmental conditions fire science still does not fully understand. Using the FPA, the study of this condition is made possible. In Chapter 5, flammability of chipboard has been studied with varying oxygen levels, heat insults, material thickness and density. Critical limits for ignition were found to be 14% O_2 above 30 kW/m^2 and 10 kW/m^2 at 21% O_2. Char formation is seen to have a large effect on the burning dynamics of chipboard. Once the first char formation has been established on the surface of the solid a regime where chipboard steadily burns has been identified. HRR, MLR and CO/CO_2 ratio are seen to be significantly affected by both changes in heat insults and oxygen levels. Material thickness and density do not seem to affect HRR and MLR significantly as long as the material is thermally thick. During pyrolysis, chipboard seems to be mostly unaffected by changes in oxygen concentrations, the effect was significant mostly during flaming showing the importance of the oxygen effect on the flame itself.

Most notably, the works highlight the importance of first establishing the dynamics of the combustion process in order to be able to extract the combustion parameter that are needed in order to model fires better in both wildland and built environments. With this taken into account, we still must be cautious of applying this knowledge to large scale fires as other large scale effects can also undermine or enhance these relations.

Scaling analysis for fires has certainly been a subject of numerours papers and reviews. Various subjects have been addressed in detail to provide a series of scaling laws currently in use [1]. Quintiere's work in [2] is a classic attempt to develop a comprehensive set of non-dimensional parameters using Buckingham Pi theorem. Zukoski presents a good review on the classic attempts of scaling mainly associated to pool fires, entrainment and compartments fires in [3]. One of the main problems,

however, is scaling and non-dimensional parameter have been mostly derived for a particular application meaning each specific case has to be considered which is not ideal. Characterization of a length scale for the combustion regime, radiation and turbulence in each problem is one of the main issues associated with scaling [1]

Recommendation for further works suggested here would be in the area of actual applicability of the data and the current use of the existing data to link this gap. Are the input variables being used for modeling representative of the processes taking place is believed to be one of the question left unanswered. There has been a reasonable amount of research on small scale and large scale tests but little research in actually trying to link the two. Due to the different length scales and problems with scaling in general, a shortage of linkage between these two hinders the overall research aim.

Many of the studies going at the small scale are maybe not representative or applicable but this cannot be known unless we see the effects of varying one parameter at the small scale and the corresponding parameter at the large scale. Torero's research in [1] is certainly an improvement on this in order to observe the problems with scaling and applications to ignition of solid fuels.

Sensitivity analysis on the different parameters affecting the combustion process is one of the necessary researches to be able to accomplish this. Jahn's [4] and Bal's [5] work could certainly be used for this aim. Their work and methodology on sensitivity of different parameters is what is needed to understand how small changes in one parameter can change the fire dynamics of the problem.

The resources are certainly there like the wide range of tests at the small scale presented here under a wide different environmental and fuel conditions, methods to extract parameters pertaining to combustion such as Gpyro [6], and large scale tests like those presented in the Dalmarnok tests [7] for built environments and Santoni's tests [8] for wildland fires. An analysis on the different parameters at both scales could certainly

provide an improvement into our understanding of the different scales and factors affecting combustion in each.

References

[1] Torero, J. L., Simeoni, A., "Heat and mass transfer in fires: scaling laws, ignition of solid fuels and application to forest fires," *The Open Thermodynamics Journal*, 2010, **4**, 145-155.

[2] Quintiere, J.G., "Scaling Applications in Fire Research," *Fire Safety Journal*, 1989, **15**, pp.3-29.

[3] Zukoski, E.E., "Properties of Fire Plumes," Chapter 3, *Combustion fundamentals of Fire*, G. Cox Editor, Academic Press, pp.101-220, 1995.

[4] Jahn, W., "Inverse modelling to forecast enclosure fire dyanmics" The University of Edinburgh, Accesible at http://www.era.lib.ed.ac.uk/handle/1842/3418 , 2010.

[5] Bal, N., rein, G., "Numerical investigation of the ignition delay time of a translucent solid at high radiant heat fluxes," *Combustion and Flame*, 2011, **158(6)**, 1109–1116.

[6] Generalized pyrolysis model for combustible solids: http://code.google.com/p/gpyro

[7] Rein, Abecassis-Empis, and Carvel, editors. "The Dalmarnock Fire Tests: Experiments and Modelling". ISBN 978-0-9557497-0-4. The University of Edinburgh, Accesible at www.era.lib.ed.ac.uk/handle/1842/2037, 1st edition, 2007.

[8] Santoni, P. A., Simeoni, A., Rossi, J. L., Bosseur, F., Morandini, F., Silvani, X., Balbi, J. H., Cancelleri, D., Rossi, L., " Instrumentation of wildland fire: Characterisation of a fire spreading through a Mediterranean shrub," *Fire Safety Journal*, 2006, **41**, 171-184.

Appendix A:

Flammability parameter graphs for live and dead Pinus halepensis needles under two different heat insults for Chapter 2

50 kW/m^2 vs 25 kW/m^2

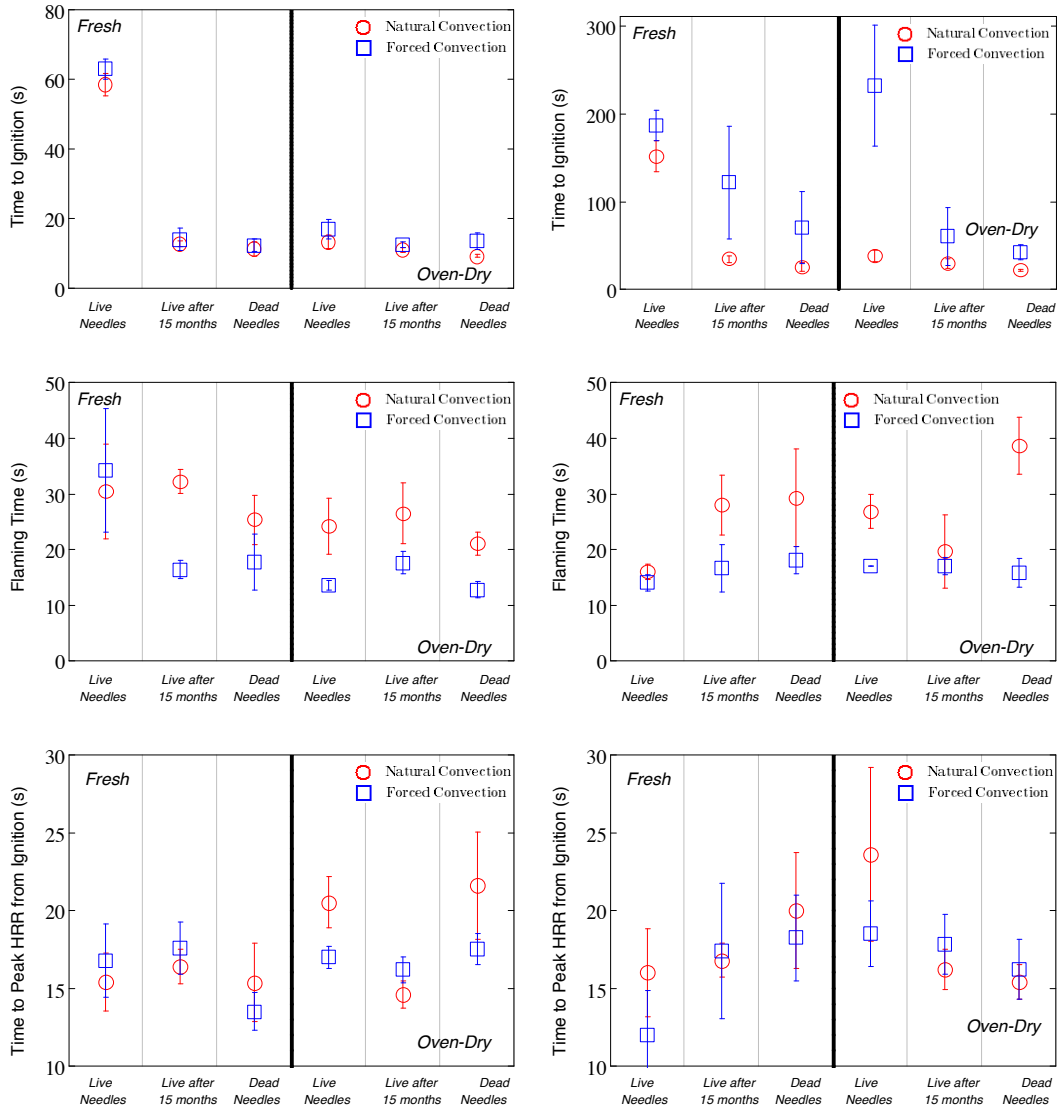

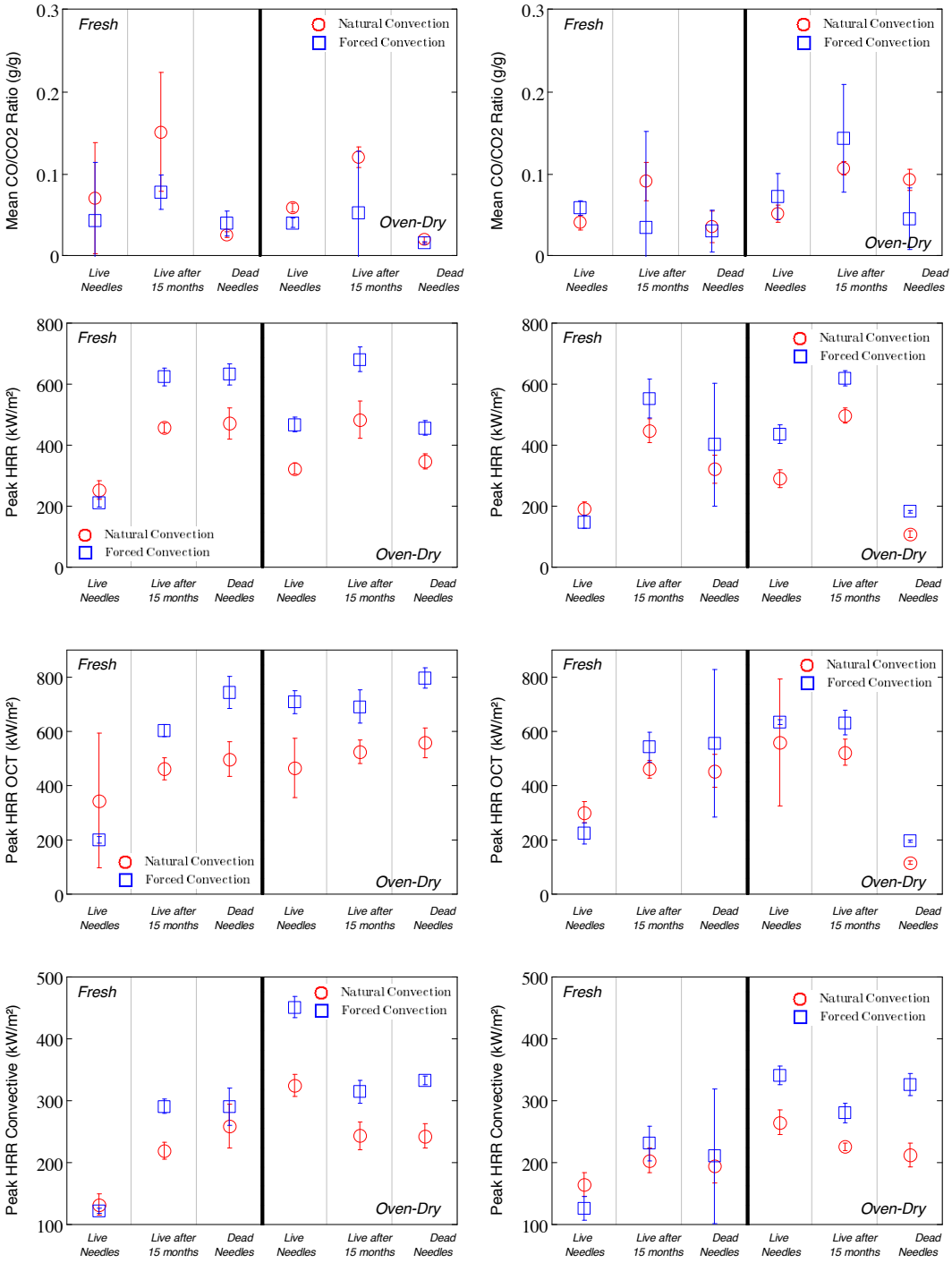
Mean CO/CO2 Ratio (g/g)
Peak HRR (kW/m²)
Peak HRR OCT (kW/m²)
Peak HRR Convective (kW/m²)
Fresh
Oven-Dry
Natural Convection
Forced Convection
Live Needles
Live after 15 months
Dead Needles

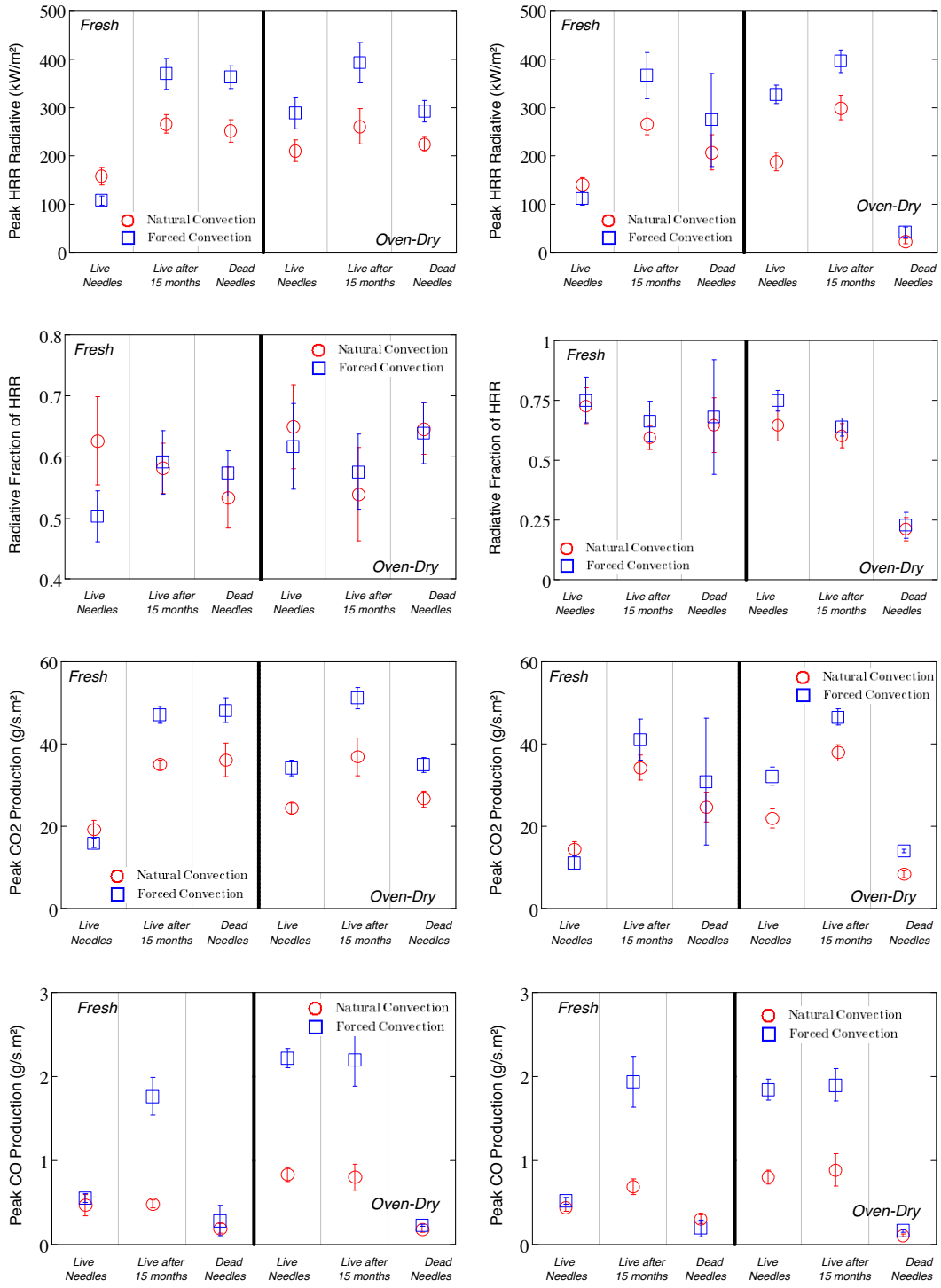
Peak HRR Radiative (kW/m²)
Radiative Fraction of HRR
Peak CO2 Production (g/s.m²)
Peak CO Production (g/s.m²)
Fresh
Oven-Dry
Natural Convection
Forced Convection
Live Needles
Live after 15 months
Dead Needles

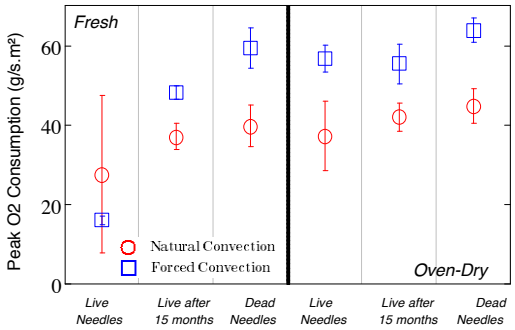
Fresh
Oven-Dry
Natural Convection
Forced Convection
Peak O2 Consumption (g/s.m²)
0
20
40
60
Live Needles
Live after 15 months
Dead Needles
Live Needles
Live after 15 months
Dead Needles

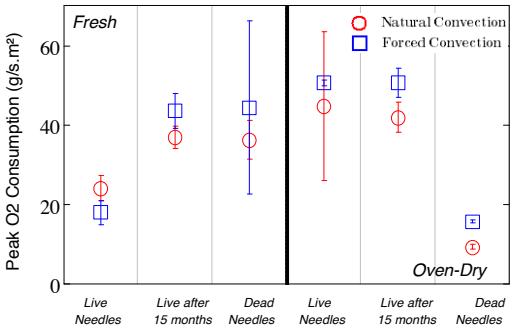
Fresh
Oven-Dry
Natural Convection
Forced Convection
Peak O2 Consumption (g/s.m²)
0
20
40
60
Live Needles
Live after 15 months
Dead Needles
Live Needles
Live after 15 months
Dead Needles

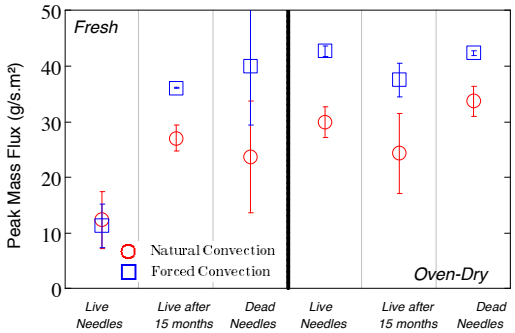
Fresh
Oven-Dry
Natural Convection
Forced Convection
Peak Mass Flux (g/s.m²)
0
10
20
30
40
50
Live Needles
Live after 15 months
Dead Needles
Live Needles
Live after 15 months
Dead Needles

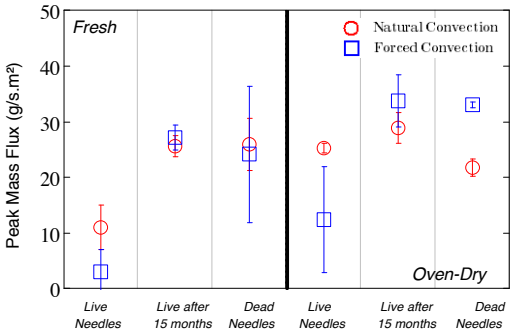
Fresh
Oven-Dry
Natural Convection
Forced Convection
Peak Mass Flux (g/s.m²)
0
10
20
30
40
50
Live Needles
Live after 15 months
Dead Needles
Live Needles
Live after 15 months
Dead Needles

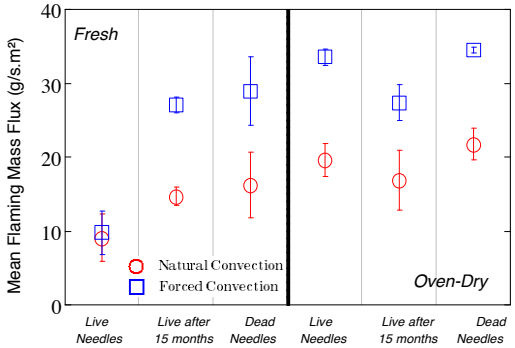
Fresh
Oven-Dry
Natural Convection
Forced Convection
Mean Flaming Mass Flux (g/s.m²)
0
10
20
30
40
Live Needles
Live after 15 months
Dead Needles
Live Needles
Live after 15 months
Dead Needles

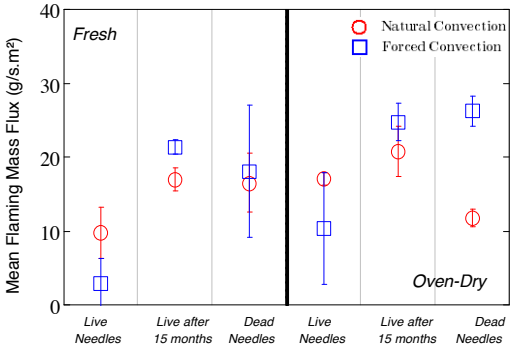
Fresh
Oven-Dry
Natural Convection
Forced Convection
Mean Flaming Mass Flux (g/s.m²)
0
10
20
30
40
Live Needles
Live after 15 months
Dead Needles
Live Needles
Live after 15 months
Dead Needles

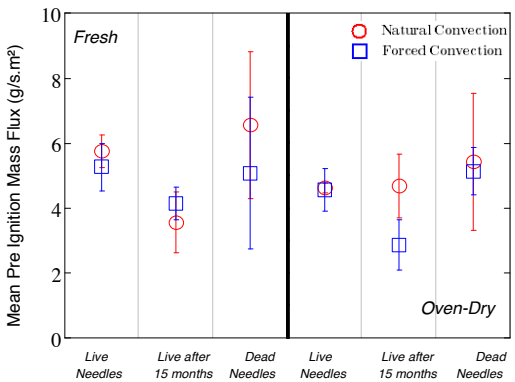
Fresh
Oven-Dry
Natural Convection
Forced Convection
Mean Pre Ignition Mass Flux (g/s.m²)
0
2
4
6
8
10
Live Needles
Live after 15 months
Dead Needles
Live Needles
Live after 15 months
Dead Needles

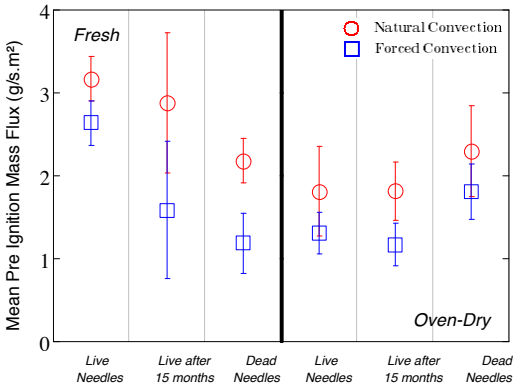
Fresh
Oven-Dry
Natural Convection
Forced Convection
Mean Pre Ignition Mass Flux (g/s.m²)
0
1
2
3
4
Live Needles
Live after 15 months
Dead Needles
Live Needles
Live after 15 months
Dead Needles

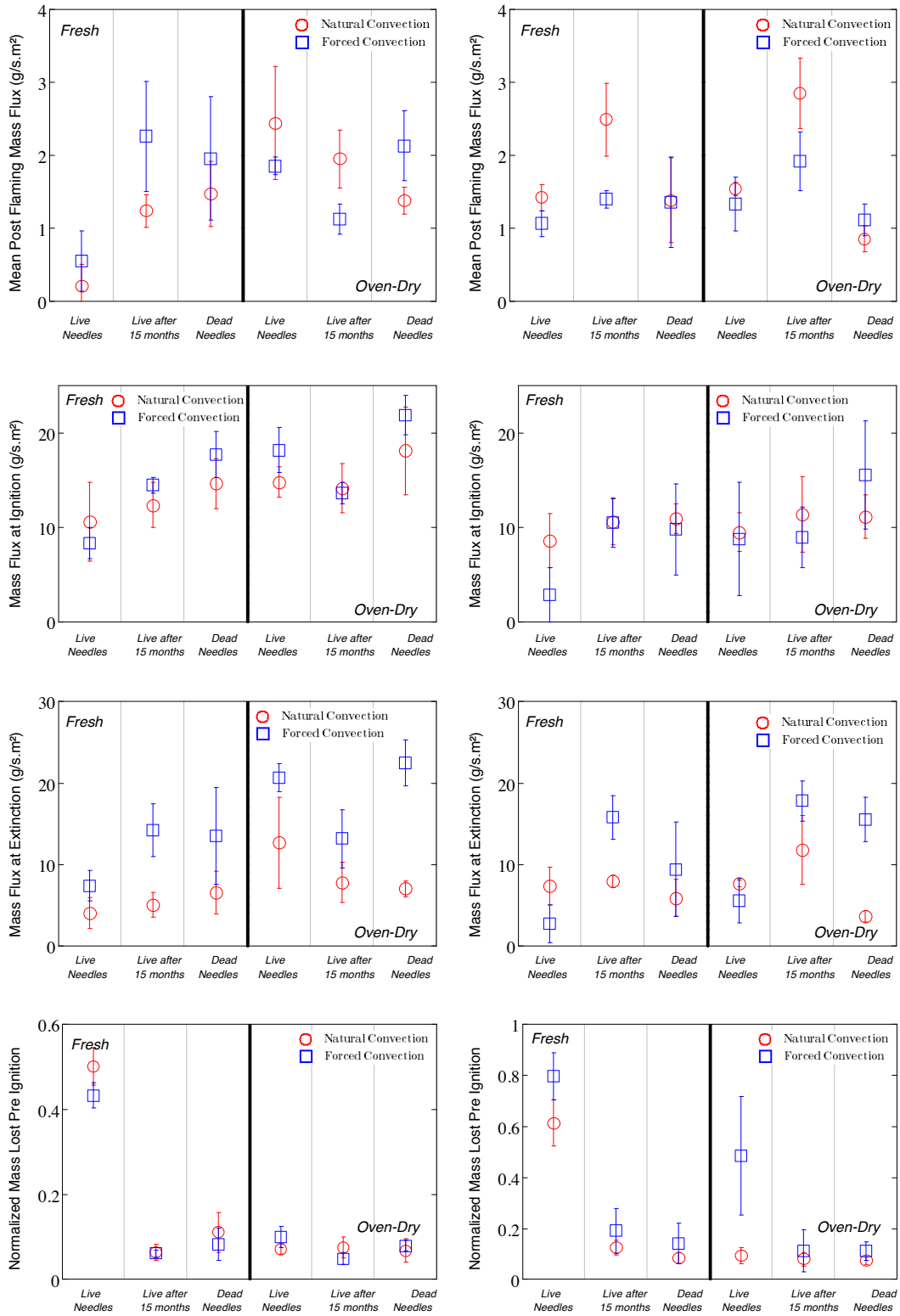
Mean Post Flaming Mass Flux (g/s.m²)
Mass Flux at Ignition (g/s.m²)
Mass Flux at Extinction (g/s.m²)
Normalized Mass Lost Pre Ignition
Fresh
Oven-Dry
Natural Convection
Forced Convection
Live Needles
Live after 15 months
Dead Needles

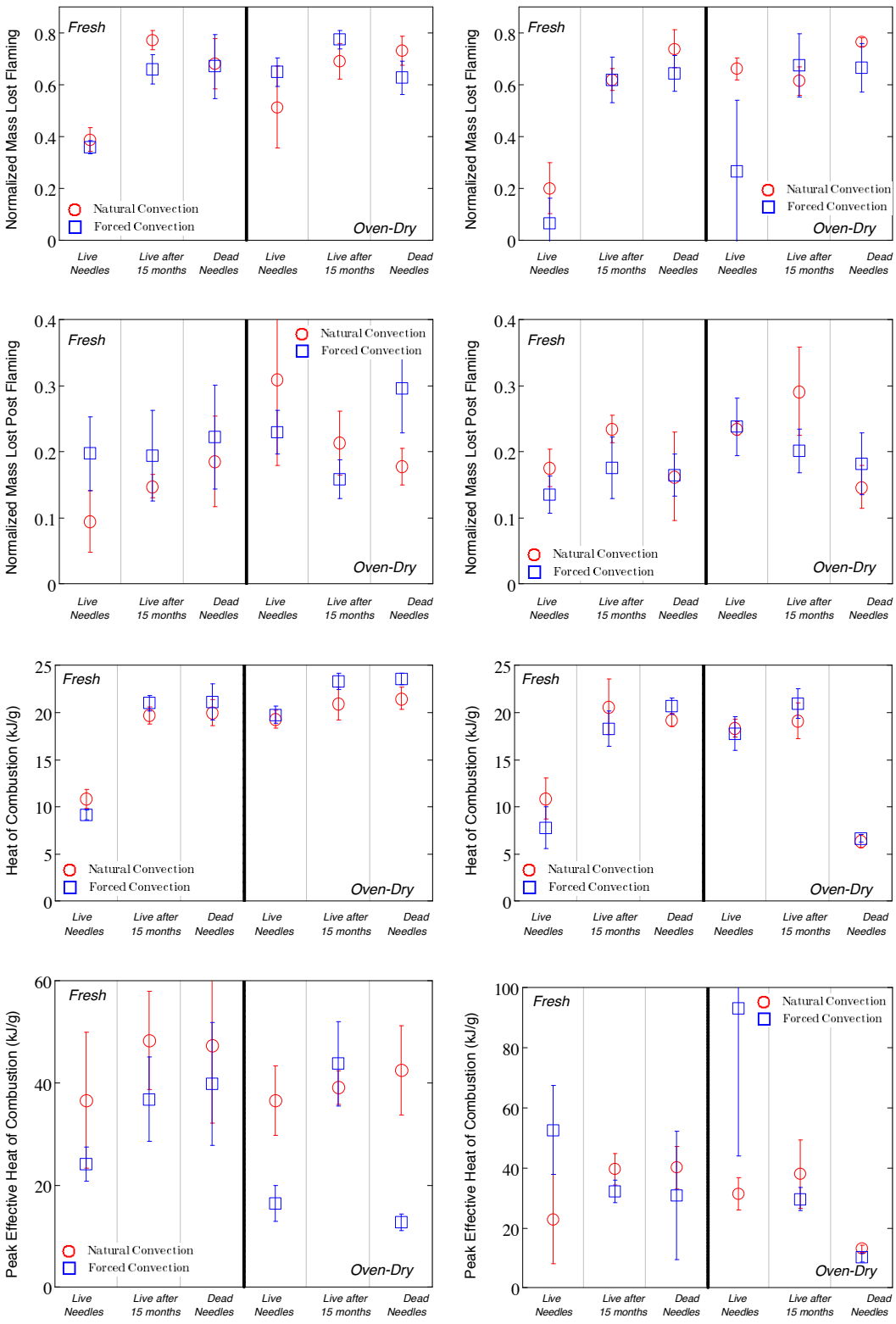
Normalized Mass Lost Flaming
Normalized Mass Lost Post Flaming
Heat of Combustion (kJ/g)
Peak Effective Heat of Combustion (kJ/g)
Fresh
Oven-Dry
Natural Convection
Forced Convection
Live Needles
Live after 15 months
Dead Needles

Appendix B:

Flammability parameter graphs for different pine needles species under two different heat insults and moisture contents for Chapter 3

50 kW/m^2 vs 25 kW/m^2

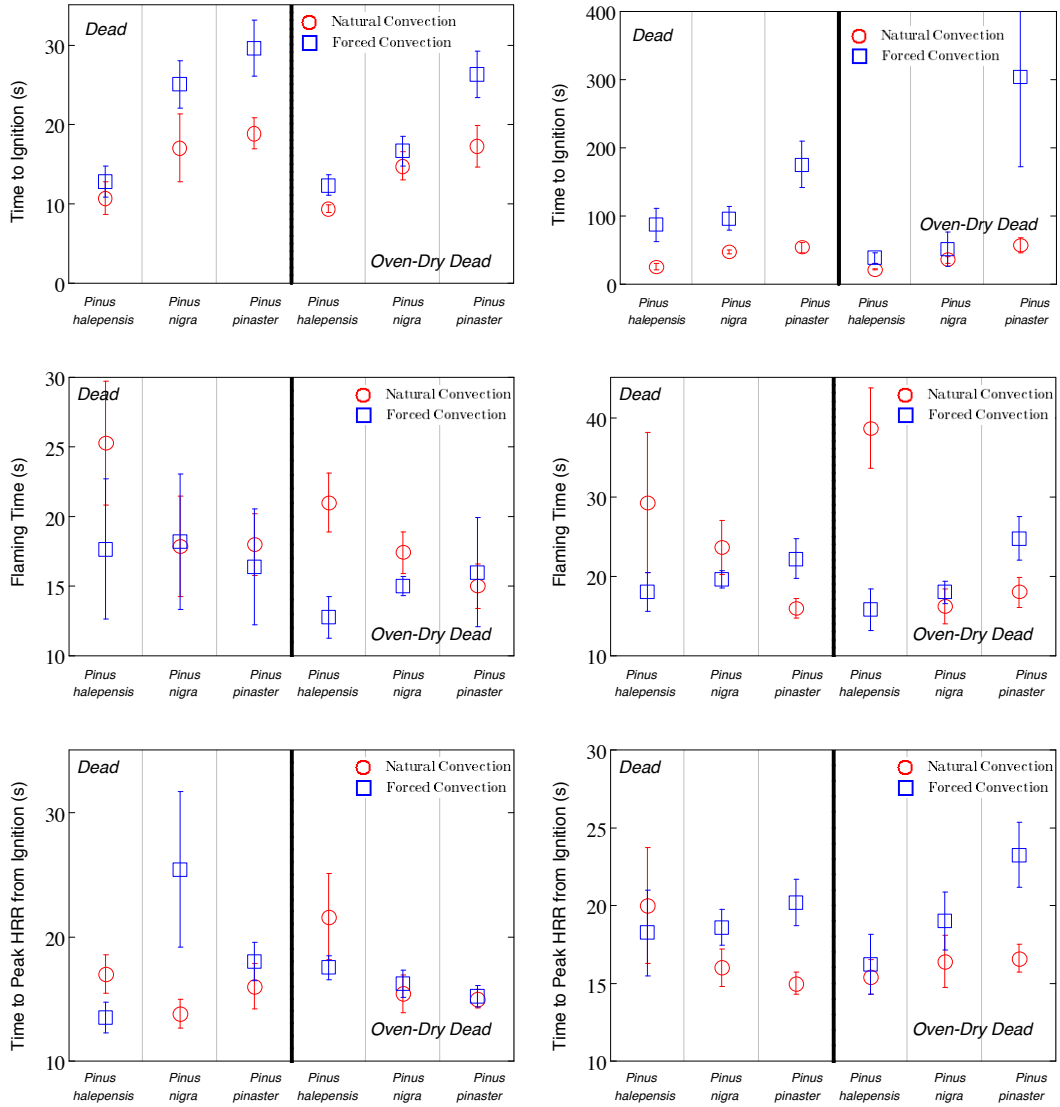

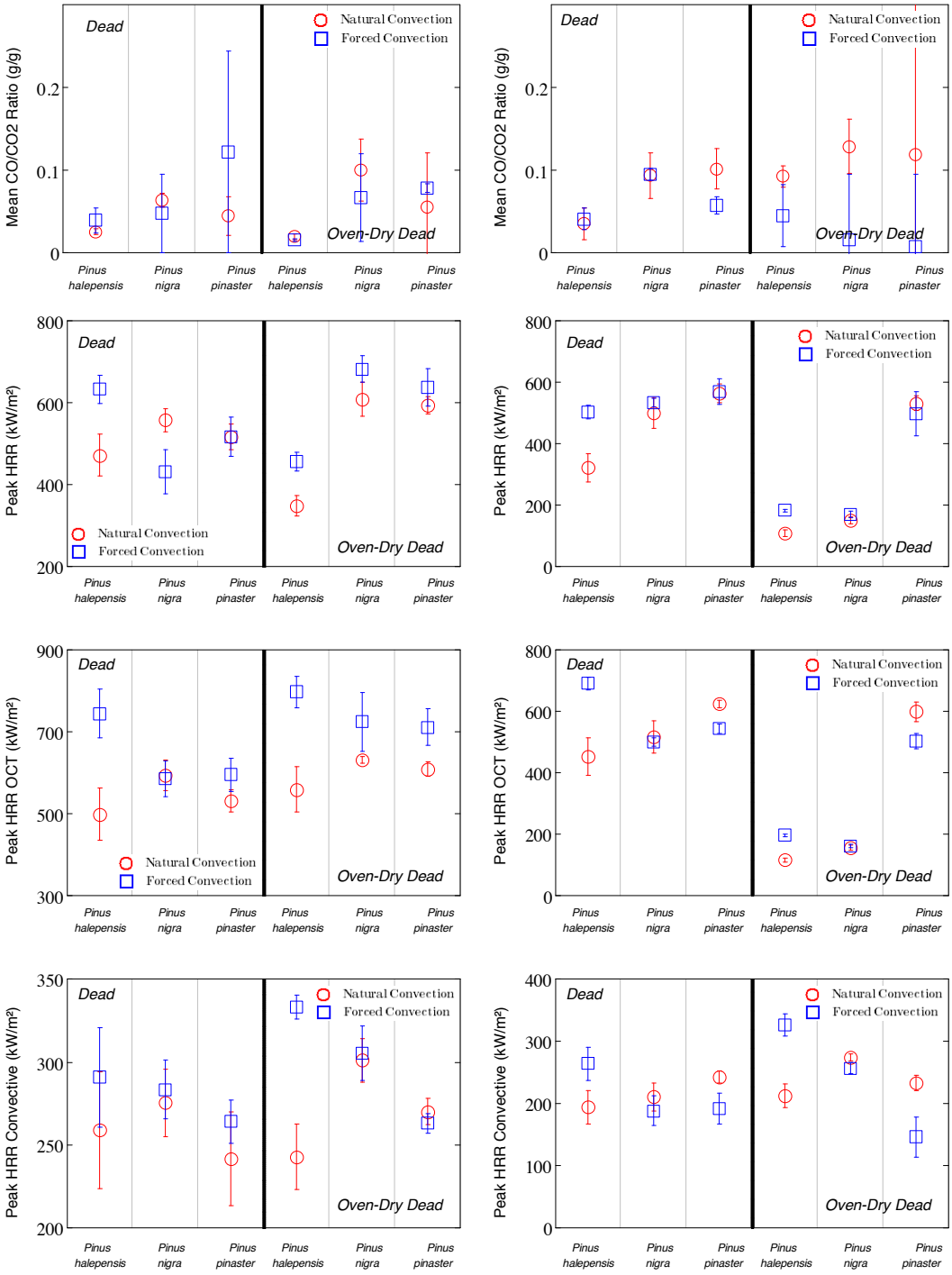
Dead
Oven-Dry Dead
Natural Convection
Forced Convection
Mean CO/CO2 Ratio (g/g)
Peak HRR (kW/m²)
Peak HRR OCT (kW/m²)
Peak HRR Convective (kW/m²)
Pinus halepensis
Pinus nigra
Pinus pinaster

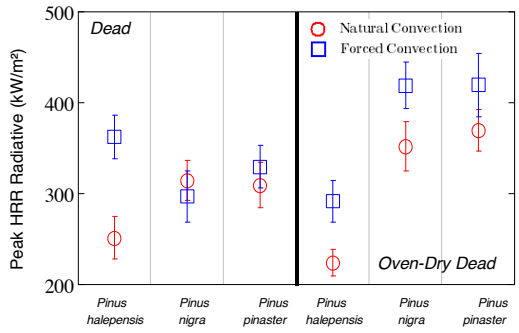
Peak HRR Radiative (kW/m²)
500
400
300
200
Dead
Oven-Dry Dead
Natural Convection
Forced Convection
Pinus halepensis
Pinus nigra
Pinus pinaster

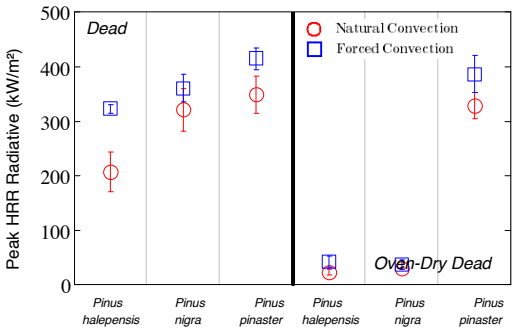
Peak HRR Radiative (kW/m²)
500
400
300
200
100
0
Dead
Oven-Dry Dead
Natural Convection
Forced Convection
Pinus halepensis
Pinus nigra
Pinus pinaster

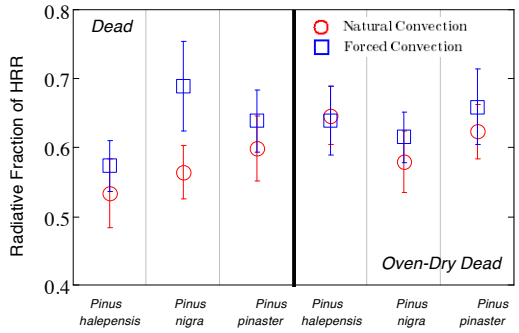
Radiative Fraction of HRR
0.8
0.7
0.6
0.5
0.4
Dead
Oven-Dry Dead
Natural Convection
Forced Convection
Pinus halepensis
Pinus nigra
Pinus pinaster

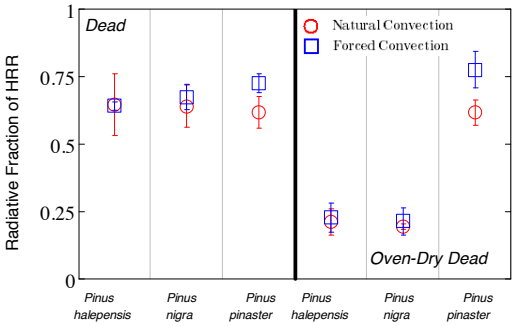
Radiative Fraction of HRR
1
0.75
0.5
0.25
0
Dead
Oven-Dry Dead
Natural Convection
Forced Convection
Pinus halepensis
Pinus nigra
Pinus pinaster

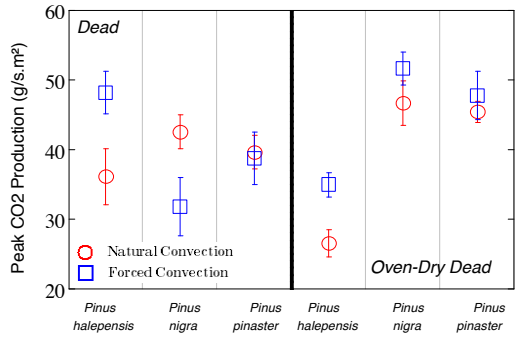
Peak CO2 Production (g/s.m²)
60
50
40
30
20
Dead
Oven-Dry Dead
Natural Convection
Forced Convection
Pinus halepensis
Pinus nigra
Pinus pinaster

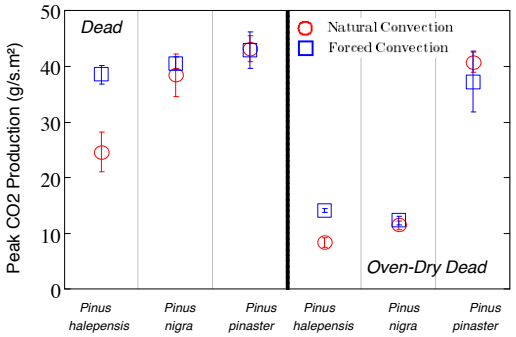
Peak CO2 Production (g/s.m²)
50
40
30
20
10
0
Dead
Oven-Dry Dead
Natural Convection
Forced Convection
Pinus halepensis
Pinus nigra
Pinus pinaster

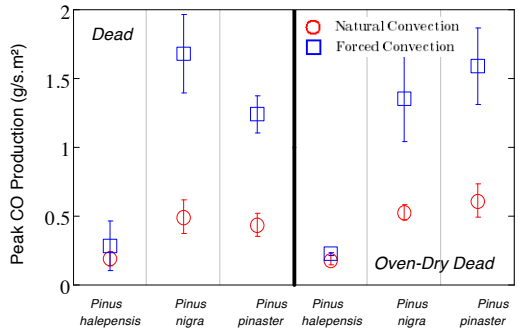
Peak CO Production (g/s.m²)
2
1.5
1
0.5
0
Dead
Oven-Dry Dead
Natural Convection
Forced Convection
Pinus halepensis
Pinus nigra
Pinus pinaster

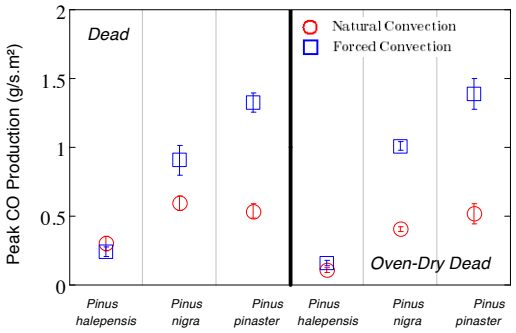
Peak CO Production (g/s.m²)
2
1.5
1
0.5
0
Dead
Oven-Dry Dead
Natural Convection
Forced Convection
Pinus halepensis
Pinus nigra
Pinus pinaster

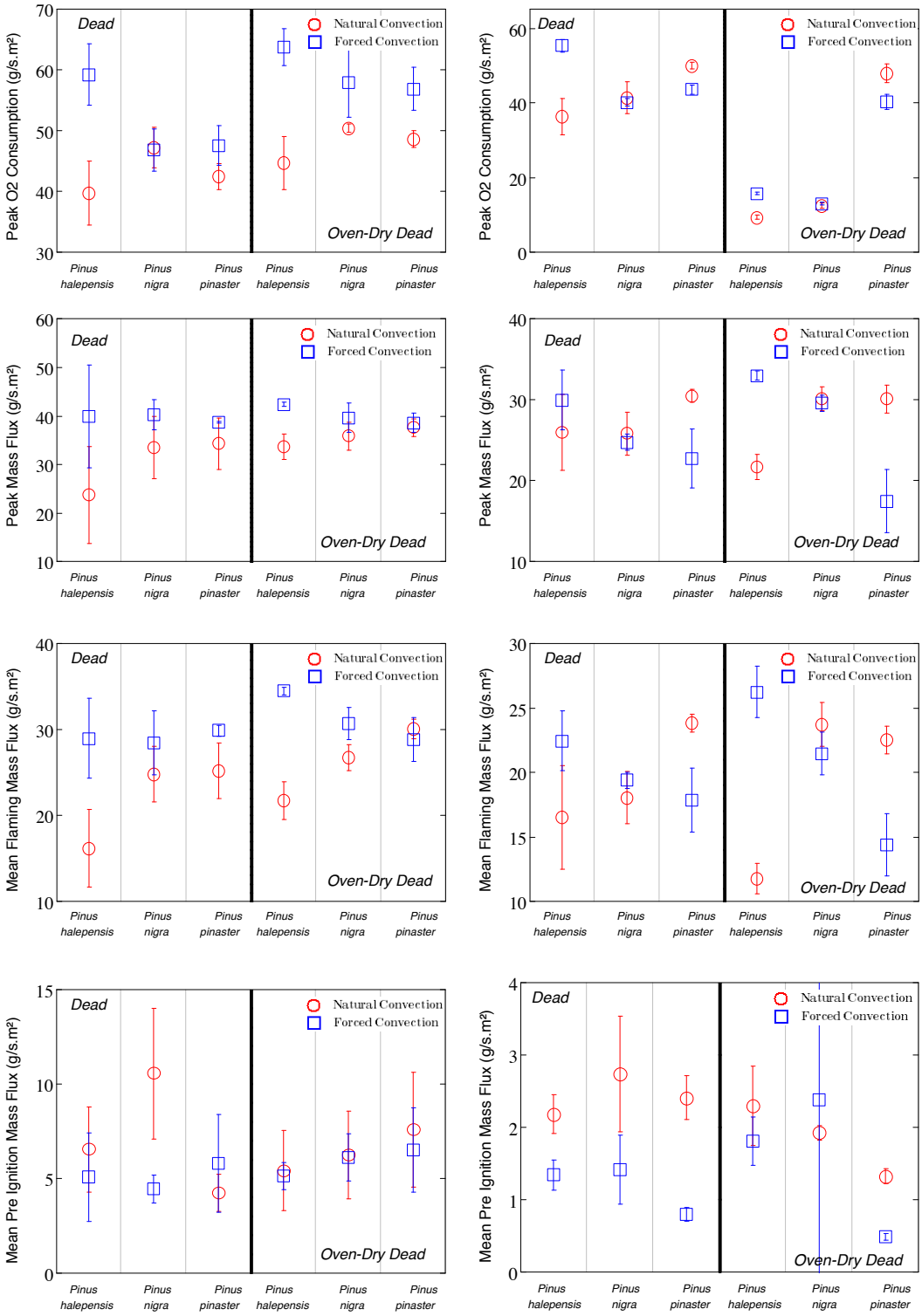
Peak O2 Consumption (g/s.m²)
Peak Mass Flux (g/s.m²)
Mean Flaming Mass Flux (g/s.m²)
Mean Pre Ignition Mass Flux (g/s.m²)
Dead
Oven-Dry Dead
Natural Convection
Forced Convection
Pinus halepensis
Pinus nigra
Pinus pinaster

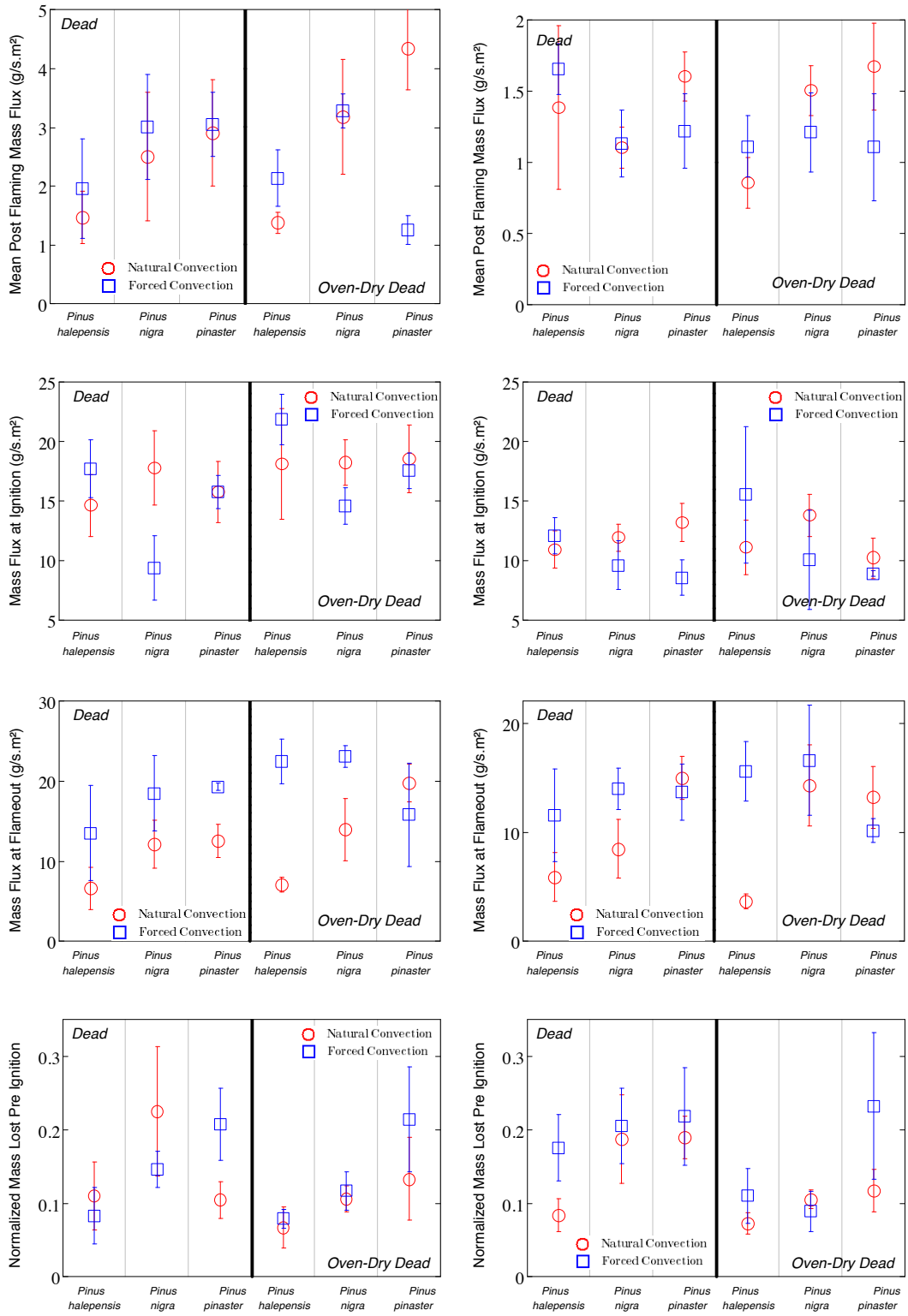
Dead
Oven-Dry Dead
Natural Convection
Forced Convection
Mean Post Flaming Mass Flux (g/s.m²)
Mass Flux at Ignition (g/s.m²)
Mass Flux at Flameout (g/s.m²)
Normalized Mass Lost Pre Ignition
Pinus halepensis
Pinus nigra
Pinus pinaster

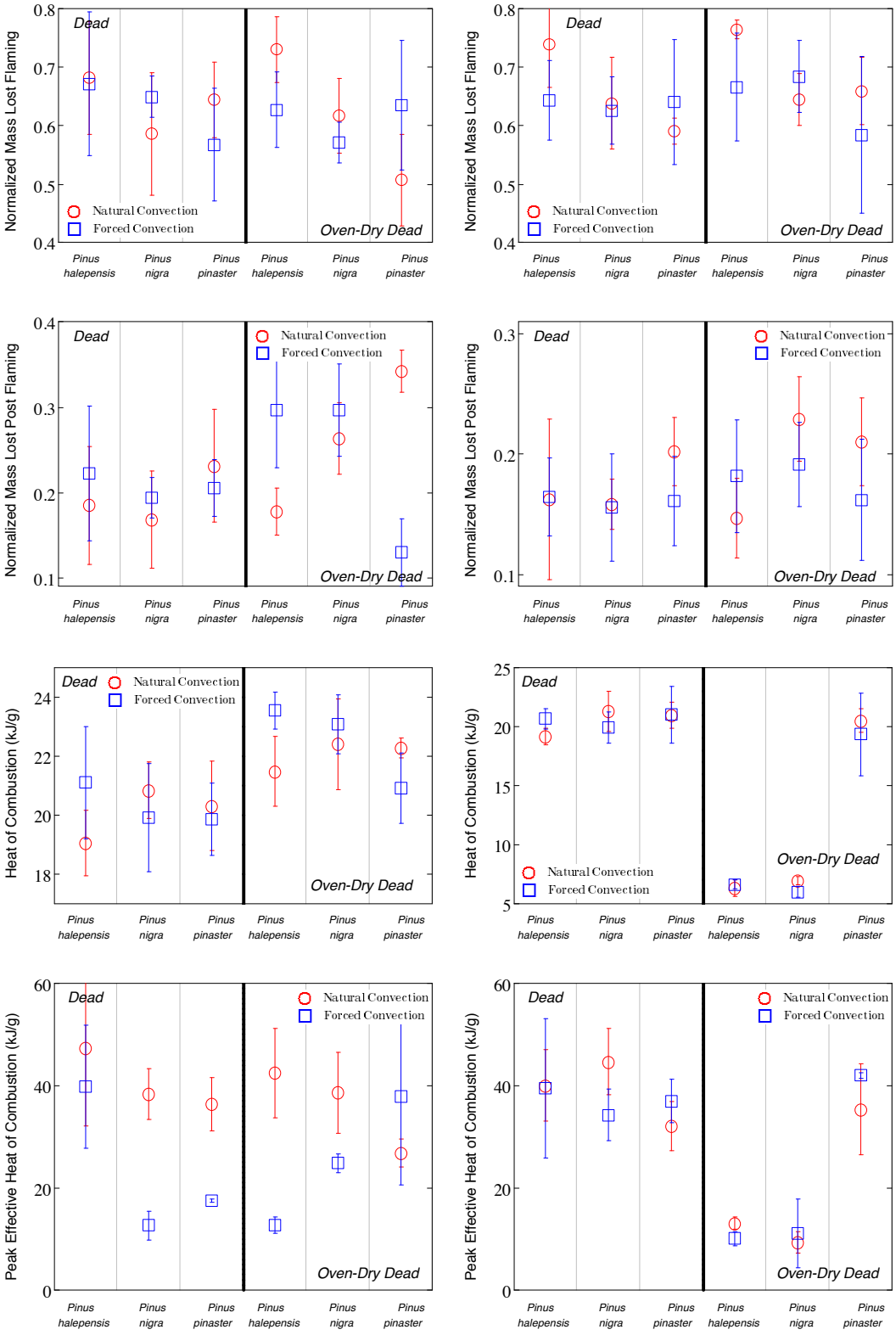
Normalized Mass Lost Flaming
Dead
Natural Convection
Forced Convection
Oven-Dry Dead
Pinus halepensis
Pinus nigra
Pinus pinaster
Normalized Mass Lost Post Flaming
Heat of Combustion (kJ/g)
Peak Effective Heat of Combustion (kJ/g)

Appendix C:

Flammability parameter graphs for different pine needle species under natural convection and Pinus halepensis needles under two different flow condition with varying fuel loads for Chapter 3

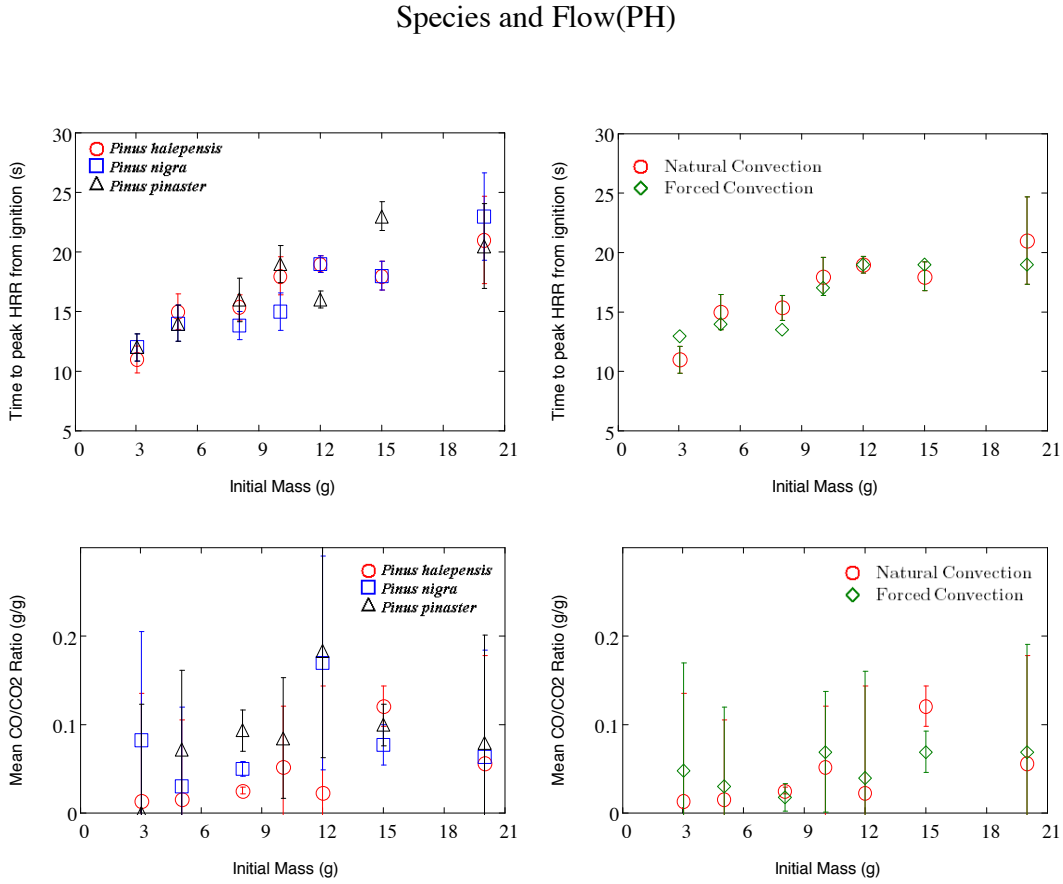

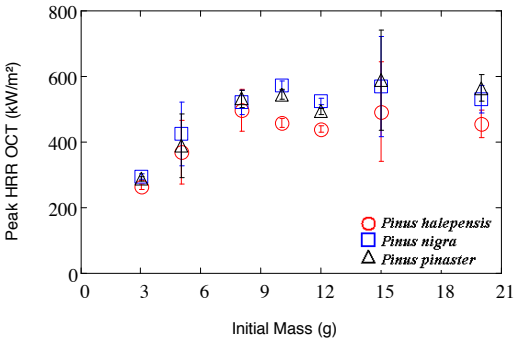
Peak HRR OCT (kW/m²)
Initial Mass (g)
Pinus halepensis
Pinus nigra
Pinus pinaster

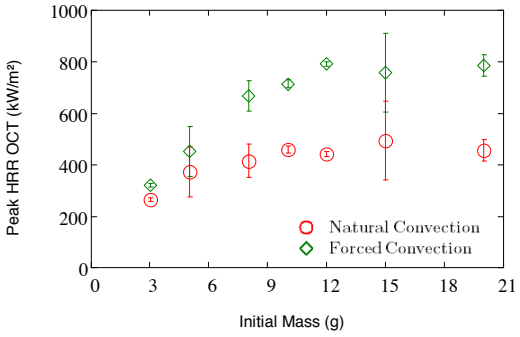
Peak HRR OCT (kW/m²)
Initial Mass (g)
Natural Convection
Forced Convection

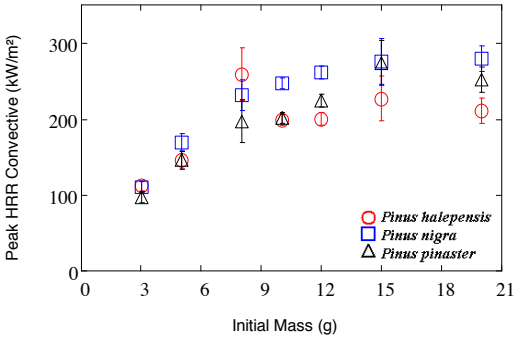
Peak HRR Convective (kW/m²)
Initial Mass (g)
Pinus halepensis
Pinus nigra
Pinus pinaster

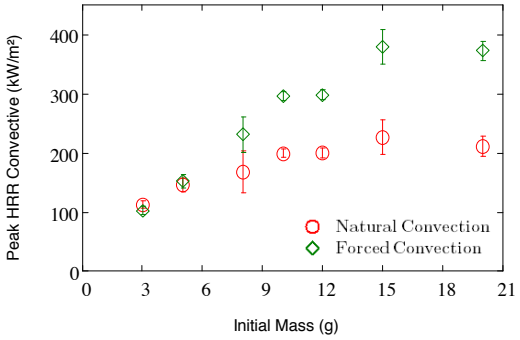
Peak HRR Convective (kW/m²)
Initial Mass (g)
Natural Convection
Forced Convection

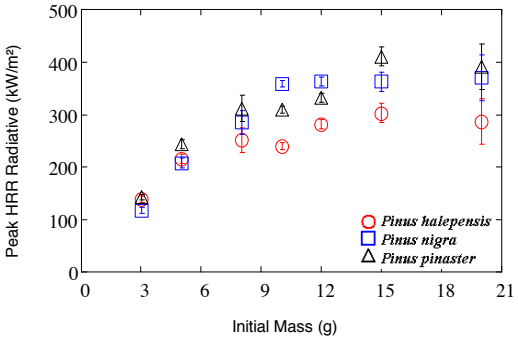
Peak HRR Radiative (kW/m²)
Initial Mass (g)
Pinus halepensis
Pinus nigra
Pinus pinaster

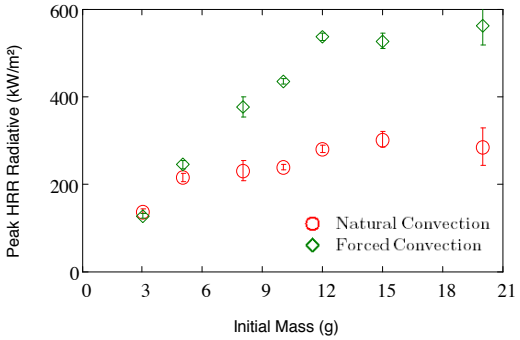
Peak HRR Radiative (kW/m²)
Initial Mass (g)
Natural Convection
Forced Convection

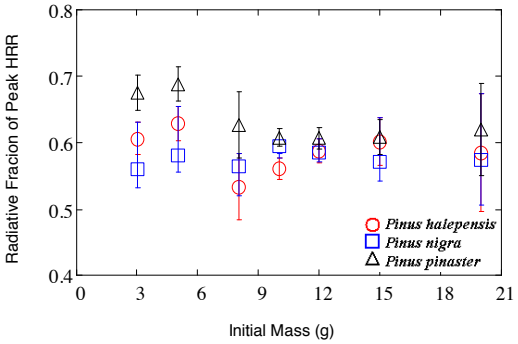
Radiative Fracion of Peak HRR
Initial Mass (g)
Pinus halepensis
Pinus nigra
Pinus pinaster

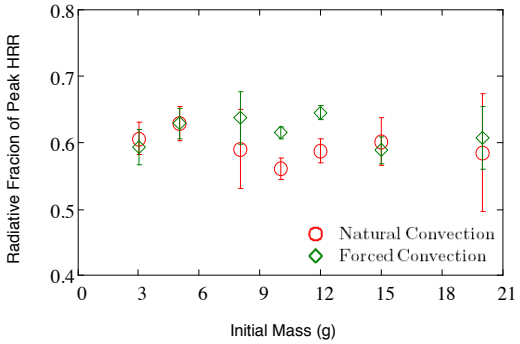
Radiative Fracion of Peak HRR
Initial Mass (g)
Natural Convection
Forced Convection

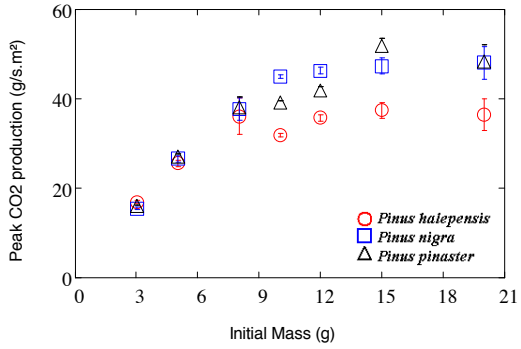
Peak CO2 production (g/s.m²)
Initial Mass (g)
Pinus halepensis
Pinus nigra
Pinus pinaster

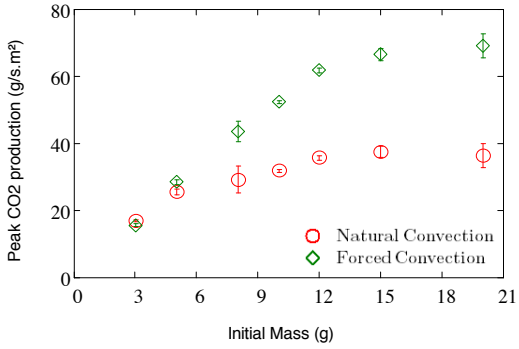
Peak CO2 production (g/s.m²)
Initial Mass (g)
Natural Convection
Forced Convection

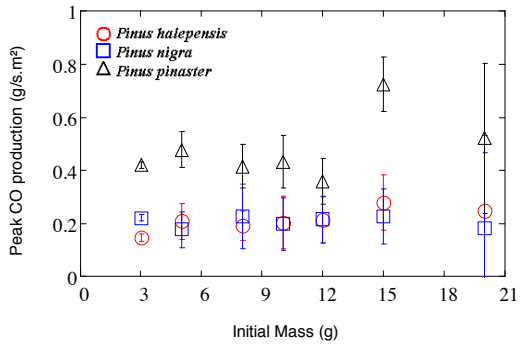
Peak CO production (g/s.m²)
Initial Mass (g)
Pinus halepensis
Pinus nigra
Pinus pinaster

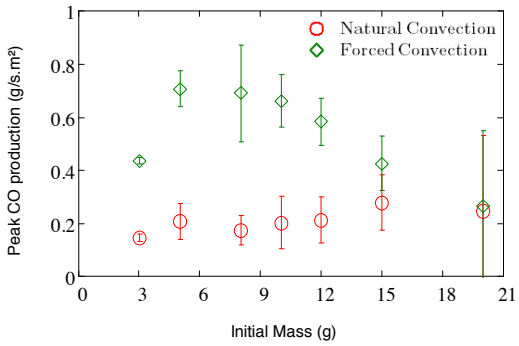
Peak CO production (g/s.m²)
Initial Mass (g)
Natural Convection
Forced Convection

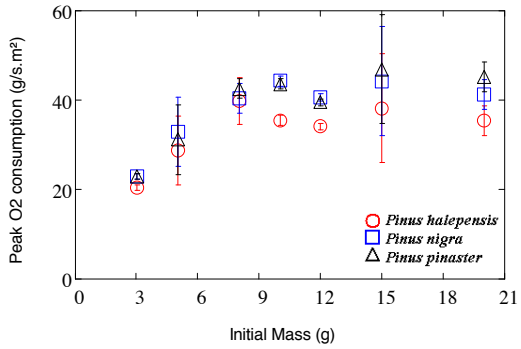
Peak O2 consumption (g/s.m²)
Initial Mass (g)
Pinus halepensis
Pinus nigra
Pinus pinaster

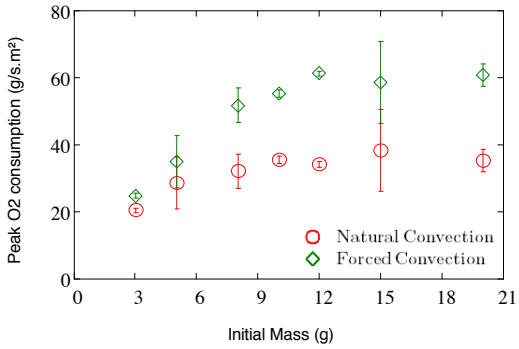
Peak O2 consumption (g/s.m²)
Initial Mass (g)
Natural Convection
Forced Convection

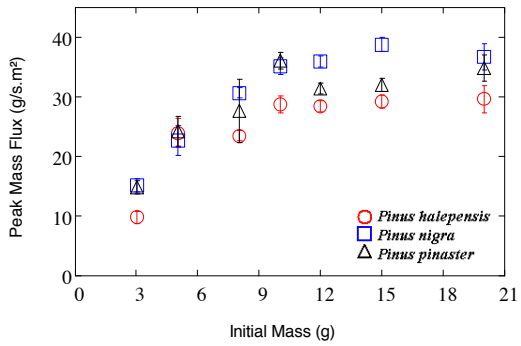
Peak Mass Flux (g/s.m²)
Initial Mass (g)
Pinus halepensis
Pinus nigra
Pinus pinaster

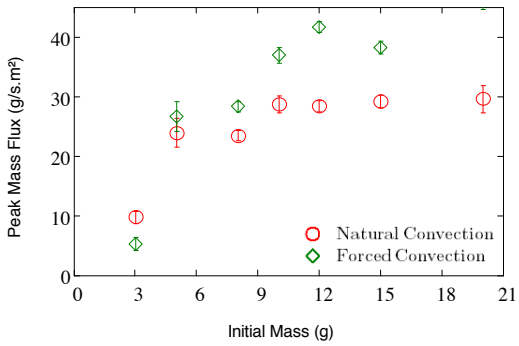
Peak Mass Flux (g/s.m²)
Initial Mass (g)
Natural Convection
Forced Convection

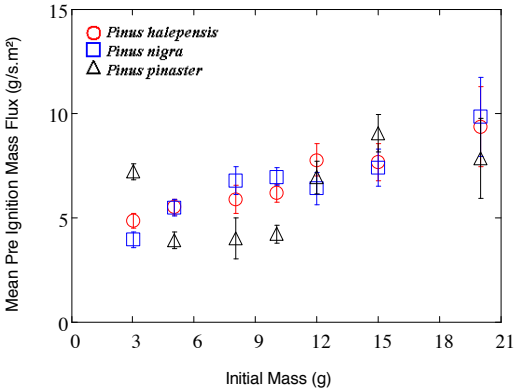
Mean Pre Ignition Mass Flux (g/s.m²)
Initial Mass (g)
Pinus halepensis
Pinus nigra
Pinus pinaster

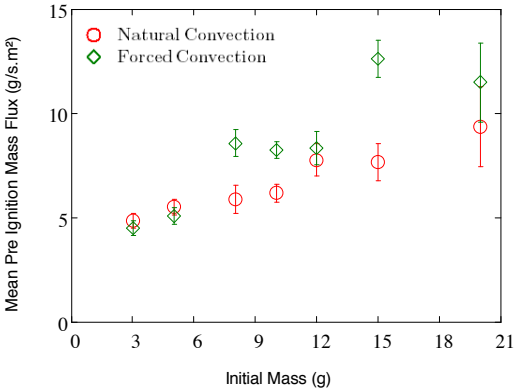
Mean Pre Ignition Mass Flux (g/s.m²)
Initial Mass (g)
Natural Convection
Forced Convection

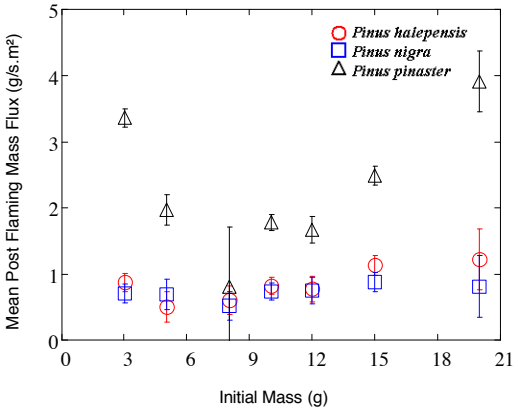
Mean Post Flaming Mass Flux (g/s.m²)
Initial Mass (g)
Pinus halepensis
Pinus nigra
Pinus pinaster

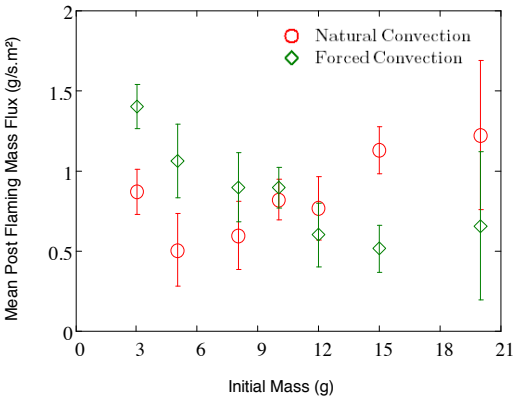
Mean Post Flaming Mass Flux (g/s.m²)
Initial Mass (g)
Natural Convection
Forced Convection

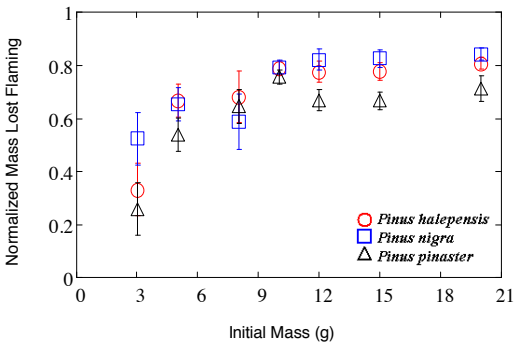
Normalized Mass Lost Flaming
Initial Mass (g)
Pinus halepensis
Pinus nigra
Pinus pinaster

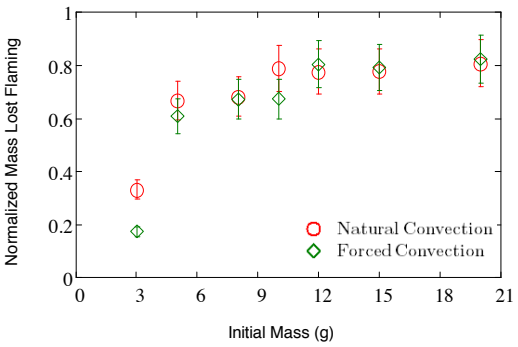
Normalized Mass Lost Flaming
Initial Mass (g)
Natural Convection
Forced Convection

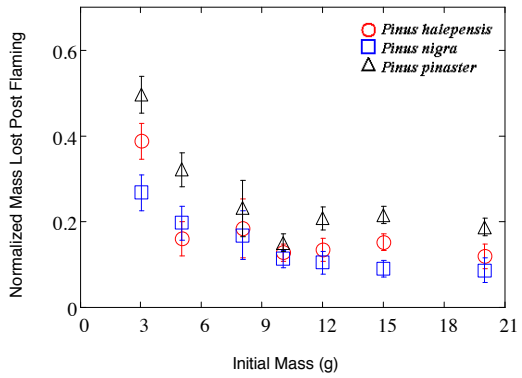
Pinus halepensis
Pinus nigra
Pinus pinaster
Normalized Mass Lost Post Flaming
Initial Mass (g)

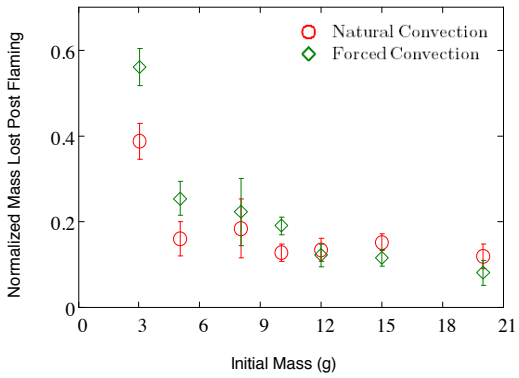
Natural Convection
Forced Convection
Normalized Mass Lost Post Flaming
Initial Mass (g)

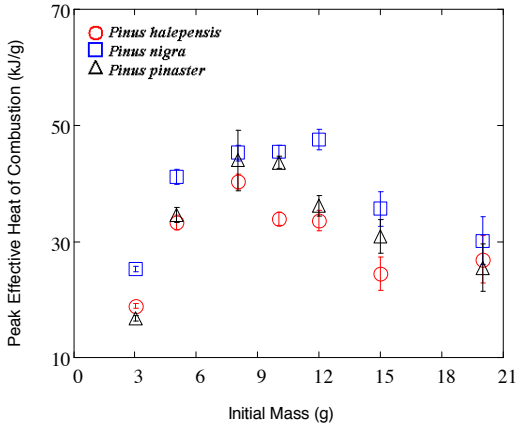
Pinus halepensis
Pinus nigra
Pinus pinaster
Peak Effective Heat of Combustion (kJ/g)
Initial Mass (g)

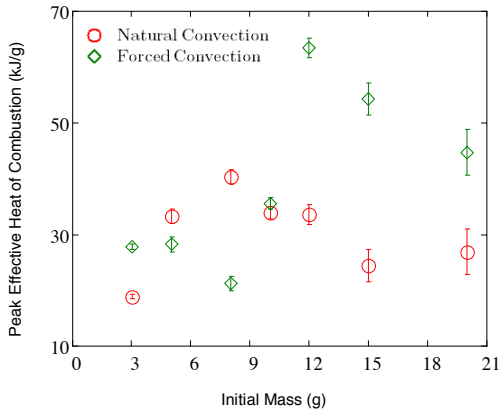
Natural Convection
Forced Convection
Peak Effective Heat of Combustion (kJ/g)
Initial Mass (g)

Appendix D:

Heat release rate, mass loss rate and flammability parameter graphs for different pine needles species under different heat insults and different flow conditions for Chapter 3

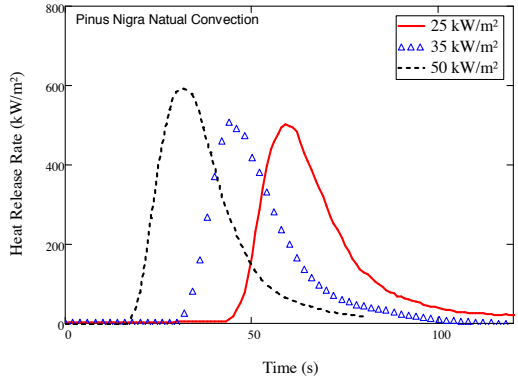

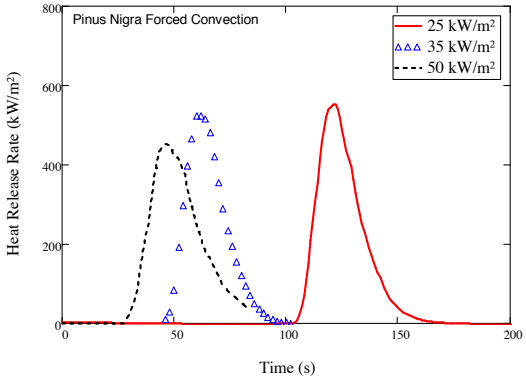

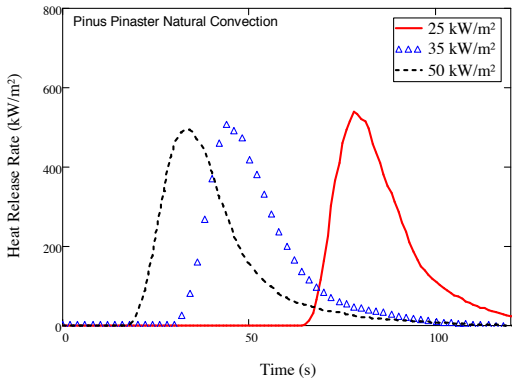

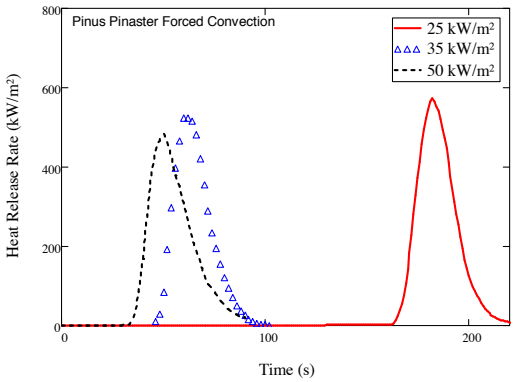

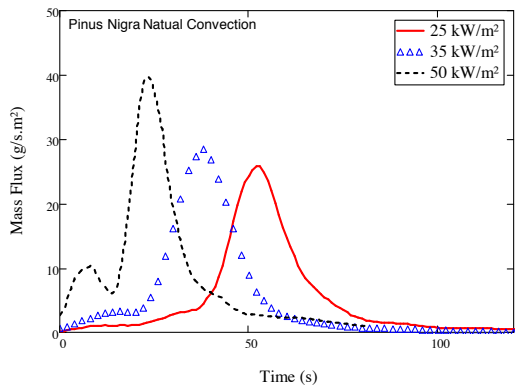

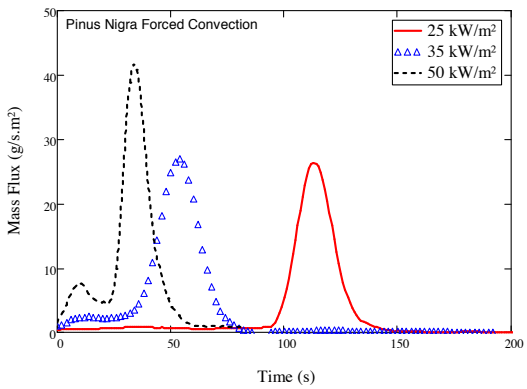

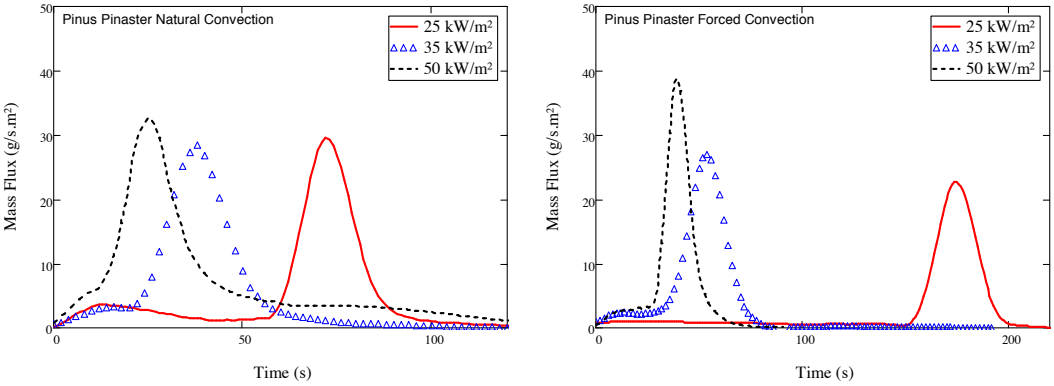

Natural Convection vs Forced Convection

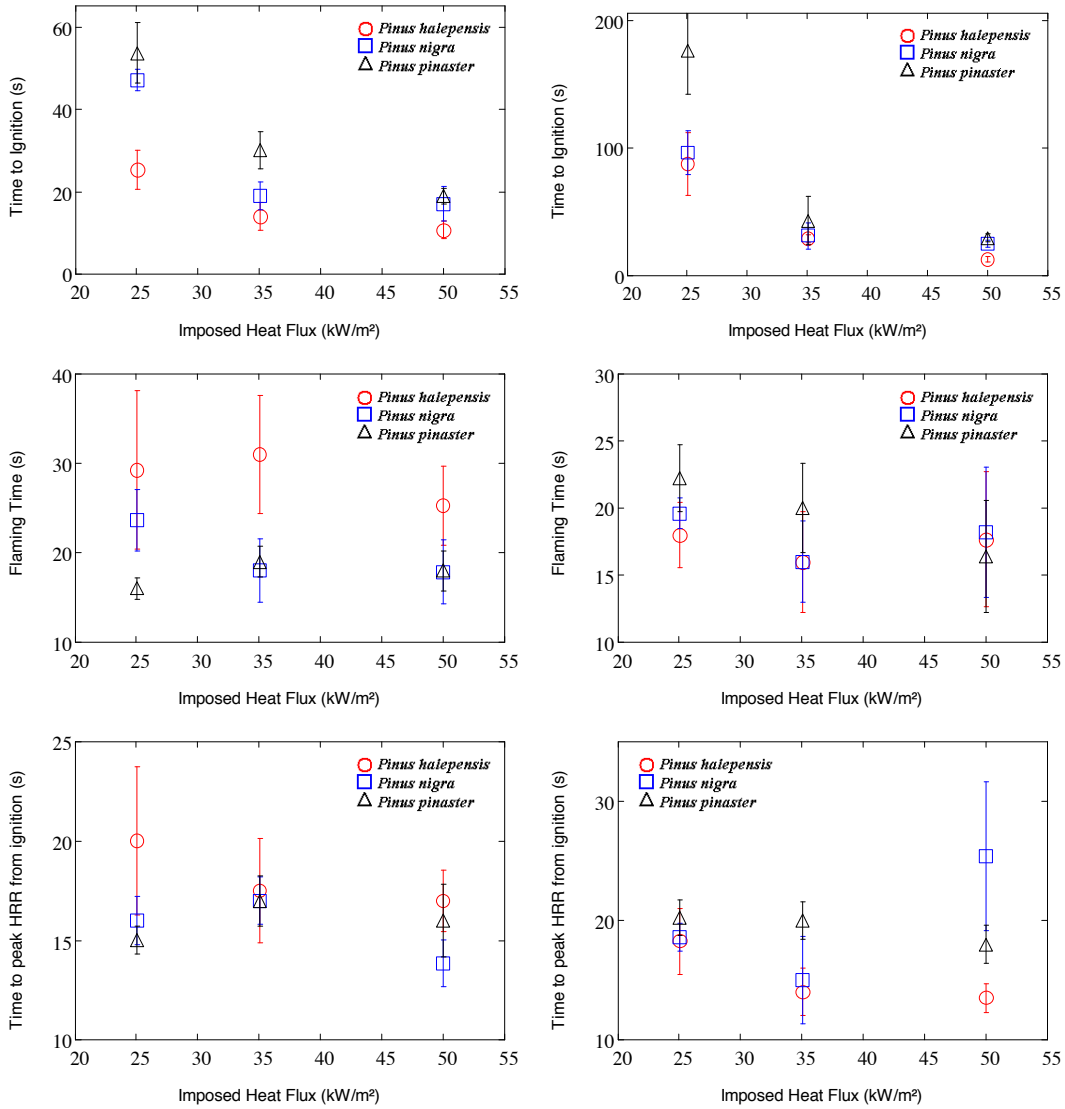

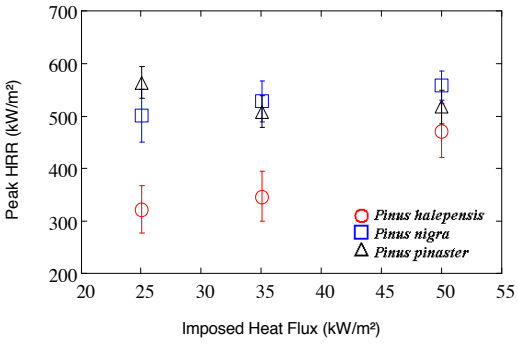
Peak HRR (kW/m²)
Imposed Heat Flux (kW/m²)
Pinus halepensis
Pinus nigra
Pinus pinaster

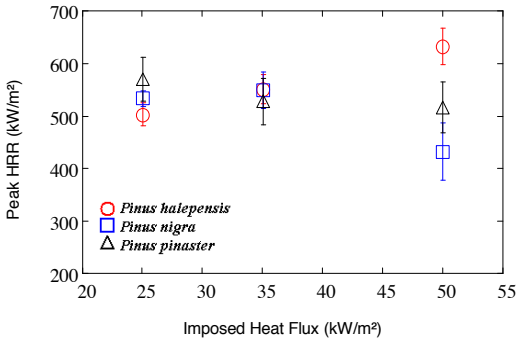
Peak HRR (kW/m²)
Imposed Heat Flux (kW/m²)
Pinus halepensis
Pinus nigra
Pinus pinaster

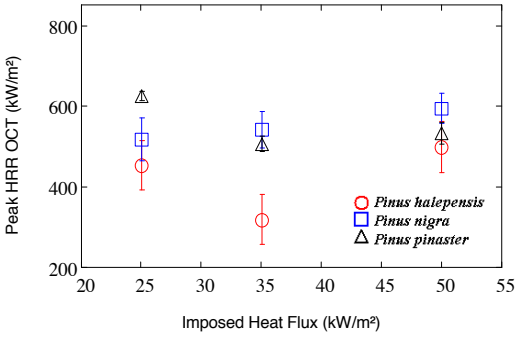
Peak HRR OCT (kW/m²)
Imposed Heat Flux (kW/m²)
Pinus halepensis
Pinus nigra
Pinus pinaster

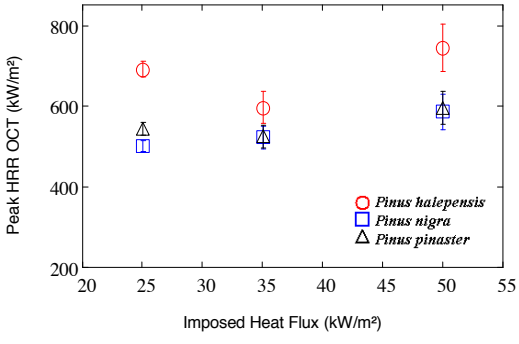
Peak HRR OCT (kW/m²)
Imposed Heat Flux (kW/m²)
Pinus halepensis
Pinus nigra
Pinus pinaster

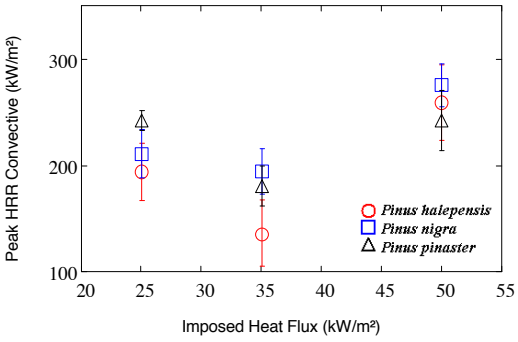
Peak HRR Convective (kW/m²)
Imposed Heat Flux (kW/m²)
Pinus halepensis
Pinus nigra
Pinus pinaster

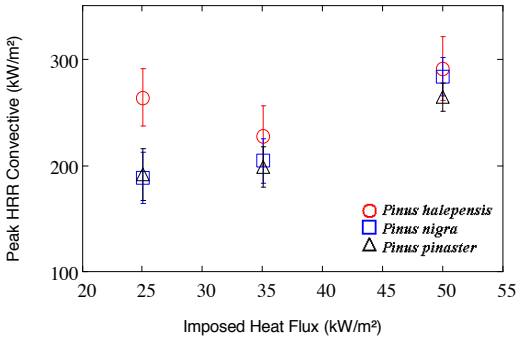
Peak HRR Convective (kW/m²)
Imposed Heat Flux (kW/m²)
Pinus halepensis
Pinus nigra
Pinus pinaster

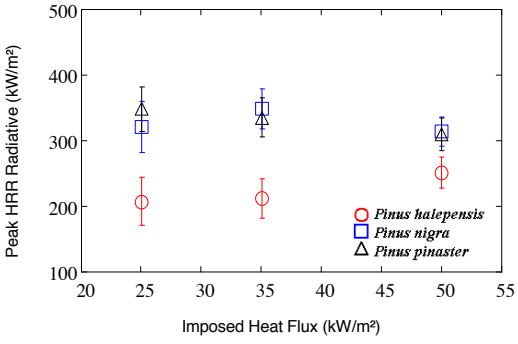
Peak HRR Radiative (kW/m²)
Imposed Heat Flux (kW/m²)
Pinus halepensis
Pinus nigra
Pinus pinaster

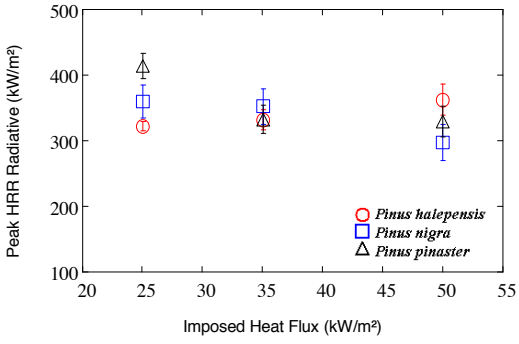
Peak HRR Radiative (kW/m²)
Imposed Heat Flux (kW/m²)
Pinus halepensis
Pinus nigra
Pinus pinaster

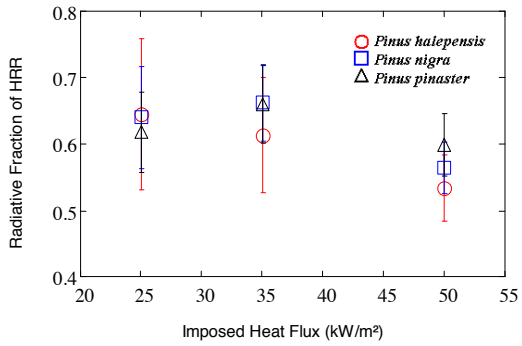
Radiative Fraction of HRR
Imposed Heat Flux (kW/m²)
Pinus halepensis
Pinus nigra
Pinus pinaster

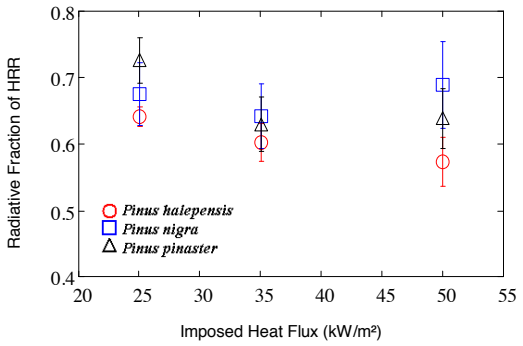
Radiative Fraction of HRR
Imposed Heat Flux (kW/m²)
Pinus halepensis
Pinus nigra
Pinus pinaster

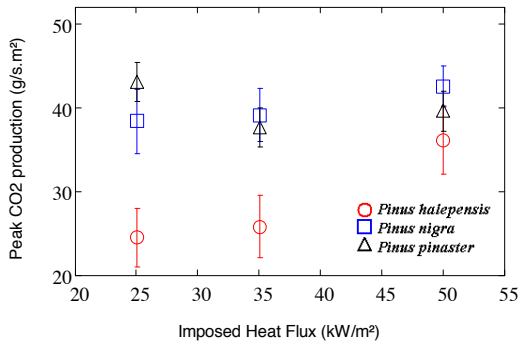
Peak CO2 production (g/s.m²)
Imposed Heat Flux (kW/m²)
Pinus halepensis
Pinus nigra
Pinus pinaster

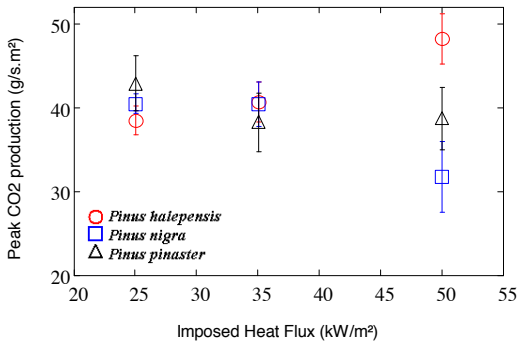
Peak CO2 production (g/s.m²)
Imposed Heat Flux (kW/m²)
Pinus halepensis
Pinus nigra
Pinus pinaster

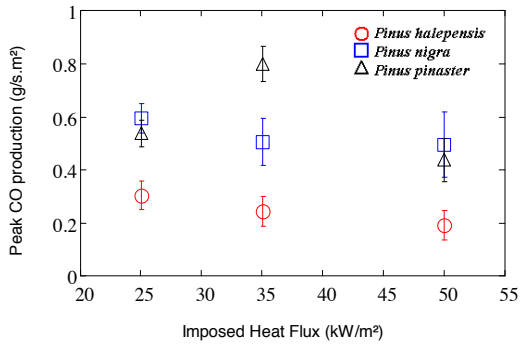
Peak CO production (g/s.m²)
Imposed Heat Flux (kW/m²)
Pinus halepensis
Pinus nigra
Pinus pinaster

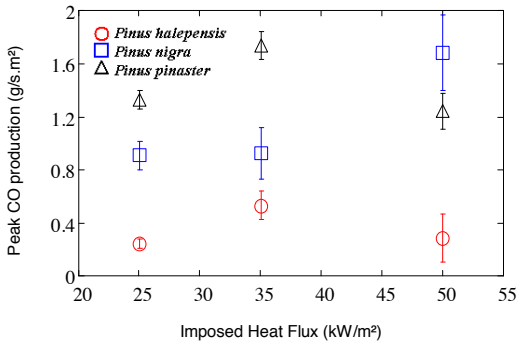
Peak CO production (g/s.m²)
Imposed Heat Flux (kW/m²)
Pinus halepensis
Pinus nigra
Pinus pinaster

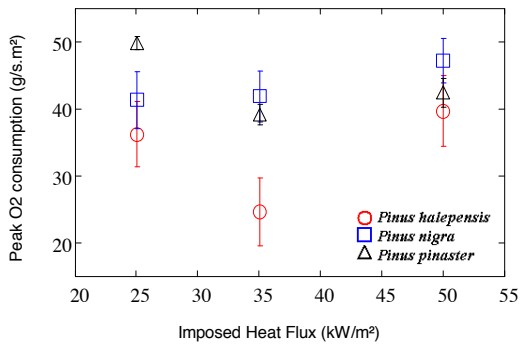
Peak O2 consumption (g/s.m²)
Imposed Heat Flux (kW/m²)
Pinus halepensis
Pinus nigra
Pinus pinaster

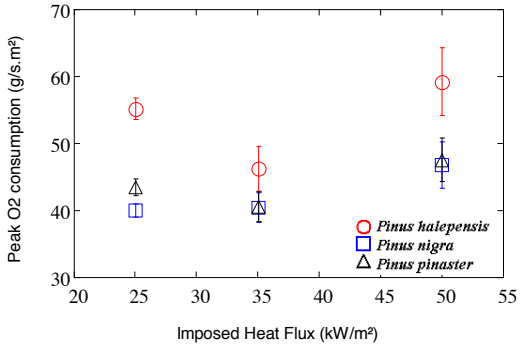
Peak O2 consumption (g/s.m²)
Imposed Heat Flux (kW/m²)
Pinus halepensis
Pinus nigra
Pinus pinaster

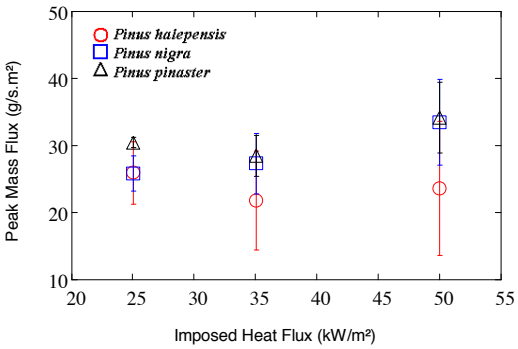
Pinus halepensis
Pinus nigra
Pinus pinaster
Peak Mass Flux (g/s.m²)
Imposed Heat Flux (kW/m²)

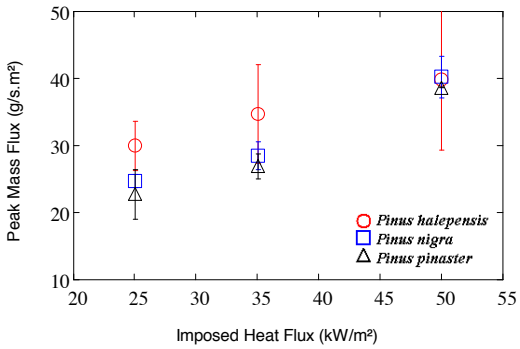
Pinus halepensis
Pinus nigra
Pinus pinaster
Peak Mass Flux (g/s.m²)
Imposed Heat Flux (kW/m²)

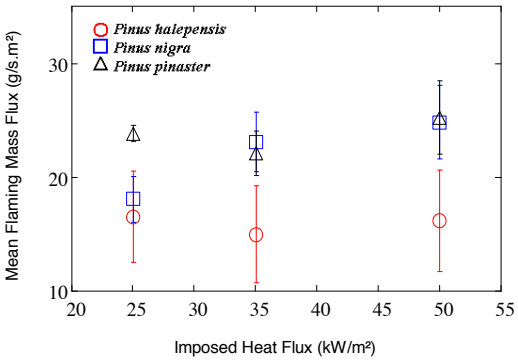
Pinus halepensis
Pinus nigra
Pinus pinaster
Mean Flaming Mass Flux (g/s.m²)
Imposed Heat Flux (kW/m²)

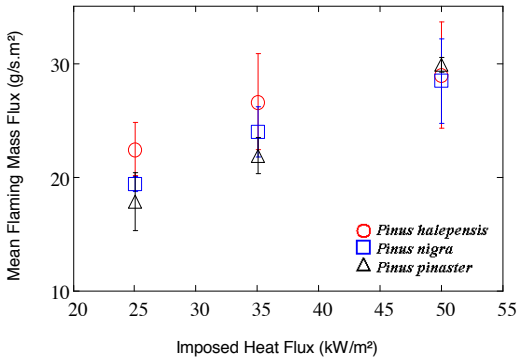
Pinus halepensis
Pinus nigra
Pinus pinaster
Mean Flaming Mass Flux (g/s.m²)
Imposed Heat Flux (kW/m²)

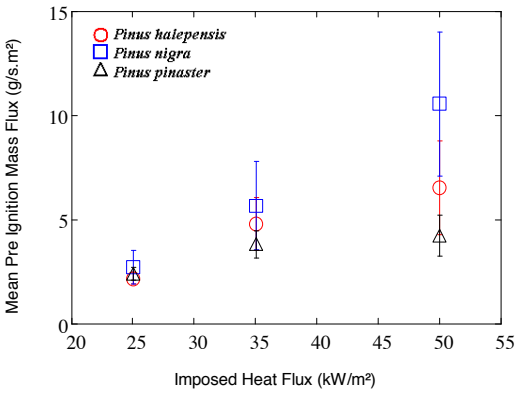
Pinus halepensis
Pinus nigra
Pinus pinaster
Mean Pre Ignition Mass Flux (g/s.m²)
Imposed Heat Flux (kW/m²)

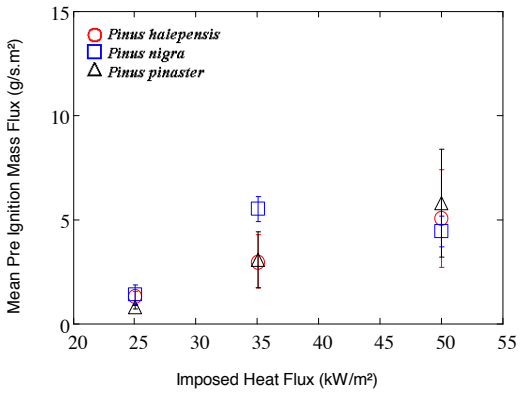
Pinus halepensis
Pinus nigra
Pinus pinaster
Mean Pre Ignition Mass Flux (g/s.m²)
Imposed Heat Flux (kW/m²)

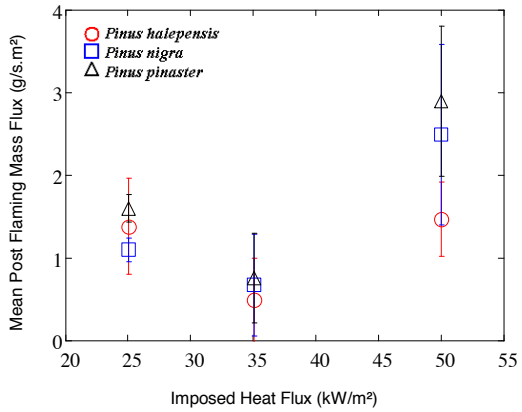
Pinus halepensis
Pinus nigra
Pinus pinaster
Mean Post Flaming Mass Flux (g/s.m²)
Imposed Heat Flux (kW/m²)

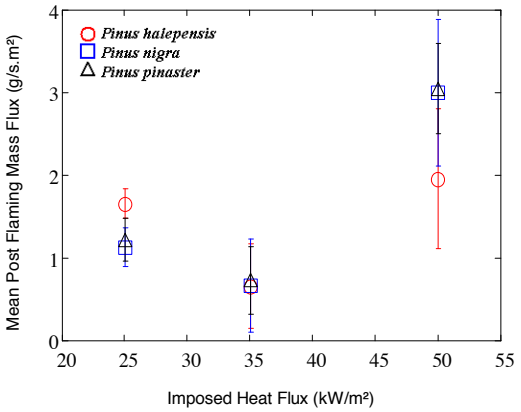
Pinus halepensis
Pinus nigra
Pinus pinaster
Mean Post Flaming Mass Flux (g/s.m²)
Imposed Heat Flux (kW/m²)

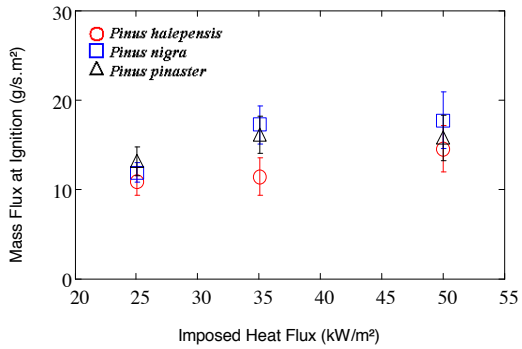
Pinus halepensis
Pinus nigra
Pinus pinaster
Mass Flux at Ignition (g/s.m²)
Imposed Heat Flux (kW/m²)

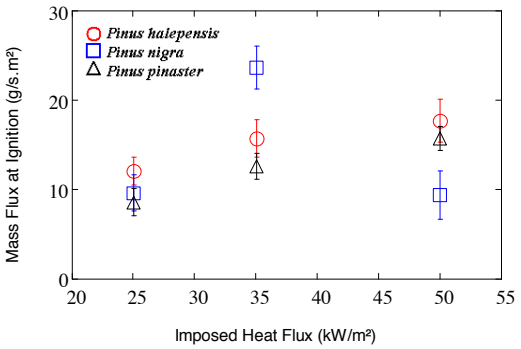
Pinus halepensis
Pinus nigra
Pinus pinaster
Mass Flux at Ignition (g/s.m²)
Imposed Heat Flux (kW/m²)

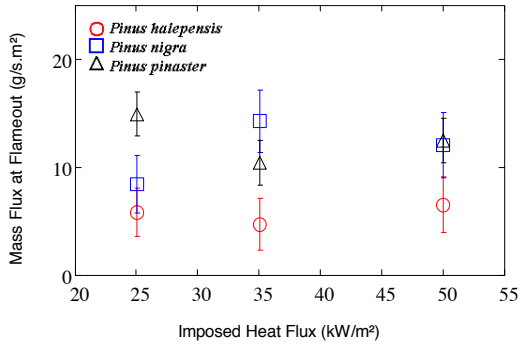
Pinus halepensis
Pinus nigra
Pinus pinaster
Mass Flux at Flameout (g/s.m²)
Imposed Heat Flux (kW/m²)

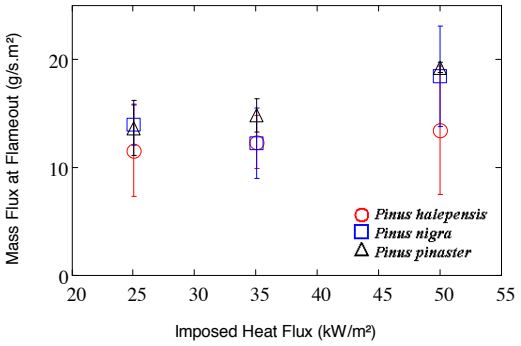
Pinus halepensis
Pinus nigra
Pinus pinaster
Mass Flux at Flameout (g/s.m²)
Imposed Heat Flux (kW/m²)

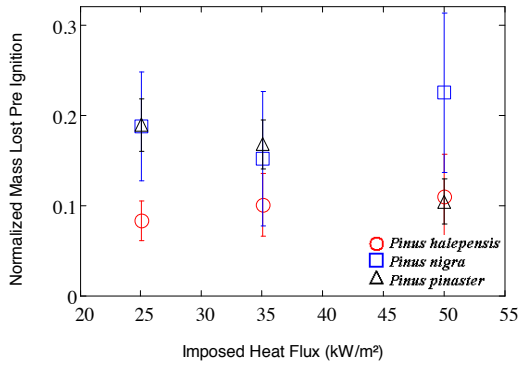
Pinus halepensis
Pinus nigra
Pinus pinaster
Normalized Mass Lost Pre Ignition
Imposed Heat Flux (kW/m²)

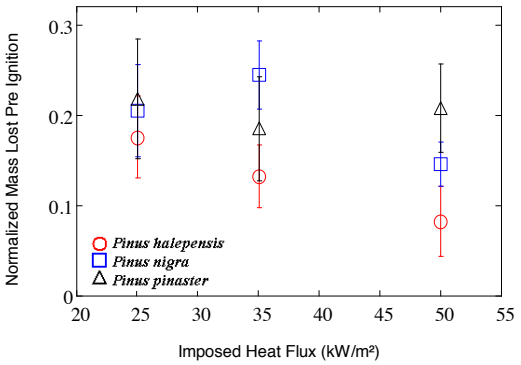
Pinus halepensis
Pinus nigra
Pinus pinaster
Normalized Mass Lost Pre Ignition
Imposed Heat Flux (kW/m²)

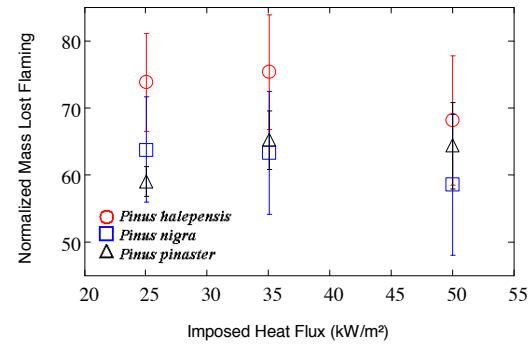
Normalized Mass Lost Flaming
Imposed Heat Flux (kW/m²)
Pinus halepensis
Pinus nigra
Pinus pinaster

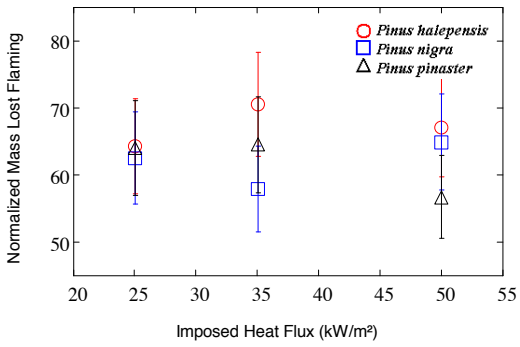
Normalized Mass Lost Flaming
Imposed Heat Flux (kW/m²)
Pinus halepensis
Pinus nigra
Pinus pinaster

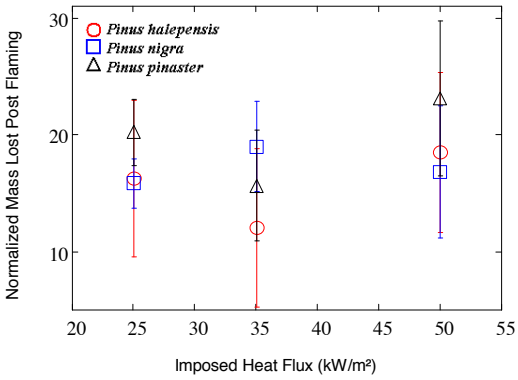
Normalized Mass Lost Post Flaming
Imposed Heat Flux (kW/m²)
Pinus halepensis
Pinus nigra
Pinus pinaster

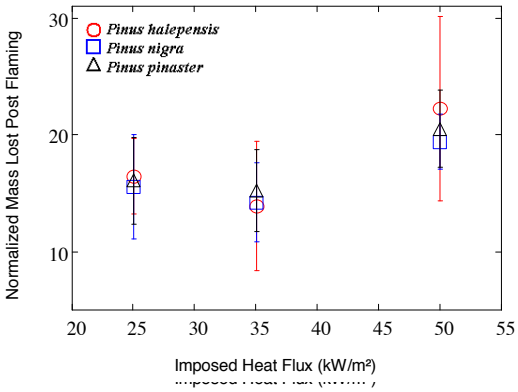
Normalized Mass Lost Post Flaming
Imposed Heat Flux (kW/m²)
Pinus halepensis
Pinus nigra
Pinus pinaster

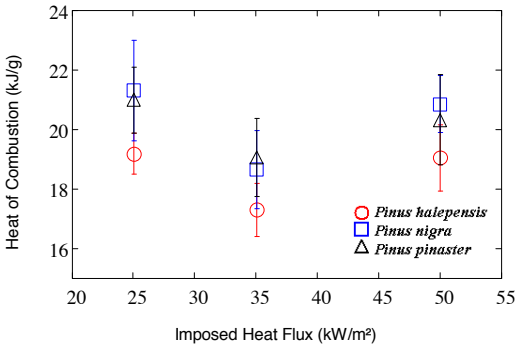
Heat of Combustion (kJ/g)
Imposed Heat Flux (kW/m²)
Pinus halepensis
Pinus nigra
Pinus pinaster

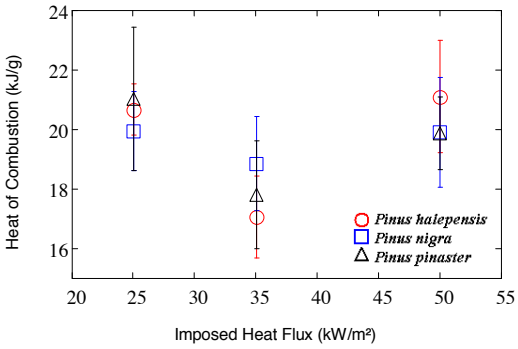
Heat of Combustion (kJ/g)
Imposed Heat Flux (kW/m²)
Pinus halepensis
Pinus nigra
Pinus pinaster

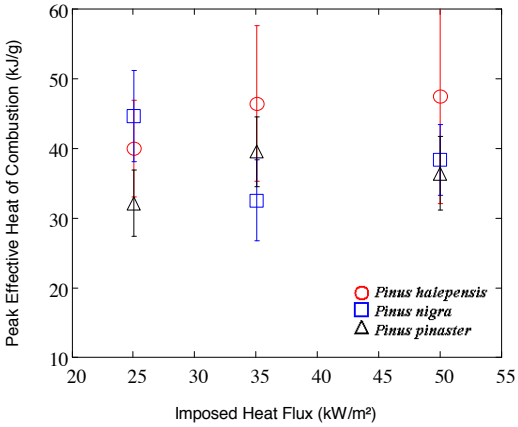
Peak Effective Heat of Combustion (kJ/g)
Imposed Heat Flux (kW/m²)
Pinus halepensis
Pinus nigra
Pinus pinaster

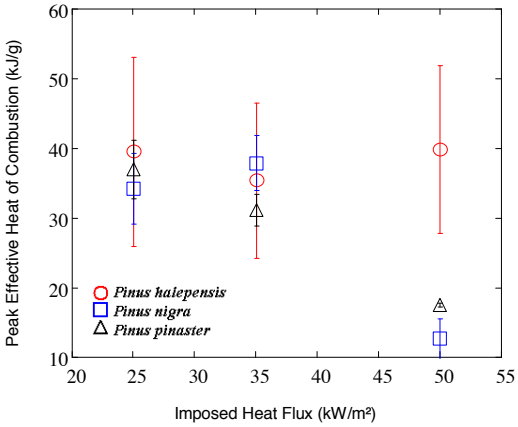
Peak Effective Heat of Combustion (kJ/g)
Imposed Heat Flux (kW/m²)
Pinus halepensis
Pinus nigra
Pinus pinaster

Appendix E

Flammability parameter graphs for leaf morphology study for Chapter 4

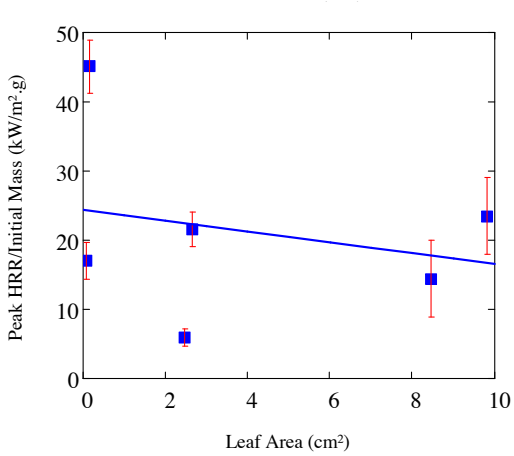

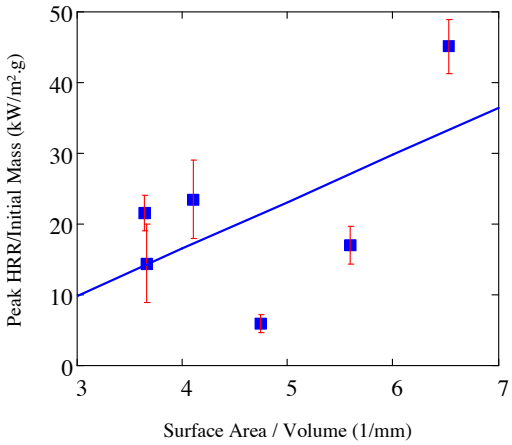

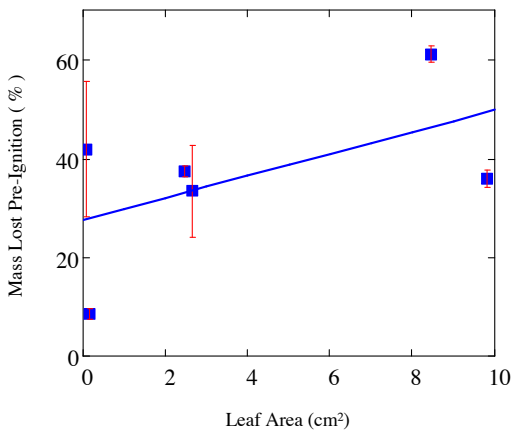

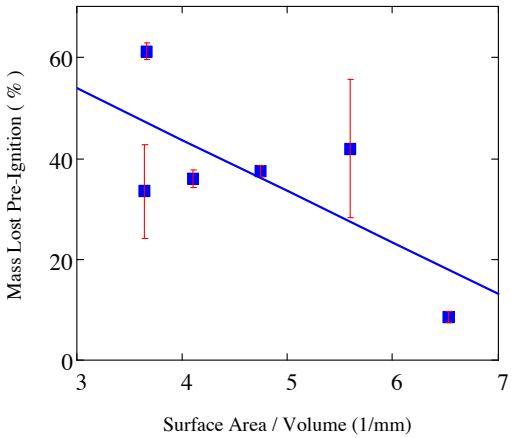

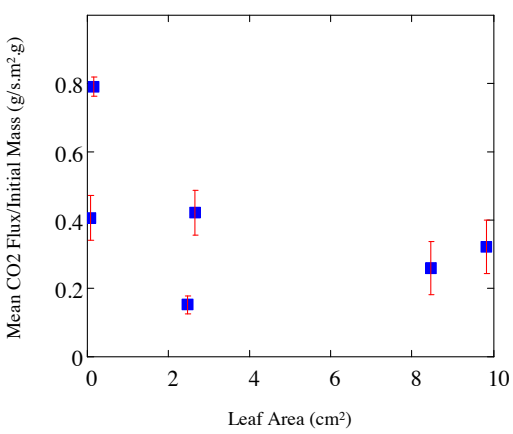
Mean CO2 Flux/Initial Mass (g/s.m².g)
0.8
0.6
0.4
0.2
0
0
2
4
6
8
10
Leaf Area (cm²)

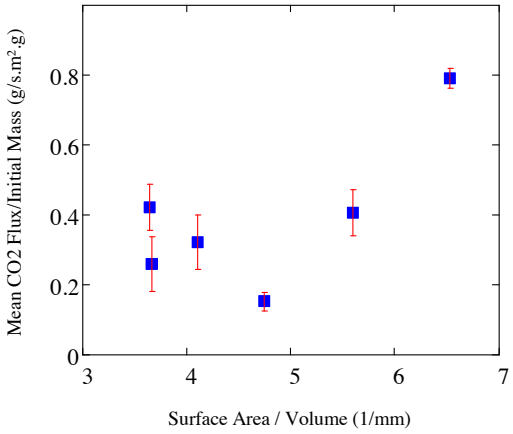
Mean CO2 Flux/Initial Mass (g/s.m².g)
0.8
0.6
0.4
0.2
0
3
4
5
6
7
Surface Area / Volume (1/mm)

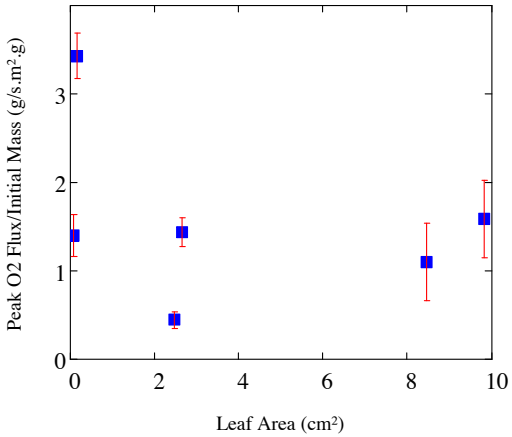
Peak O2 Flux/Initial Mass (g/s.m².g)
3
2
1
0
0
2
4
6
8
10
Leaf Area (cm²)

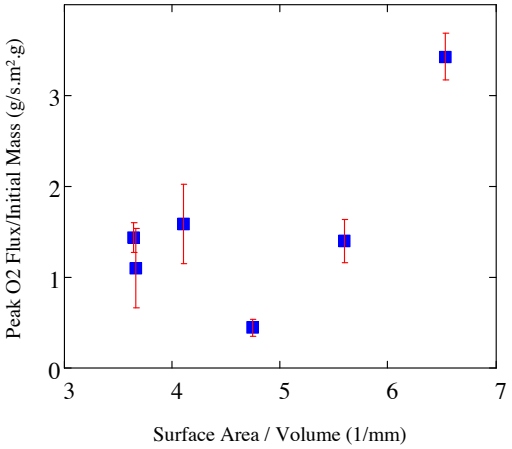
Peak O2 Flux/Initial Mass (g/s.m².g)
3
2
1
0
3
4
5
6
7
Surface Area / Volume (1/mm)

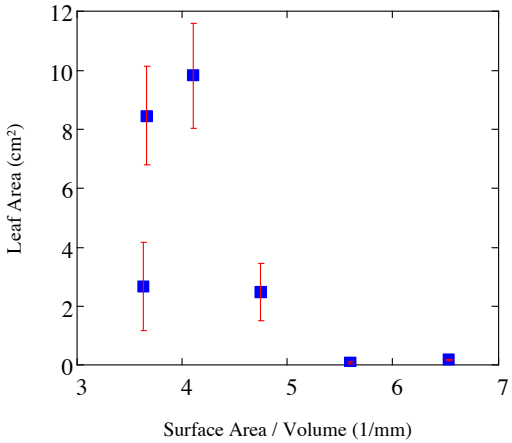
Leaf Area (cm²)
12
10
8
6
4
2
0
3
4
5
6
7
Surface Area / Volume (1/mm)